UNIVERSITY OF MANITOBA

FACTORS AFFECTING PULMONARY VASCULAR PRESSURES AND EDEMA FORMATION

A DISSERTATION SUBMITTED TO
THE FACULTY OF GRADUATE STUDIES
IN CANDIDACY FOR THE DEGREE OF
DOCTOR OF PHILOSOPHY

DEPARTMENT OF PHYSIOLOGY

BY

ZOHEIR BSHOUTY

WINNIPEG, MANITOBA

SEPTEMBER 1990

ISBN 0-315-71859-5

Canada

FACTORS AFFECTING PULMONARY VASCULAR PRESSURES AND EDEMA FORMATION

BY

ZOHEIR BSHOUTY

A thesis submitted to the Faculty of Graduate Studies of the University of Manitoba in partial fulfillment of the requirements of the degree of

DOCTOR OF PHILOSOPHY

Dedicated to my wife and children

ACKNOWLEDGMENTS

I would like first to thank my supervisor Dr. M.K. Younes for his financial assistance, guidance, and continuous critique without which this work would not have been possible.

I also thank Krika Duke, Andrew Gourdie, Donna Lobchuk, Dave Jung for their technical assistance, and Kathy Harlos for preparation of this manuscript.

Finally I would like to extend my thanks to the Canadian Heart Foundation for granting me a three year fellowship and thus providing me with financial assistance from July 1st, 1986 to July 1st, 1989.

Table of Contents

I. SUMMARY

Water content in the lung is determined by rates of fluid filtration and removal. Under normal conditions both rates are small and cancel each other out so that there is no net accumulation of fluid in the lung. An increase in lung water, at a given microvascular pressure, implies an increase in filtration, a decrease in clearance, or both. Rate of fluid filtration (J_v) is governed by the Starling equation:

$$J_v = K_{f,c} \cdot [(P_c - P_{ti,f}) - \sigma \cdot (\pi_c - \pi_{ti})]$$

where, P_c is intravascular hydrostatic pressure, $P_{ti,f}$ is interstitial tissue fluid pressure, σ is the reflection coefficient for plasma proteins, and π_c and $\pi_{ti,f}$ are plasma and tissue colloid osmotic pressures, respectively. Fluid removal (J_l) is effected primarily by the lymphatics.

Physiologic and pathophysiologic factors affecting one or more elements in the Starling equation can have substantial influence on the potential for and rate of fluid accumulation in the lungs. Increasing pulmonary blood flow in the absence of elevated left atrial pressure (such as occurs in exercise), hypoxia (such as occurs upon ascent to altitude), and breathing pattern (because of mechanical interdependence between vascular walls and lung parenchyma) are only a few of these factors.

The goal of this series of studies is to examine some of the physiologic and pathophysiologic factors that affect one or more parameters in the Starling equation, and therefore, enhance or attenuate fluid accumulation in the lung under edema forming conditions. Emphasis will be placed on attempting to identify mechanisms for increased fluid filtration rather than on ultimate outcome. More specifically to determine the effects of increasing pulmonary blood flow, changes in breathing pattern and level of ventilation, and hypoxia on rate of edema formation.

In addition, an in depth look at the behavior of distensible vessels (pulmonary arteries and veins) with and without smooth muscle tone, using computer modeling, is presented. Subsequently, a multibranched computer model of the pulmonary circulation is developed and a detailed discussion of the mechanisms (recruitment and distensibility) responsible for the characteristic behavior of the pulmonary circulation under physiologic and pathophysiologic conditions is entertained.

We first developed an *in situ* left upper lobe preparation, in dogs, that enabled us to monitor lung weight continuously while pulmonary vascular pressures and flow could be accurately controlled and manipulated. A major advantage to our preparation is that changes in pulmonary blood flow and vascular pressures, or lung volume in the experimental lobe had virtually no effect on other variables such as systemic blood pressure and arterial blood gas tensions outside the lobe. Accordingly, many of the

variables that confound interpretation of results in intact preparations were eliminated. As an adjunct to this basic preparation we have established that the hydrostatic pressure at the filtration site, effective filtration pressure (EFP), can be accurately estimated over the entire relevant range of pulmonary blood flow (up to 5 times normal) by the arterial occlusion technique (CHAPTER 4). This permitted the very simple and frequent determination of EFP as experimental variables were changed.

Longitudinal distribution of pulmonary vascular resistance. The longitudinal distribution of pulmonary vascular resistance (PVR) has long been a subject of investigation. The proportion of resistance contributed by vascular segments upstream to and downstream from specific anatomic and functional sites has been assessed in a large number of studies using a variety of techniques. The partitioning of PVR relative to the fluid filtration site is of particular importance; for a given set of inflow and outflow pressures the distribution of resistance determines the intravascular pressure at the filtration site, and hence the potential for, and rate of, edema formation. Several previous studies addressed this question at normal, or near normal, flow rates. Despite marked differences in experimental design, the results were quite similar indicating that the pressure at the fluid filtration site is approximately midway between pulmonary arterial and left atrial pressures.

By contrast, there is little information about the distribution of pulmonary vascular resistance, relative to fluid filtration site, under conditions of very high pulmonary blood flow. There is reason to believe that it may be different. Because arteries are situated upstream along the vascular pathway, they are subject to a greater increase in pressure as flow increases. The relation between pressure and cross-sectional area also varies considerably in different segments along the pulmonary vascular tree.

Our results indicate that during high pulmonary blood flow EFP is closer to PA pressure than it is to left atrial (LA) pressure, and that this becomes progressively more so as a function of flow. As a result the lung accumulates edema at flow rates in excess of four times normal, despite a normal left atrial pressure.

Effect of tidal volume and PEEP. As opposed to the extensive literature on the effects of sustained changes in lung volume (e.g. by PEEP and CPAP), on edema formation and resolution, there is little information on the effect of cyclic changes in lung volume on lung fluid dynamics. In order to maintain adequate ventilation, it is necessary to cycle lung volume. There is a variety of tidal volume/frequency combinations by which a given alveolar ventilation can be achieved. Because of the profound effect of lung volume on almost all factors (Starling factors) that govern lung fluid

filtration and removal, it is quite reasonable to suspect that breathing pattern influences rate of edema formation ($\Delta W/\Delta t$) under edematogenic conditions. It is conventional to ventilate patients in pulmonary edema with fairly large tidal volumes despite high distending pressures, although the spontaneous breathing pattern of patients in pulmonary edema is rapid and shallow. It has not been established, however, whether this imposed pattern is superior to the natural response pattern with respect to edema formation.

Using the same preparation, we were able to show that, for a given filtration pressure, ventilating the lung with larger tidal volumes was associated with greater $\Delta W/\Delta t$ as compared to *base line*. Interestingly, when operating (i.e. mean) lung volume was increased from *base line*, using PEEP, to match that of the large tidal volume, $\Delta W/\Delta t$ changed in the opposite direction. This confirmed that the pattern of ventilation influences $\Delta W/\Delta t$ through mechanisms that are independent of changes in operating lung volume.

Effect of alveolar hypoxia. The effect of alveolar hypoxia on the pulmonary circulation has also been extensively investigated. While there is agreement that the predominant vasoconstrictor effect of hypoxia is at the arterial level, there is no agreement on whether hypoxia causes venoconstriction or has a direct effect on capillary permeability.

In reviewing existing evidence on the effect of alveolar hypoxia on permeability one cannot exclude that the observed increase in fluid flux could not have been attributed to changes in EFP. Because of the complex and somewhat uncertain effects of alveolar hypoxia on the parallel and longitudinal distributions of pulmonary vascular resistance, it is not possible to obtain an accurate estimate of microvascular filtration pressure during hypoxia in the presence of even modest levels of blood flow. Accordingly, using a modification of our basic preparation we have studied the effect of alveolar hypoxia on fluid flux in dog lungs under conditions of very low flow rates, where hydrostatic filtration pressure can be controlled and estimated with certainty.

Our results indicate that alveolar hypoxia does not alter the threshold for edema formation or the rate of edema formation at a given microvascular pressure.

Arterial occlusion versus isofiltration pulmonary capillary pressures. When the arterial supply to a lobe is suddenly occluded, inflow pressure declines in two distinct stages, an initial rapid decline followed by a gradual decline. The point of inflection (between the fast and slow components) describes the pressure at the site of major compliance in the pulmonary circulation (P_M). We wished to determine how P_M, as determined by arterial occlusion, relates to EFP in our preparation. Similarity between P_M and EFP would have two significant

implications: First, it would establish that the sites of fluid filtration and major compliance are the same. Second, it would greatly facilitate the measurement of EFP since arterial occlusion is very simple, and rapid (ca. 2-3 seconds) to achieve, whereas gravimetric techniques are very cumbersome.

Our results indicate that the arterial occlusion technique yields a pressure that is equivalent to EFP even during very high pulmonary blood flow, where the longitudinal distribution of resistance is quite different from that obtained during normal flow.

Distensibility and pressure-flow relationship of the pulmonary circulation. Single vessel model. To ascertain the relative contributions of vascular distensibility and non-homogeneous behavior within the pulmonary circulation to the distinctive non-linear relation between inflow pressure (P_{in}) and flow (F, P-F relation) and between P_{in} and outflow pressure (P_{out}) at constant F (P_{in}-P_{out} relation), we developed a multibranched model in which the elastic behavior of, and forces acting on, individual branches can be independently varied. We first describe the methods used and the responses of single components of the larger model. Perivascular pressure is modeled as a function of intravascular and transpulmonary pressures (P_v and P_{TM}, respectively), and vessel length as a function of lung volume. These, and the relation between vascular area (A) and P_{TM} were modeled primarily from dog data of Smith and Mitzner (*J.*

Appl. Physiol. 48:450-467, 1980). Vasomotor tone is modeled as a radial collapsing pressure (P_T) in the same plane as P_{TM}. In view of lack of information about the relation between P_T and *A* for a given active state, different patterns were assumed which span a wide range of possible relations. The *P-F* and P_{in}-P_{out} relations of single vessels were very similar to those reported for the entire intact circulation. Of note, the slope of the P_{in}-P_{out} relation in the low P_{out} range (0-5 mmHg) was very low (<0.25) and increased gradually with P_{out}, toward unity. Vasomotor tone caused an apparent parallel shift in the *P-F* relation in the physiologic flow range of the dog (2-8 *l*/min) regardless of pattern used to model the P_T vs. *A* relation; different patterns affected the *P-F* relation only over the low flow range before the parallel shift was established.

Distensibility and pressure-flow relationship of the pulmonary circulation. Multibranched model. The contribution of distensibility and recruitment to the distinctive behavior of the pulmonary circulation is not known. To examine this question we developed a multibranched model in which an arterial vascular bed bifurcates sequentially up to 8 parallel channels that converge and reunite at the venous side to end in the left atrium (LA). Separating the arterial and venous beds are 8 resistors representing the capillary bed. The elastic behavior of capillaries and extraalveolar vessels were modeled after Fung and Sobin (*Circ. Res.* 30:451-490, 1972) and Smith and Mitzner (*J.*

Appl. Physiol. 48(3):450-467, 1980), respectively. Forces acting on each component are modified and calculated individually thus enabling the user to explore the effects of parallel and longitudinal heterogeneities in applied forces (e.g. gravity, vasomotor tone). Model predictions indicate that the contribution of distensibility to non-linearities in the pressure-flow (*P-F*) and left atrial-pulmonary artery pressure (P_{LA}-P_{PA}) relations is substantial, whereas gravity-related recruitment contributes very little to these relations. In addition, P_{LA}-P_{PA} relations, obtained at a constant flow, have no discriminating ability in identifying the presence or absence of a waterfall along the circulation. The *P-F* relation is routinely shifted in a parallel fashion, within the physiologic flow range, whenever extra forces (e.g. lung volume, tone) are applied uniformly at one or more branching levels, regardless of whether a waterfall is created. For a given applied force, the magnitude of parallel shift varies with proportion of the circulation subjected to the added force and with LA pressure.

II. CHAPTER 1

LONGITUDINAL DISTRIBUTION OF PULMONARY VASCULAR RESISTANCE WITH VERY HIGH PULMONARY BLOOD FLOW

A. BACKGROUND

The longitudinal distribution of pulmonary vascular resistance relative to the fluid filtration site in the lung is of considerable importance. For a given set of inflow and outflow pressures this distribution determines intravascular pressure at the filtration site (effective filtration pressure, EFP) and hence, the potential for and rate of edema formation. Several studies have previously addressed this question at normal or near normal flow rates (1, 21, 22, 49). Despite marked technical differences, the results of these studies were quite similar, indicating that EFP is approximately midway between pulmonary arterial and left atrial pressures.

In contrast, there is little information about the distribution of pulmonary vascular resistance, relative to the fluid filtration site, under conditions of very high pulmonary blood flow. There are reasons to believe that it may be different. First, because arteries are situated upstream along the vascular pathway, they are subjected to a greater increase in distending pressure as flow increases. Second, the relationship between the distending pressure and cross-sectional area (and hence, the change in resistance for a given change in pressure) also varies considerably between different segments along the pulmonary vascular tree (for review see *ref.* 13).

B. HYPOTHESIS

It has been previously shown that pulmonary arteries continue to distend with increasing transmural pressure (P_{TM}), whereas the distensibility of veins decreases markedly at relatively low P_{TM}. As a result, when pulmonary blood flow increases, arterial resistance continues to decrease while venous resistance remains constant. Vascular pressure at the filtration site becomes closer to pulmonary artery pressure than left atrial pressure. This enhances the potential for and rate of edema formation with increasing pulmonary blood flow.

C. METHODS

1. General

A schematic representation of the preparation used is shown in Figure 1. An isolated *in situ* perfused left upper lobe (LUL) preparation was used. Mongrel dogs weighing roughly 25 kg were anesthetized with intravenous sodium pentobarbital (30 mg/kg body wt), intubated, and ventilated with a dual Harvard pump (initial V_T 10-15 ml/kg, respiratory rate 10 breaths/min, and 50% O_2). An arterial line was inserted into the right carotid artery to monitor systemic blood pressure (BP) and to obtain blood gas samples. A Swan-Ganz catheter was introduced into the right external jugular vein and advanced into the main pulmonary

artery (PA). The animal was then placed in the right lateral decubitus position and a wide thoracotomy was done in the left fifth intercostal space. Once the thoracic cavity was open the animal was placed on 2.5 cmH_2O of positive-end-expiratory pressure (PEEP) to prevent lung atelectasis.

The main branch of the left lower lobe (LLL) PA was isolated and ligated at its entrance into the lobe. A ringed "Y" shaped cannula (7 mm I.D., 8 mm O.D.) was introduced immediately proximal to the ligature. One opening of this cannula was used to perfuse the LUL while the other opening contained a special catheter that served two purposes: 1) to obtain lateral inflow pressure to the LUL and 2) to separate the left and right pulmonary circulations (see below). A heparin sodium drip was then started through this special catheter (the tip of which, at this stage, was still at the stem of the Y cannula) to prevent clotting in the cannula. Left atrial (LA) pressure was monitored through a catheter that was inserted into the LLL pulmonary vein and advanced into the LA.

A second cannula was introduced into the LLL bronchus. Through this cannula, an 8F Fogarty catheter was introduced and inflated with saline at the junction of the left main bronchus and trachea. V_T to the left lung was adjusted to match the volume of the LUL. The LLL was then excised. The LUL was ventilated with a gas mixture of 5% CO_2 in oxygen while the right lung continued to be ventilated with 50% O_2. This combination

was chosen to maintain a constant arterial PCO_2 (P_aCO_2) in case V_T to the LUL had to be modified. High concentrations of oxygen were used to prevent arterial PO_2 (P_aO_2) from dropping substantially as edema formed. Continuous recording of LUL airway pressure (P_{aw}) throughout the respiratory cycle was obtained through a side opening on the bronchial cannula. Ventilation to the LUL was adjusted to pause for 10% of the respiratory cycle at end-inspiration enabling us to obtain static end-inspiratory airway pressure (EIP).

A No. 9 endotracheal tube was introduced into the LA through the LA appendage and secured. At this point the animal was fully heparinized (300 IU per kg body wt). The LA cannula was then connected to the Y arm with 9 mm Tygon tubing primed with saline, and the tubing was placed in a Cobe-Stöckert roller pump.

2. Separation of the right and left pulmonary circulations

The left main PA, after it exits from the pericardium, travels subpleurally for about 1 cm before the takeoff of the LUL branch. A small incision in the overlying pleura near the pericardial exit, avoiding nerves and lymphatics in this region, was made. By blunt dissection a silk thread (No. 2) was passed around the left main PA.

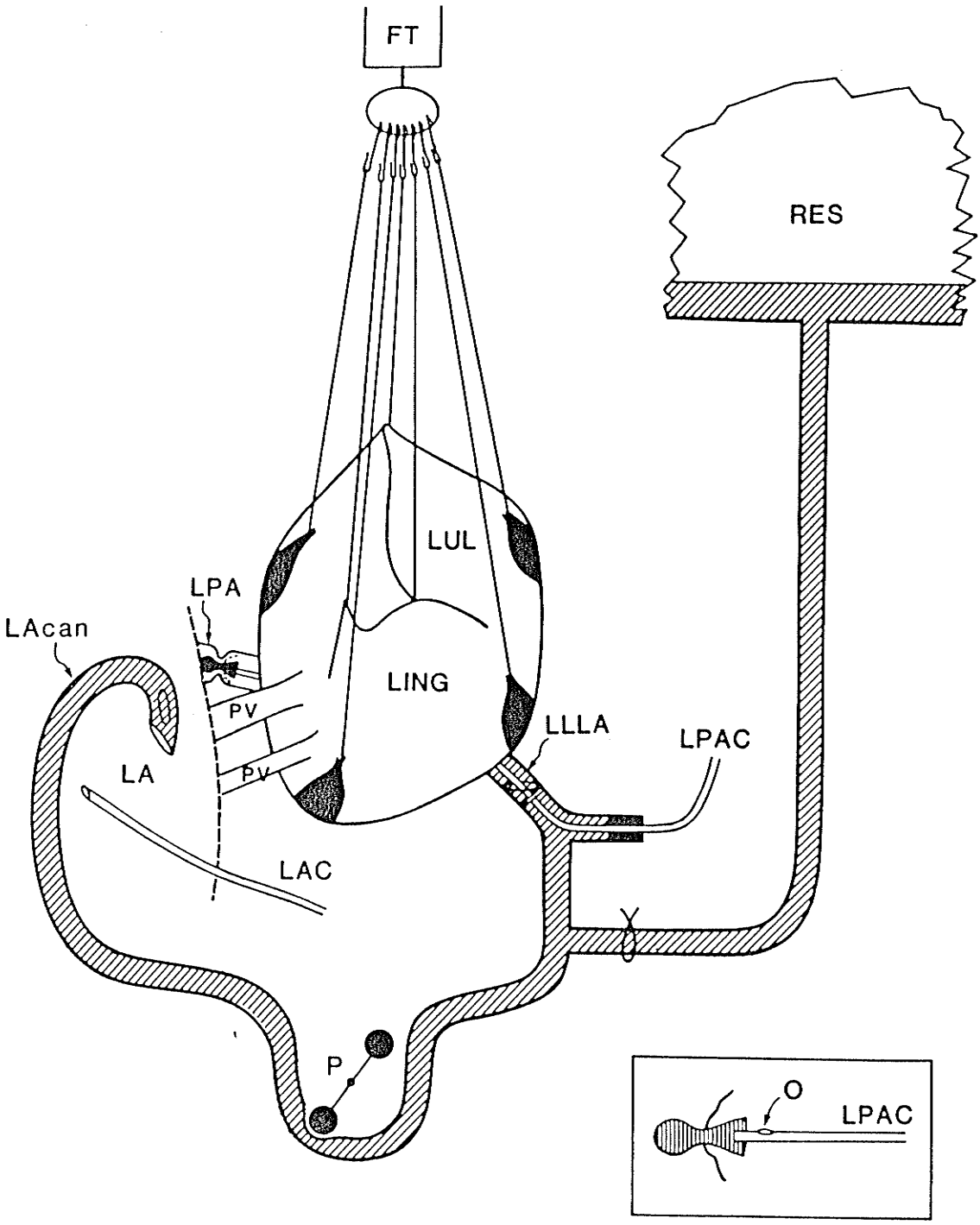

FIGURE 1. Preparation. FT, force transducer; LA, left atrium, LAC, left atrial catheter; LA can, left atrial cannula; LING, lingula; LLLA, left lower lobe artery; LPA, left pulmonary artery; LPAC, left pulmonary arterial catheter; LUL, left upper lobe; P, pump; PV, pulmonary vein; RES, reservoir. *Inset*, details of tip of LPAC. O, orifice for monitoring LPA pressure.

The tip of the special catheter in the Y tube consisted of a small sphere, 5 mm in diameter connected to a cone with a neck measuring 2 mm with a base and height of 5 mm each. The tip of a finger from a surgical glove was tied to the apex of the cone. The width of this rubber material was adjusted so that, when folded over the cone, it did not extend beyond the cone's base. An aperture in the catheter near the cone's base permitted measurement of left PA pressure. The catheter was advanced until the narrow neck of this device was at the level of the silk thread around the left main PA. The thread was then tightened until a pressure gradient was established between the right and left PA without completely occluding the vessel. The roller pump was then immediately started. Flow rate was adjusted so that left PA pressure just exceeded right PA pressure. Under these conditions the remaining space between the left PA and the thread was occluded by expansion of the rubber membrane, thus establishing complete separation between the right and left circulations. At post-mortem, we confirmed that the neck of the catheter moved freely inside the ligature so that there was no undue tension or strangulation of the artery wall.

3. Suspension of the LUL

The LUL was then prepared for suspension in the following manner: Four thin rubber patches (1 mm thick, 12 mm wide, and 40 mm long) were glued with "Krazy" glue to the surface of the

lobe, one on the medial surface and one on the lateral surface of each of the LUL proper and the lingula. Attention was paid to place the patches near the posterior surface of the lobe so that the base was supported. Silk threads were attached around the free end of each strip. The free anterior tips of the LUL and lingula were each tied with additional threads and finally, the anterior borders of the LUL and lingula were joined with a thread. Each of the seven threads was attached to a hook and all hooks were suspended from a force transducer. The height of the transducer was adjusted until the lobe was clear of posterior structures and the threads are taut. In this fashion lobar weight was evenly distributed. To calibrate the force transducer, known weights were placed on several locations on the lobe and the deflections were recorded. Because of large variations in weight with ventilation, data were obtained at end-expiration.

All pressure lines (systemic BP, left and right PA pressures, LA pressure, and P_{aw}) were connected to appropriate pressure transducers and zeroed at the level of the LUL pulmonary veins as they entered the LA. Continuous recording of these pressures was maintained throughout the study on a 6-channel Gould chart recorder. Care was taken to readjust V_T to the right lung only, to maintain P_aCO_2 between 30 and 40 mmHg. Sodium bicarbonate was infused as necessary to maintain arterial pH between 7.30 and 7.40, although this was rarely necessary.

Body temperature was maintained between 36 °C and 38 °C with heating pads. Blood gases and hematocrit were drawn at random order throughout the experiment to make sure that no major drop in hematocrit or pH occurred.

At the end of the experiment the animals were rapidly exsanguinated by pumping blood from the LA into a reservoir. The LUL was excised, drained from blood and weighed immediately.

D. PROTOCOL

With the lobe in its normal position before suspension, flow was increased in steps (each lasting approximately 30 sec) up to a flow rate of 4 *l*/min or PA pressure of 60 mmHg, whichever came first. Subsequently, flow was returned in steps to *base line*. This process was repeated following the lobe suspension to ensure that suspension, per se, caused no kinking or stretching of the pulmonary vessels.

1. Dynamic measurements

Flow was increased in steps from *base line* to various levels (up to 10 times normal flow) and was maintained for about 4 minutes. Following each step, flow was returned to *base line* and maintained until lobar weight stabilized. The above sequence was

repeated until 5 to 7 different flow rates were examined (at least twice each)[1]. The order in which the various flow levels were applied was randomized.

2. Static measurements

At the end of the dynamic measurements, snares were placed around the two LUL veins as they enter the pericardium. Pump flow was stopped and the snares were tightened. A reservoir, primed with the dog's blood and connected to the PA inflow tubing, was used to induce edema statically. Edema was produced by raising the reservoir level from a *base line* of 7-10 mmHg to varying degrees of pulmonary vascular pressure for about 4 minutes. The reservoir level was returned to *base line* between observations. The highest pressure used was one that was associated with a rate of weight gain comparable to the highest rate observed during the dynamic measurements. Again, the order at which the various pressure levels was applied was randomized.

3. Determination of rate of edema formation ($\Delta W/\Delta t$)

$\Delta W/\Delta t$ was determined gravimetrically. Following a step increase in vascular pressure (by increasing flow or raising the reservoir level) there was an initial fast phase of weight gain. When vascular pressure at the filtration site exceeds a critical value, this fast phase was followed by a phase of slow weight gain. The rate of weight gain during this period was constant as

long as vascular pressure remained constant. $\Delta W/\Delta t$ was derived from the slope of this slow weight gain segment over a period of 3 minutes.

4. Estimation of effective filtration pressure (EFP)

$\Delta W/\Delta t$ beyond the first minute of step increase in flow was measured and the average value of all determinations (in the same animal and for the same flow) was calculated. Next, all static data for which there was a measurable $\Delta W/\Delta t$ and the highest pressure point during which there was no progressive weight gain (i.e. $\Delta W/\Delta t = 0$) was plotted ($\Delta W/\Delta t$ vs. pressure) and a best linear fit was obtained. EFP in the presence of flow was estimated from the relevant regression equation at a point that resulted in a weight gain identical to that observed in the dynamic state.

Following the determination of EFP, it was possible to calculate the pressure drop upstream from the filtration site (difference between left PA pressure and EFP, ΔP_{US}), downstream pressure drop (difference between EFP and LA pressure, ΔP_{DS}), and the upstream and downstream resistances ($\Delta P_{DS}/\dot{Q}$ and $\Delta P_{DS}/\dot{Q}$, R_{US} and R_{DS}, respectively).

E. RESULTS

An example of the response observed during step increases in lobar flow is shown in Figure 2. *Base line* flow to LUL was 0.324±0.04 (mean±SD; range 0.3-0.4) *l*/min, corresponding to the

normal blood flow of this lobe [12.2% of cardiac output (7)]. At this flow (mean±SD) systemic blood pressure, right PA, and left PA and LA pressures were 128±7.3, 11.1±1.7, 11.8±1.8, and 2.6±1.6 mmHg, respectively. There was no systematic tendency for any of these *base line* pressures to change over the duration of the dynamic measurements (~2 h). The change in *base line* (mean±SE) systemic blood pressure from beginning to end of the dynamic measurements was 1.8±3.4 mmHg. The corresponding changes in (mean±SE) right PA, left PA, and LA pressures were -0.42±0.44, -0.33±0.44, and -1.1±1.3 mmHg, respectively.

The highest flow used to perfuse the LUL (mean±SD) was 2.97±0.45 (range 2.50-3.50) *l*/min. This corresponds to a cardiac output of 24 *l*/min or 1,000 ml/kg body wt. Changing flow from *base line* to the highest value had no effect on right PA pressure in any of the animals (e.g., Figure 2), confirming the complete separation between right and left lung circulations. Left atrial pressure either did not change or changed slightly and inconsistently in response to a step increase in flow. With the largest step increase, the range of LA pressure change was -1.0 to 1.5 (e.g., Figure 2) mmHg (mean±SD = 0.4±0.85; NS). Within each animal, however, the change in LA pressure was always in the same direction and its magnitude was related to the magnitude of flow. The lack of an appreciable effect of pump flow on LA pressure was predictable, since blood aspirated from the LA is returned at the same rate via the LUL veins. The inconsistency

of the change in different animals is probably due to differences in position or orientation of the tip of the LA pressure catheter relative to the currents created by the LA cannula. The change in LA pressure with a step increase in flow (if any) occurred at the point of flow transition. There was no subsequent change.

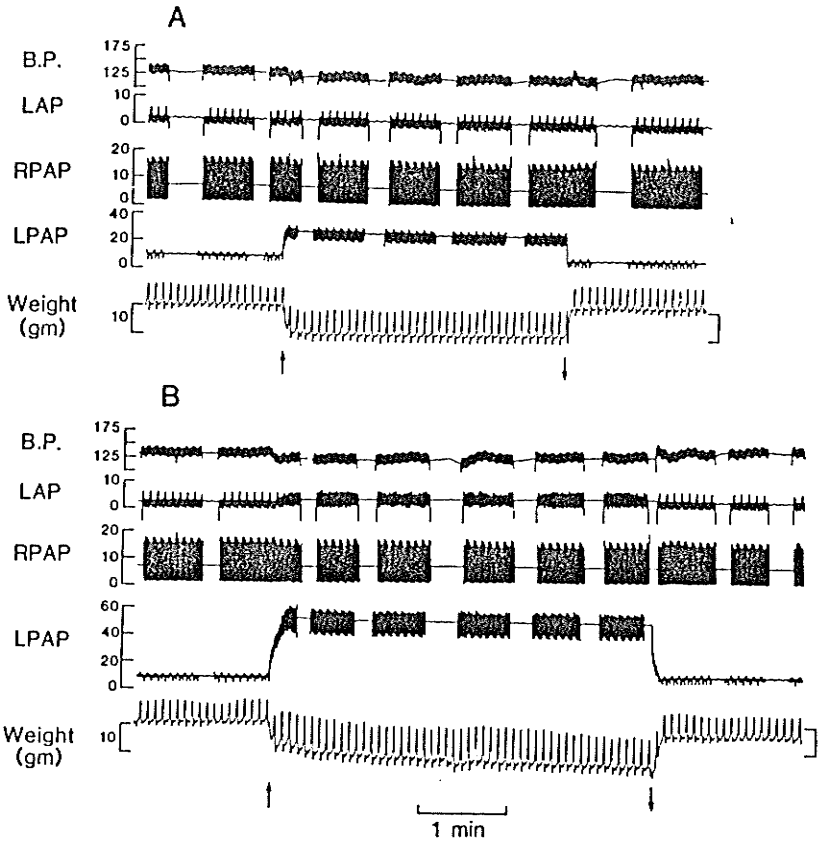

FIGURE 2. Representative examples of response to step increase in flow in one animal. A: flow increased from 0.4 to 1.5 *l*/min. B: flow increased to 3.5 *l*/min. BP, arterial blood pressure; LAP, left atrial pressure; LPAP, left pulmonary artery (PA) pressure; RPAP, right PA pressure. All pressures are in mmHg. *Thin lines* in pressure tracings represent mean pressures. *Arrows* indicate times at which flow was increased (*left*) and then returned to *base line*. Note lack of change in RPAP, slight increase in LAP, and slight decrease in BP. *Brackets* on either side of weight tracing are at the same horizontal level. A downward deflection in weight tracing signifies weight gain. Note that end-expiratory lobe weight (horizontal segment within each respiratory cycle) is stable in A and progressively increases in B.

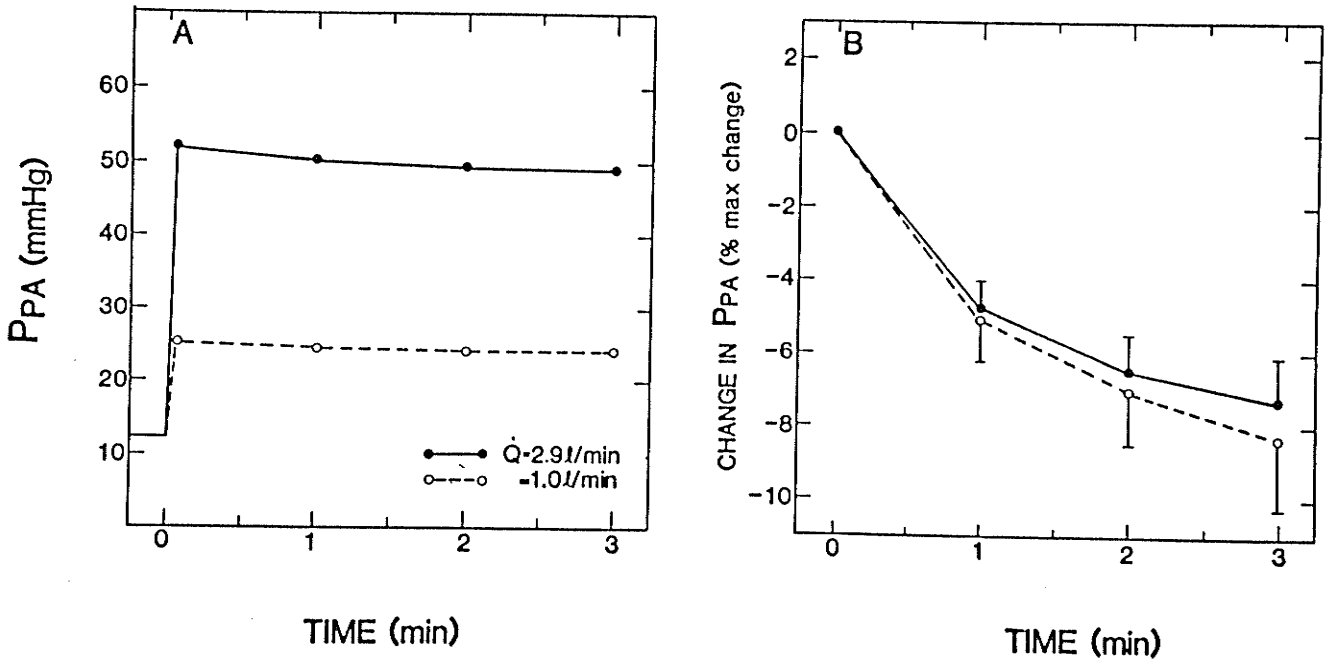

FIGURE 3. Changes in left pulmonary artery pressure with time after a step increase in flow. A: average results of response at highest flow in all animals (*solid line*). *Dashed line*, response during step increases in flow to ~1.0 *l*/min. B: data of A, but change in pressure is expressed as % of initial step increase in left pulmonary artery pressure. *Bars*, ±SE.

Systemic blood pressure decreased in all animals in response to step increase in lobar flow. The change in blood pressure, while small, was consistent and related to the magnitude of flow. At the highest flow blood pressure decreased, on average 6.2±1.6 (SD) mmHg (range -4 to -7.5 mmHg). The reason for this decrease is not clear.

Left PA pressure increased as a function of lobar flow. With each step increase in flow left PA pressure rose rapidly to a maximal value. It subsequently declined slightly over the 3-4 min. of observation (e.g., Figure 2). This gradual decline was observed with all flow rates. Figure 3A shows the average temporal change in left PA pressure with the highest step increase in flow in the seven animals. Pressure decreased, on average, 2.8 mmHg from peak to 3 min, with most of the change occurring in the 1st min (1.8 mmHg). The same phenomenon was observed at lower flow rates. The lower line in Figure 3A shows the response following a step increase in flow from *base line* to, on average, 1.0 *l*/min. Pressure decreased 1.0 mmHg over the corresponding time interval. When the time-dependent change in pressure is expressed as percent of the step change in pressure (i.e., peak pressure minus *base line* pressure), the pressure responses at the two flow rates were similar (Figure 3B). Since flow and LA pressure were constant in each case, changes in left PA pressure reflect changes in lobar pulmonary vascular

resistance (PVR). Figure 3B indicates that PVR decreased 5.0±1.1% by 1 min. with an additional decrease of 3% between 1 and 3 min.

The relation between flow and left PA pressure was determined before and immediately after lobe suspension (n=7). Three flow rates were compared: 0.5, 1.5, and 2.5 *l*/min. The change in left PA pressure as a result of suspension was 0.0±0.3, -0.9±1.4, and -2.2±1.1 (SE) mmHg at the three flow rates, respectively. None of these differences was significant, indicating that suspension per se did not alter the conductance of lobar vessels.

Following a step change in flow, weight changed acutely, presumably reflecting changes in blood volume. When flow was above a critical level, weight continued to increase at a steady rate beyond the initial weight gain (Figure 2, *bottom*). At lower flow rates end-expiratory lobe weight remained stable beyond the 1st min (Figure 2, *top*). Weight accrued during the phase of slow weight gain was not lost after returning flow to *base line* (Figure 2, *bottom*).

Figure 4 illustrates examples of the response to step changes in static vascular pressures in the same animal as in Figure 2. Increasing vascular pressure in LUL had no effect on systemic blood pressure, LA pressure, or right pulmonary arterial

pressure. When static pressure exceeded a critical value (P_{TH}) the acute increase in lobe weight was followed by a steady gain at a constant rate[2].

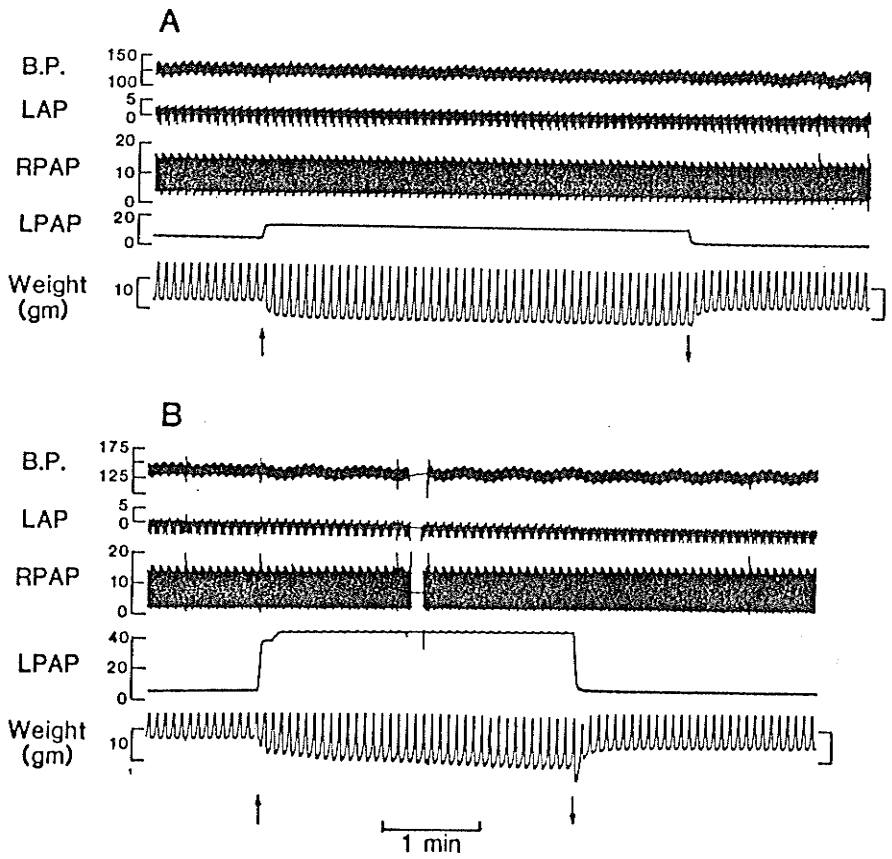

FIGURE 4. Representative tracings of response to step increases in static pressure. Same animal as in Figure 2. Legend of abbreviations as in Figure 2. Note stability of weight at static pressure of 18 mmHg (A) and progressive weight gain at pressure 44 mmHg (B).

Figure 5 shows the pressure and weight data for all animals. The left panels illustrate the relation between flow and left PA pressure (*solid lines*) in the seven animals. Each data point (*solid symbols*) represents the pressure measured 2 min after the specified step increase in flow. Because these relations did not conform to specific functions, lines of best fit were drawn by eye. As indicated in METHODS, the order of applying different flow rates was random, and more than one series of measurements was obtained in each animal.

The middle panels of Figure 5 show the relation between flow and rate of slow weight gain measured beyond the first minute. In six of seven animals the relation appeared linear. For these animals, the relation was obtained with linear regression analysis using all data points displaying slow weight gain. Excellent correlation coefficients were obtained in each case (r = 0.79-0.98; Figure 5). In the seventh animal (Figure 5, *bottom*) the relation was convex to the flow axis and the average relation was obtained by interpolating between the mean of the two points at each flow. The flow intercept for this animal was determined by extrapolating the first segment.

The minimal flow associated with slow weight gain (flow intercept, $\dot{Q}_{TH}$) ranged from 1.35 to 1.75 *l*/min (mean±SE = 1.47±0.056 *l*/min). The slope of the six linear relations varied from 0.41 to 3.17 $g \cdot min^{-1} \cdot l^{-1} \cdot min$ (mean±SE = 1.17±0.42).

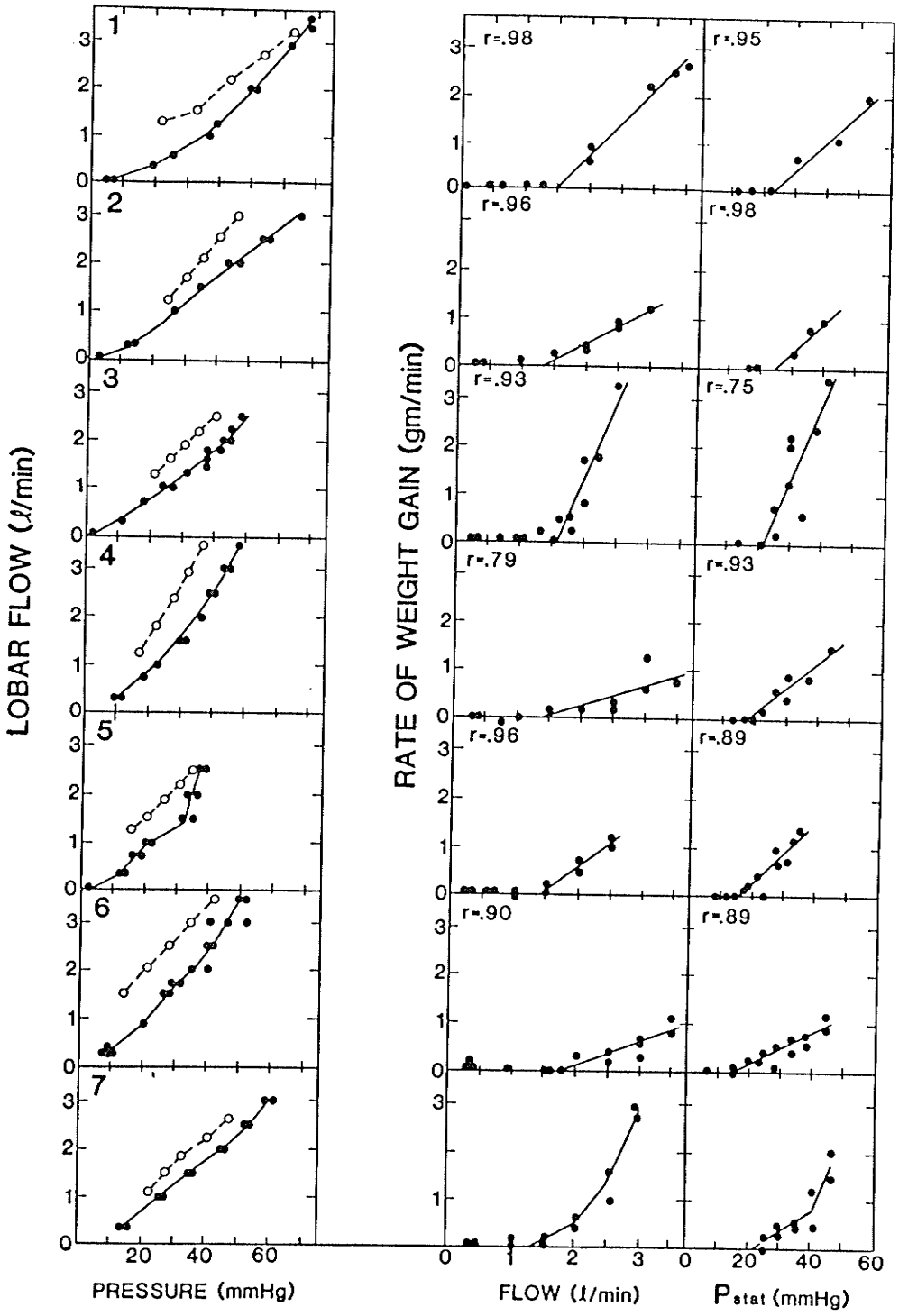

FIGURE 5. *Left*: relation between lobar flow and left pulmonary artery pressure (*solid symbols*) in 7 animals. *Open symbols*, effective filtration pressure (see text). *Middle*: relation between lobar flow and rate of weight gain. *Right*: relation between static pressure and rate of weight gain.

The relation between static pressure and $\Delta W/\Delta t$ is shown in Figure 5, right. As with the dynamic data the relations for the first six animals were linear (r = 0.75-0.98), whereas in the last animal it was convex to the pressure axis. P_{TH} ranged from 14.0 to 24.5 mmHg (mean±SE = 19.7±1.5 mmHg) and the slope for the first six animals varied from 0.032 to 0.15 $g \cdot min^{-1} \cdot mmHg^{-1}$ (mean±SE = 0.06±0.017). Given an estimated normal wet weight for LUL of 1.35 g/kg body wt. (7), the normalized slope values were 0.188±0.052 $g \cdot min^{-1} \cdot mmHg^{-1} \cdot 100\ g^{-1}$ (SE). There was an excellent correlation (r = 0.95) between the slopes of the dynamic and static measurements. The relation was given by the equation

$$S_{ST} = 0.038\ S_{DYN} + 0.024 \qquad \ldots\ldots (2)$$

where S_{ST} and S_{DYN} denote static and dynamic slopes, respectively.

We looked for evidence of systematic changes in the relation between flow and rate of weight gain over the duration of the dynamic measurements and in the relation between static pressure and weight gain during the static measurements. First, we compared the rate of weight gain during a step increase in flow at the end of the dynamic measurements with the weight gain obtained when the same flow was tested early in the experiments. Six animals provided this opportunity. There was no significant difference by paired t test ($P>0.50$), in $\Delta W/\Delta t$ between early and

late observations. $\Delta W/\Delta t$ for the early observations averaged 1.02±0.37 (SE) g/min compared with 0.96±0.30 g/min for the late observations. PA pressure also was not different (47.8±5.2 vs. 48.8±4.7) in these paired flow observations. A similar analysis (n=5) also failed to show a significant difference ($P>0.50$) in $\Delta W/\Delta t$ at a given pressure tested early and late in the course of static measurements. Average $\Delta W/\Delta t$ (mean P_{ST} = 35 mmHg) was 1.14±0.26 (SE) and 1.26±0.30 g/min for early and late observations, respectively.

In the event that the above negative results were fortuitously related to too few comparisons relative to the inherent variability of the measurement (type II error) we carried out a modified analysis of residuals to identify time-dependent trends. We thus considered that the regression lines (or lines of best fit for animal 7) for the dynamic and static measurements ($\Delta W/\Delta t$ vs. $\dot{Q}$ and $\Delta W/\Delta t$ vs. P_{ST}) represent the average response over the entire period of dynamic and static data collection, respectively. If there were a systemic tendency for weight gain to be relatively higher later in the course of data collection, then data points collected late in the experiment should be preferentially located above the regression line, and vice versa. The time of occurrence of each data point (associated with weight gain) relative to total time of dynamic or static data collection was identified. The horizontal deviation of the data point from the corresponding regression

line was measured. The results for all data points are shown in Figure 6, top. A positive value denotes that the point was to the left of the regression line, and vice versa. There was no correlation (r = 0.10) between time and magnitude of deviation in the static measurements (Figure 6, *right*). A marginally significant correlation (r = 0.32, $P<0.05$) was found between magnitude of deviation in the dynamic measurements. However, inspection of the plot of Figure 6, top left, suggested that the relation may not be a simple linear function. To reduce the effect of random (i.e., time independent) variability that accounts for 90% of the variance, we obtained the average deviation in 10% time bins (*middle*). This plot shows that in the first 30% of the time of dynamic measurements the data points appear to systematically deviate from average by ~0.21 *l*/min but that, within this time range, there is no time dependence. Following a transitional zone (30-50% of dynamic time) there is a shift to positive deviation, which again shows no clear time dependence (average deviation in the second 50% of time = 0.14 *l*/min). This time independence continues into the static measurements, which were done immediately following the dynamic measurements. In fact, there was no significant correlation between deviation and time when the data for the first and last 50% of dynamic time were considered separately (r = 0.06 and -0.09, respectively). It follows that there is a step change in rate of weight gain that occurs between 30 and 50%

of dynamic measurements time. This is particularly interesting in view of the observations by Drake et al. (12) that the rate of lobar weight gain changes from one value to a higher but also a constant value when lobe weight increases more than 50% of its original wet weight. The middle of the time of dynamic measurements would be about the time our lobes gained 15 g or 50% of their estimated normal wet weight (7).

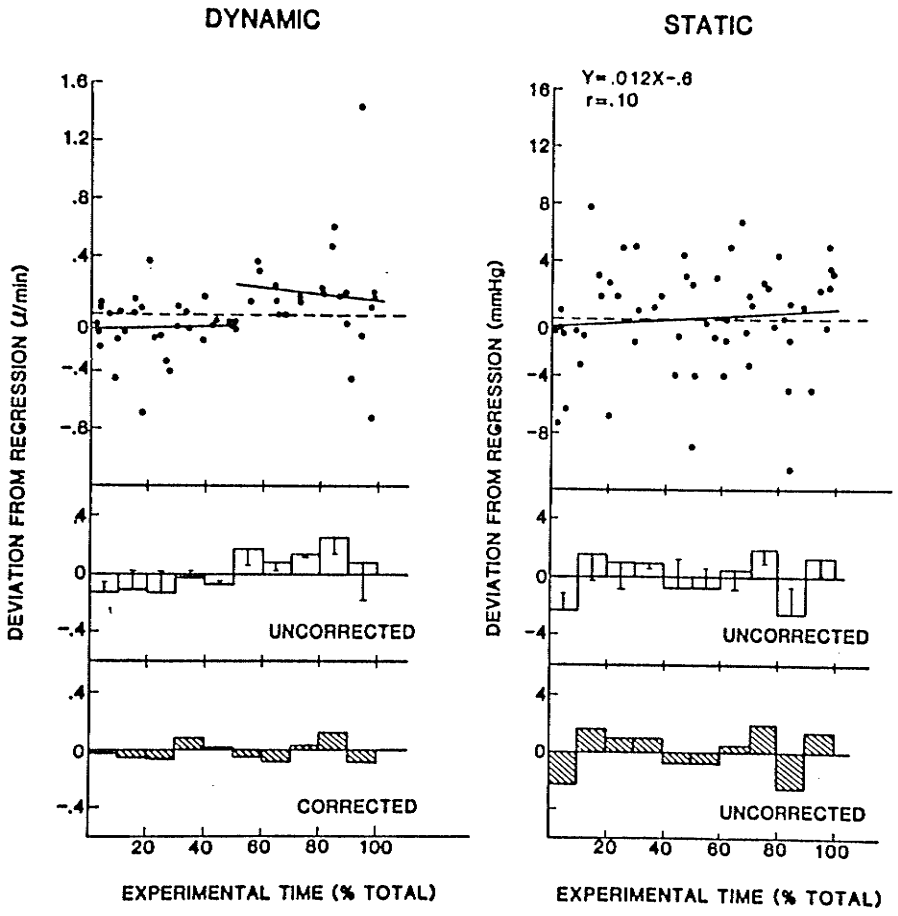

FIGURE 6. Determination of time-dependent changes in relation between flow rate and rate of weight gain (*left*) and between static pressure and rate of weight gain (*right*). See text for explanation.

The data for each half of the dynamic measurements were further divided into two groups of equal number according to flow. In the first 50% of time the average deviation for points with high flow [2.79±0.50 (SE) *l*/min] was -0.091±0.17 *l*/min compared with -0.091±0.22 *l*/min for the low flow data points (1.89±0.32 *l*/min). Similarly, there was no significant difference between high and low flow points in the second half of the measurements (0.138±0.23 vs. 0.163±0.50, $P>0.50$). Our lobes thus behave as if, after accumulating about 50% of their initial weight, a change occurs in one of the factors in the Starling equation, which causes rate of weight gain to increase by a constant amount that is independent of flow (and hence intravascular hydrostatic pressure). The change in rate of weight gain is comparable with that which would have been produced by a flow increment of 0.26 *l*/min (sum of negative and positive deviations in first and second halves of dynamic measurements: 0.12+0.14 = 0.26). Judging from the relation between S_{DYN} and S_{ST}, this is equivalent to a pressure change of 5.0 mmHg ($0.26\ S_{DYN}/S_{ST}$).

The data points obtained in the first half of dynamic measurements in each experiment were shifted 0.26 *l*/min to the left and the regression equations were recalculated. The correlation coefficient improved in each case. Average of *r* values increased to 0.93±0.03 (SE) from 0.91±0.03. The flow intercept ($\dot{Q}_{TH}$) decreased in each case. Average $\dot{Q}_{TH}$ became

1.27±0.05 (SE) compared with 1.47±0.06 *l*/min before correction. There were minor and inconsistent changes in slope (1.05±0.30 vs. 1.17±0.42, NS).

Recalculation of average deviation from the recalculated regression lines now showed no time-dependent trends (Figure 6, *bottom*).

The elimination of time- (or lobe weight) dependent trends makes it possible to relate static and dynamic measurements to each other. It must be reiterated that only a few minutes separated the end of dynamic measurements and beginning of static measurements and that there was no fluid accumulation in the interim.

The remaining analysis will be based on corrected data, but the effect of the correction, if any, on the results will be indicated.

Partitioning of Pulmonary Vascular Resistance. For a given flow, the hydrostatic pressure at the filtration site (effective filtration pressure, EFP) was estimated from the static pressure that resulted in a similar rate of weight gain in the same animal. For this purpose, the dynamic and static regression lines (Figure 5, *right*) were used instead of actual data points to eliminate the effect of random measurement noise. For each animal we determined EFP at five flow levels. These were $\dot{Q}_{TH}$, the highest flow for which static measurements with comparable

$\Delta W/\Delta t$ were available ($\dot{Q}_{HI}$) and three equally spaced intermediate levels ($\dot{Q}_2$, $\dot{Q}_3$, and $\dot{Q}_4$). The data are shown in Figure 5, left (*open circles*). From these plots it was possible to calculate the pressure drop upstream to the filtration site (horizontal distance between PA and EFP lines, ΔP_{US}), downstream pressure drop (difference between EFP and LA pressure, ΔP_{DS}), upstream and downstream resistances ($\Delta P_{US}/\dot{Q}$ and $\Delta P_{DS}/\dot{Q}$, R_{US}, and R_{DS}, respectively) and the contribution of R_{DS} to total pulmonary vascular resistance (R_{DS}/PVR). The results are summarized in Table 1. In addition, the relation between flow and ΔP_{US} and ΔP_{DS} in individual animals is shown in Figure 7.

Rus decreased. The decrease was sufficiently pronounced so that ΔP_{US} did not change or decreased as flow increased in six of seven animals (Figure 7, *left*). On average R_{US} decreased from 8.3 to 2.9 mmHg·l^{-1}·min (Table 1). In contrast, ΔP_{DS} increased progressively with flow in all animals and the relations were linear (Figure 7, *right*). The regression had a small pressure intercept in three animals (3, 4 and 8 mmHg) while intercepting the flow axis in the other four (0.2, 0.3, 0.5, and 0.7 *l*/min). On the average, there was no significant change in R_{DS} as a result of increasing flow over the range of measurements (Table 1). R_{DS}/PVR increased progressively from 0.61 at $\dot{Q}_{TH}$ to 0.83 at $\dot{Q}_{HI}$.

TABLE 1. *Average hemodynamic data in seven dogs at five flow rates*

	$\dot{Q}$, l/min	PAP, mmHg	EFP, mmHg	LAP, mmHg	ΔPus, mmHg	ΔPds, mmHg	Rus, mmHg·l^{-1}·min	Rds, mmHg·l^{-1}·min	Rds/PVR
$\dot{Q}$th	1.27 (0.05)	30.4 (1.7)	19.7 (1.5)	2.6 (0.3)	10.7 (1.7)	17.0 (1.7)	8.3 (1.3)	13.7 (1.7)	0.61 (0.05)
$\dot{Q}_2$	1.70 (0.07)	36.8 (1.8)	25.7 (1.7)	2.7 (0.3)	11.1 (0.9)	22.9 (1.9)	6.6 (0.5)	13.7 (1.4)	0.67 (0.03)
$\dot{Q}_3$	2.12 (0.10)	42.5 (2.3)	31.8 (2.1)	2.8 (0.2)	10.5 (0.6)	29.0 (2.2)	5.0 (0.2)	13.8 (1.2)	0.73 (0.01)
$\dot{Q}_4$	2.55 (0.13)	47.8 (3.0)	38.4 (2.9)	2.9 (0.2)	9.7 (1.5)	35.5 (2.9)	3.8 (0.6)	14.1 (1.3)	0.78 (0.03)
$\dot{Q}$hi	2.97 (0.17)	53.0 (3.7)	44.4 (3.5)	2.9 (0.2)	8.7 (2.1)	41.4 (3.6)	2.9 (0.7)	14.1 (1.3)	0.83 (0.03)

Values are means±SE. $\dot{Q}$, flow; PAP, pulmonary artery pressure; EFP, effective filtration pressure; LAP, left atrial pressure; ΔP_{Ds}, pressure difference between EFP and LAP; ΔP_{Us}, pressure difference between PAP and EFP; R_{Ds}, downstream resistance; R_{Us}, upstream resistance; R_{Ds}/PVR, contribution of downstream resistance to pulmonary vascular resistance; $\dot{Q}_{TH}$, lowest flow at which lobe weight progressively increased; $\dot{Q}_{HI}$, highest flow tested. $\dot{Q}_2$, $\dot{Q}_3$, $\dot{Q}_4$ intermediate flow rates.

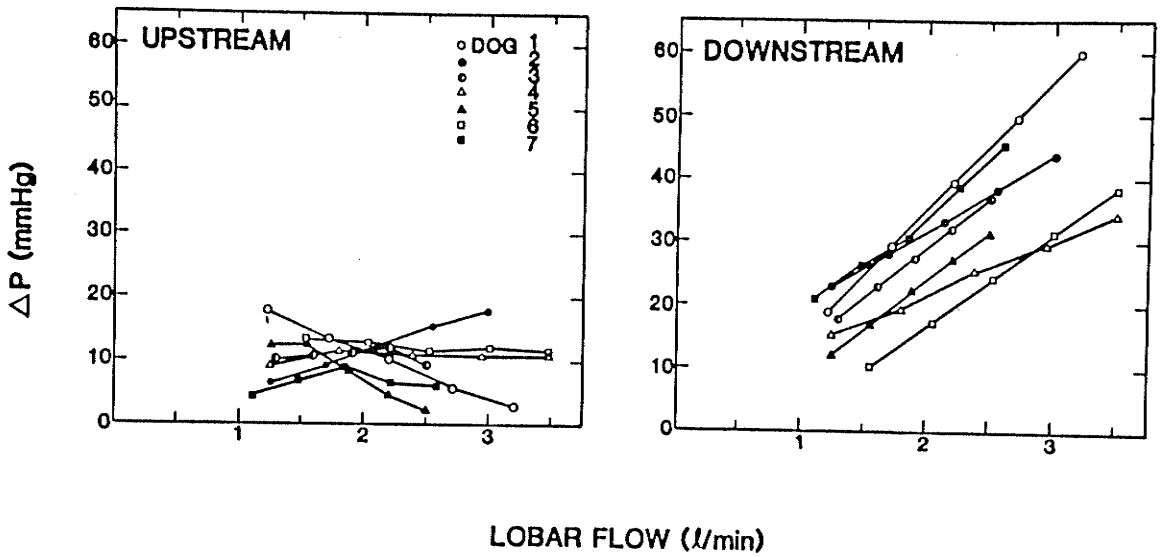

FIGURE 7. Changes in upstream (*left*) and downstream (*right*) pressure gradients as a function of lobar flow. Pressure change (ΔP) in *left panel*, difference between PA pressure and EFP. ΔP in *right panel*, effective pressure at filtration site - left atrial pressure.

Whereas these results were based on corrected data, results with uncorrected data were only marginally different. As indicated earlier $\dot{Q}_{TH}$ was higher with the uncorrected data. R_{US} was slightly higher and R_{DS} was slightly lower with the uncorrected data, but the trends with increasing flow were the same. R_{DS}/PVR was 0.55 at $\dot{Q}_{TH}$ (compared with 0.61 in the corrected data) and increased to 0.79 $\dot{Q}_{HI}$ (compared with 0.83). The main effect of the correction, therefore, was to cause a slight systematic increase in the contribution of R_{DS} to PVR.

Figure 8 shows the average change in various vascular pressures and resistances as a function of lobar flow. Equivalent cardiac output values are shown in the upper abscissa [8 times lobar flow (7)]. Solid lines show data obtained from the present study (as in Table 1). In addition, we attempt to infer the behavior of these pressures and resistances over the flow range below $\dot{Q}_{TH}$. This extrapolation is justified by virtue of the linear relation (r = 1.00) between $\dot{Q}$ and ΔP_{DS} with an intercept very near zero (-1.46 mmHg; Figure 8B). We reasoned that the actual relation between $\dot{Q}$ and ΔP_{DS} in the range for which data do not exist (i.e, 0 to $\dot{Q}_{TH}$) cannot deviate substantially from a line joining zero and the $\dot{Q}_{TH}$ point (Figure 8B, *dark dashed line*). Extrapolated ΔP_{DS} was then added to LA pressure to arrive at EFP over this range (Figure 8A, *dots*). The changes in ΔP_{US}, R_{DS}, R_{US}, and R_{DS}/PVR were then derived. This analysis shows that R_{DS} and R_{US} should be equal

(R_{Ds}/PVR = 0.5) at a lobar flow of 0.62 *l*/min (Figure 8D), about twice normal blood flow, and that at normal flow rates R_{Ds} should account for 45% of the pressure gradient between PA and LA. In this analysis we assume that the critical opening pressure is not much higher than LA pressure. This treatment is justified in this preparation, since in several animals we measured PA pressure when the pump was briefly stopped ($\dot{Q}$ = 0). In each case (Figure 5, *left*) PA pressure was not different by >1 mmHg from LA pressure.

The wet weight at the end of the experiment in four animals averaged 77.4±10.7 (SE) g. Given an estimated normal wet weight of 31.0 [i.e. 1.35 x body wt (7)], this represents an average increase of 46.4 g. The average cumulative increase in force transducer signal was 49.5±7.5 (SE) g, and there was a significant correlation between excess weight determined by the two methods. The values of r (0.88) and slope (1.14) were similar to those reported by Gabel and Drake (19) in another *in situ* preparation (r = 0.82 and S = 1.05).

P_aCO_2 changed little (31 to 32 mmHg) as a result of increasing flow from *base line* to the highest level. Likewise, arterial pH did not change (7.37 to 7.35). P_aO_2 increased from an average of 90 mmHg to 167 mmHg. since both values are above the physiologically relevant range, it can be concluded that

increasing flow caused no functionally significant changes in arterial or lobar inflow blood gas tensions (both are derived from LA).

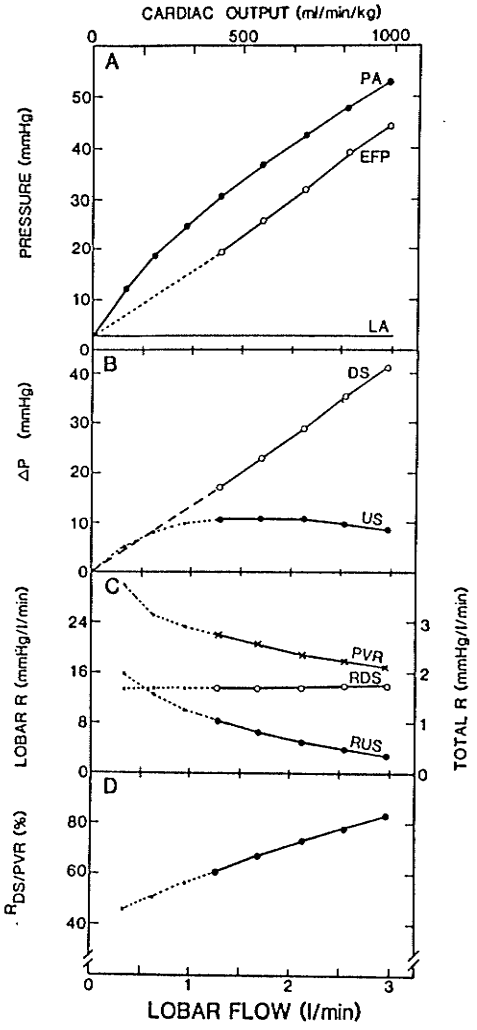

FIGURE 8. Average changes in various pressures (A), pressure gradients (B), resistances (C) and fraction of downstream resistance (R_{DS}) to total resistance (PVR) (D), as a function of lobar flow (*lower abscissa*) or equivalent cardiac output (*top abscissa*). *Right ordinate of panel C* is equivalent resistance value for total circulation (i.e. lobar resistance/8). PA, pulmonary arterial pressure; EFP, effective filtration pressure; LA, left atrial pressure; DS, downstream; US, upstream; PVR, pulmonary vascular resistance; R_{US}, upstream resistance. *Solid lines*, data obtained from present study. See text for explanation of dotted and dashed lines.

F. DISCUSSION

1. Critique of Methods

The preparation we used combines the advantages of in vivo and in vitro gravimetric preparations while minimizing the disadvantages of both. It permits the precise control of flow over the entire physiologically relevant range while lobar weight is being continuously monitored. The choice of upper lobe perfusion offers several advantages over the more commonly used *in situ* lower lobe perfusion. For gravimetric measurements of either lobe, it is necessary to remove the other lobe. The lower lobe, being distal relative to the hilum, can be removed without any risk of compromising nerve supply, lymphatic drainage, or bronchial circulation to the upper lobe. Because pump perfusion is necessary to achieve flow rates such as those studied here, the choice of upper lobe perfusion permits access via the more distal left lower lobe artery, again minimizing the risk of damage to vascular, lymphatic, and nerve supply of the lobe to be studied. This mode of access also permits instant transition from natural flow to pump flow without an intervening period of no perfusion (see METHODS). The upper lobe is also much smaller, making it easier to suspend from a force transducer with its surfaces free of contact from the chest wall despite a normal end-expiratory transpulmonary pressure (2-3 cmH_2O). Admittedly,

the proximity of LUL to the mediastinum renders lobar weight more vulnerable to mediastinal movement and changes in cardiac size. Indeed, in the process of developing this technique (experiments not reported here), lobar weight was frequently erratic, displaying wide fluctuations that appeared to correlate with spontaneous changes in systemic blood pressure which are common in the anesthetized animal and are associated with alterations in cardiac size. These problems were subsequently averted by attention to details outlined in METHODS, notably animal position, method of suspension, and ensuring complete separation between the medial surface of the lobe and the mediastinum.

Withdrawal of blood from the left atrium permits an almost unlimited increase in lobar flow, independent of ventricular function, with no effect on perfusion to the right lung and only minimal changes in such variables as blood pressure, left atrial pressure, or systemic blood gas tensions that may alter the distribution of pulmonary vascular resistance (10, 15, 21). As a result, any readjustment of pulmonary vascular resistance consequent to changing flow must have its origin (passive, pharmacological, or reflex) within the perfused lobe and is not secondary to extraneous changes produced by the method used to increase flow. This degree of isolation was only possible in the past with perfusion systems that are totally independent and separate from the animal's circulation. These systems require

cannulation of the lobar veins (i.e. more surgical intervention) and do not permit the removal of blood degradation products that may otherwise accumulate and may cause vascular injury (36).

In agreement with the behavior of intact lobes and contrary to the behavior of in vitro lobes (30), our lobes did not accumulate fluid until a critical vascular pressure was reached (Figure 5, *right*). This threshold (19.7±1.50 mmHg) is comparable with that reported by Drake et al. (19.7±1.8 mmHg; *ref.* 12) using an isolated *in situ* left lower lobe preparation. Also, in keeping with responses of intact lobes (12, 30), the rate of weight gain at vascular pressures above threshold was constant. After correction for differences in lobe size, the filtration coefficient in our preparation (0.188±0.052 $g \cdot min^{-1} \cdot mmHg^{-1} \cdot 100\ g^{-1}$) was somewhat higher than the values reported by Drake et al. [mean±SE = 0.11±0.02 $g \cdot min^{-1} \cdot mmHg^{-1} \cdot 100\ g^{-1}$, (12)] and by Morriss et al. [mean±SE = 0.09±0.01, (30)]. In comparing these results we found no significant difference from the results of Drake et al. ($P>0.20$) and a marginally significant difference from the results of Morriss et al. ($P<0.05$). It is not clear whether this represents a true difference in the filtration coefficients of upper and lower lobes or is the result of differences in experimental preparation and protocol. It must be emphasized that the present experiments were not designed to obtain the filtration coefficient of the lobe. This would have required

rigorous attention to specific details with respect to pattern of increase in pressure (12). Such precautions, while providing a more accurate filtration coefficient, would have precluded the acquisition of the information we set out to obtain.

The approach we used to estimate EFP in the presence of flow is similar in principle to that used by Gabel and Drake (isofiltration technique; *ref.* 19); EFP at a given high flow is similar to the pressure that produces an equal rate of slow weight gain during very low flow. At zero flow, EFP can be determined with certainty, since the pressure throughout the vascular tree is the same. Two major assumptions underlie the validity of this approach: 1) slow weight changes are due to fluid filtration and not the result of progressive changes in intravascular volume; and 2) the relation between hydrostatic intravascular pressure and rate of weight gain is the same in the two sets of measurements (i.e. dynamic and static). Gabel and Drake (19) concluded that these factors did not influence their results. However, since our experimental approach was substantially different, these points should be re-addressed.

Changes in vascular volume. The progressive increase in lobe weight over the 3-4 min of observation may in part or in total be the result of progressive vascular dilatation in response to a step increase in pressure. Indeed, we documented a decrease in pulmonary vascular resistance over the period of observation (Figure 3). To the extent that a decrease in

resistance indicates vascular dilatation, progressive increase in vascular blood volume must have contributed to the slow weight gain. We believe, however, that this contribution was negligible for the following reasons. 1) The change in resistance beyond the 1st min (during which weight change was ignored) was minimal and amounted to ~3%. 2) The change in resistance was observed with low and high step increases in flow, whereas slow weight gain was observed only when flow exceeded a critical level. 3) In several instances we deliberately maintained high flow beyond the point at which pressure stabilized (usually 4 min). There was no measurable change in the rate of weight gain. 4) When flow was returned to *base line*, after a period of high flow, *base line* PA pressure was lower (at the same *base line* flow), reflecting the dilatation that occurred in the course of increased flow. In each case, *base line* pressure returned to control before a new high flow was instituted, thereby establishing the restoration of *base line* resistance. Lobar weight at this point was invariably higher than at *base line* before the observation that resulted in a slow weight gain, and the magnitude of increase in *base line* weight agreed very well with the amount of slow weight gain beyond the first minute. 5) The wet weight of the blood-drained lobe at the end of the experiment was substantially increased, and there was good agreement between the increase in wet weight and the cumulative increase in force transducer signal. We conclude that any

contribution vascular dilatation may have made to slow weight gain was very small in relation to total weight gain. A similar conclusion was reached by other investigators who used gravimetric techniques (19, 31). Evidently, the vascular dilatation occurring between 1 and 4 min after a step flow change is not only small but must also involve vessels that do not contribute significantly to intravascular blood volume.

Relation between intravascular pressure and rate of weight gain. As discussed by Drake and associates (12, 30) the rate of weight gain represents the balance between the rate of fluid filtration and rate of fluid removal by lymphatics and possibly by airways (in case of alveolar edema) and pleural surface. The rate of fluid filtration is in turn a function not only of intravascular pressure but also of several other factors included in the Starling equation, namely filtration coefficient (including membrane permeability), tissue hydrostatic pressure, membrane reflection coefficient to proteins, and plasma and tissue oncotic pressures. Accordingly, a similar rate of weight gain measured at two different times implies the same intravascular pressure only if it can be shown that all other factors that affect filtration and removal of fluid are the same, or, in the event of any differences, the net effect of changes in these factors is nil.

Over the long period of data collection (~4 h), and particularly with progressive edema accumulation as a result of repeated challenge with high flow or static pressures, it would be reasonable to expect that one or more of the above factors will change. It is clearly not practical to monitor all these variables throughout the experiment. To address this complication, we had initially planned to alternate dynamic and static measurements throughout the experiment on the premise that any systematic changes in the filtration or clearance factors would apply equally to both measurements. After attempting several potential approaches for reversible occlusion of the pulmonary veins in preliminary experiments, we concluded that this design was not feasible.[3]

As a compromise, static measurements were carried out after the completion of the dynamic measurements but safeguards were incorporated in the protocol. These included randomization of order of various step changes in flow or static pressures, to eliminate the possibility of systematic drifts affecting EFP estimation more with some flow values than with others, and by additional experimental steps and analyses (see METHODS and RESULTS) designed to permit detection, and correction for, any systematic trends in the relation between flow and static pressure on one hand and rate of weight gain on the other.

As indicated in RESULTS (also Figure 6), there was only a suggestion of a step increase in rate of weight gain (at a given flow) early in the course of dynamic measurements, and correcting for this small change had no material effect on the results. Otherwise, the relation between flow or pressure and rate of weight gain was stable (Figure 6). The reason for this stability is not clear. It is possible that all the relevant filtration and clearance factors remained constant. Indeed several studies (see *ref.* 35 for review) have shown that tissue pressure changes little once a critical amount of edema has accumulated. This critical amount (35) appears to be quite small in relation to the total weight accumulated by our lobes throughout the experiment. It is thus likely that this saturation point was reached very early in the experiment. It has also been shown that rate of lymph flow reaches a maximum early in the course of edema formation (11, 12). The perfusion system we used should minimize permeability changes (see above), and there was no reason for plasma oncotic pressure to change. There was little blood loss and fluid administration was minimal and likely no more than insensible losses. The experiments were terminated before any audible bubbling occurred so that losses via the airway were unlikely. Alternatively, multiple changes may have occurred which canceled each other out. Finally, it is possible that our protocol, consisting of brief periods of edema formation alternating with periods of no edema formation, may have

permitted restoration of *base line* values before initiation of a new step change in flow or pressure. Regardless of the reason, the results indicate that inferring EFP during flow from static measurements done later is valid under the conditions of our experiments.

While our lobes were technically in zone II perfusion (i.e. $P_{PA} > P_A > P_{LA}$), they were functionally in zone III. EFP, presumably reflecting pressure at or near alveolar vessels, ranged from 19.7 to 44.4 mmHg during the flow rates used (Table 1). It is difficult to envision this pressure decreasing to less than alveolar pressure (2.5 cmH_2O) as blood traverses alveolar vessels with no further change down to left atrium. It follows that pressure downstream from alveolar vessels was higher than alveolar pressure, effectively placing the lobe in perfusion zone III. This conclusion is further supported by the findings of Hyman (24) that, with comparable flow rates, pressure in medium-sized veins (2-3 mm) is substantially higher than LA pressure.

Fluid filters out of the pulmonary vessels not at a unique point but rather over a region (segment) that includes the capillaries and a variable amount of adjoining larger vessels (2, 25). To the extent that this filtration segment possesses a finite resistance, there is no unique hydrostatic intravascular pressure at the filtration site in the presence of flow. Rather, there is a gradient. Also, it would be unreasonable to expect

the distribution of resistance upstream and downstream from the filtration site to be the same in all parallel units, so that for a given set of inflow and outflow pressures mean vascular pressure at the filtration site will be different in different units. This is independent of the effect of gravity, which applies equally to static and dynamic measurements. Furthermore, the presence of a longitudinal pressure gradient along the filtration site in the dynamic but not the static state dictates that for a comparable overall filtration rate in the two states relatively more fluid filters out at the proximal end of the filtration site and less at the distal end, in the dynamic state. Distribution of tissue pressure in the two states may thus not be similar. Furthermore, factors that govern the relation between vascular pressure and edema formation (see above) may not be uniform along the entire filtration site. It follows that estimates of filtration pressure in the dynamic state, from static measurements, are necessarily functional. They simply state that, at a given flow, the pulmonary circulation behaves as if the pressure at the filtration region were uniform and of the specified magnitude. Hence our use of the term effective filtration pressure (EFP).

2. Longitudinal Distribution of Resistance During Very High Pulmonary Blood Flow

With the qualification indicated immediately above, the major finding of the present study is that as flow increases resistance upstream from the predominant filtration site decreases, whereas resistance of the downstream segment stays the same. As a result, EFP during high flow is closer to PA pressure than it is to LA pressure and becomes progressively more so as a function of flow. The lung routinely accumulates edema when lobar flow exceeds 53 ml/kg, corresponding to a cardiac output of ~430 ml/kg, even when LA pressure is normal.

The decrease in upstream resistance (R_{us}) may be apparent (i.e. no actual dilatation) or real. An apparent decrease in R_{us} may result from 1) specific effect of flow on permeability, 2) dissipation of the kinetic energy contained in inflowing blood, or 3) upstream migration of the filtration midpoint. A real decrease in R_{us} may follow 1) recruitment of parallel units, 2) active dilatation, or 3) passive dilatation.

Increased permeability. An increase in permeability should cause a faster rate of weight gain at the same vascular pressure. If permeability increased progressively with flow, EFP would be overestimated and ΔP across the upstream segment would thus be underestimated. For increased permeability to account for the measured decrease in R_{us}, the change in permeability must be

specific to flow (e.g. shearing) and not a consequence of vascular distention (under the influence of high pressures), since any effect of vascular distention on permeability applies equally to the static and dynamic measurements. Furthermore, Erdmann et al (14) found no change in filtration coefficient as a result of increasing capillary pressure. We believe that this mechanism does not contribute significantly to the observed decrease in Rus for at least two reasons. First, damage to vascular endothelium as a result of high flow should be progressive. As a result, rate of weight gain should have progressively increased as a step increase in flow was maintained. This was not observed. Second, if permeability progressively increased as a function of flow the relation between flow and $\Delta W/\Delta t$ should be convex to the flow axis or, at least , its shape should be different from the relation between static pressure and $\Delta W/\Delta t$. A relation that is convex to the flow axis was observed in only one animal (animal 7, Figure 5, *middle*), but the static relation was similar (Figure 5, *right*). In the other six animals, the relation was described well with a linear function and there was no significant difference in r values between static and dynamic measurements [r = 0.93±0.07 (SD) for dynamic measurements versus 0.90±0.08 for static measurements].

Kinetic energy. The pressure measured across a conducting system (ΔP_T) is the sum of pressure drop secondary to frictional resistance (ΔP_{FR}), which is a function of vascular dimensions and fluid properties, and the pressure gain or loss secondary to deceleration or acceleration of the fluid, respectively ($\pm\Delta P_{CA}$). The blood enters the LUL artery at high speed, and its kinetic energy is not included in the lateral pressure measured at the inflow port. Since blood slows substantially at the filtration site, this energy is converted into lateral pressure. Accordingly, measured ΔP_T underestimates ΔP_{FR}, and the magnitude of underestimation increases as a function of the square of blood velocity at the entrance to the LUL. We estimate this effect (ΔP_{CA}) to be no more than 1.0 mmHg at the highest flow in our preparation[4]. Table 1 shows that, as flow increased from 1.27 *l*/min (at $\dot{Q}_{TH}$) to 2.97 *l*/min (at $\dot{Q}_{HI}$), ΔP across the upstream segment decreased 2.0 mmHg instead of the expected increase of 14.3 mmHg had resistance remained the same. The pressure deficit is, accordingly, 16.3 mmHg. It is evident that blood deceleration can account for only a small fraction of the measured decrease in R_{US}.

The conclusion that deceleration had little to do with the measured reduction in R_{US} applies only to this preparation. The low estimate of ΔP_{CA} results from the fact that lateral PA pressure was measured at a location (left main PA) that is much larger than the artery supplying LUL. A flow of 3.0 *l*/min, while

very large in relation to LUL, is relatively small in relation to left main PA, which is designed to handle three to four times the flow to the LUL. If the entire left lung were perfused at the same relative flow (i.e. ~10 *l*/min), ΔP_{CA} would have been much higher (~10-15 mmHg), and measured R_{US} would have decreased even more as a function of flow. Since ΔP_{US} at the highest flow was only 8.7 mmHg (Table 1), it is quite possible that at these high flow rates (in the natural state) EFP could be the same or even higher than lateral PA pressure (i.e. negative R_{US}).

Upstream migration of filtration midpoint. As indicated earlier, there is evidence that extra-alveolar vessels (arteries and veins) participate in fluid filtration (2, 25). Because as flow increases arterial pressure rises more than venous pressure (as dictated by the presence of an inflow to outflow pressure gradient), it is possible that precapillary vessels contribute relatively more to filtration at the higher flow rates. The filtration midpoint would thus move upstream as flow increased, and calculated upstream resistance would decrease simply because that segment covered by the midpoint migration is no longer part of the calculated upstream resistance. We do not believe this mechanism could account for any more than a small fraction of the observed decrease in R_{US}. First, to the extent that venous pressures also increase substantially as a function of flow (24), the contribution of postcapillary vessels to filtration must also increase thereby offsetting (at least partly) the increased

contribution of precapillary vessels and restraining upstream migration of the midpoint. Second, as shown in Table 1, R_{US} at the highest flow decreased to approximately one-third of its value at $\dot{Q}_{TH}$. If that were primarily the result of migration of the filtration midpoint, the latter must have migrated upstream of the major arterial resistance sites during the highest flow. This would place the predominant site of fluid filtration in thick-walled arteries, a most improbable development.

Recruitment of parallel units. For recruitment of new units to explain the decrease in R_{US} between $\dot{Q}_{TH}$ and $\dot{Q}_{HI}$ (Table 1), some units must have been closed at $\dot{Q}_{TH}$ and opened subsequently. PA pressure at $\dot{Q}_{TH}$ was 30.4 mmHg (Table 1), and the vertical distance between PA catheter and the most independent lobe region was ~12 cm (8.8 mmHg). Since airway pressure was 2.5 cmH_2O, if units were closed at $\dot{Q}_{TH}$, then closure was maintained by active smooth muscle tone that can withstand a distending pressure of at least 25 mmHg. This proposition is untenable, particularly in an animal preparation that displays little evidence of active tone (see *ref.* 15 and 21). Furthermore, recruitment of parallel units should decrease downstream as well as upstream resistance. This was not the case.

Active dilatation. For active dilatation to effect a substantial decrease in resistance, there must be a substantial pre-existing tone. This is not the case (15, 21). Active dilatation may have contributed to the gradual decrease in

resistance in the course of sustained flow. However, as indicated in RESULTS (also Figure 4), the total decrease in resistance was very small and can readily be accounted for on the basis of stress relaxation (17).

Passive dilatation. The major contributors to R_{US} are undoubtedly the arteries, and arteries distend under pressure. Arterial distensibility varies from 1 to 4% of circumference per millimeter of mercury depending on size (17, 27, 33). As flow increased from $\dot{Q}_{TH}$ to $\dot{Q}_{HI}$, the pressure at both ends of the upstream segment (i.e. P_{PA} and EFP) increased approximately to the same extent (~20 mmHg). It follows that arteries of all sizes were subjected to nearly the same increase in pressure. A decrease in resistance from 8.3 to 2.9 mmHg·l^{-1}·min (i.e. a 65% decrease, Table 1) would result from a 30% increase in radius (or circumference), or 1.5% per mmHg. As indicated above, this is well within the documented distensibility of pulmonary arteries. This mechanism (passive dilatation) would also explain failure of downstream resistance to decrease despite the pronounced decrease in R_{US}. The upstream segment is necessarily subjected to a larger increase in distending pressure. Furthermore, unlike arteries, the distensibility of veins decreases markedly once their distending pressure reaches a modest value of 7-8 mmHg (27). This pressure was most likely reached well below $\dot{Q}_{TH}$.

We conclude that the progressive decrease in R_{Us}, and hence the closer proximity of EFP to PA pressure, with progressive increases in flow is largely the result of passive dilatation of arteries.

3. Relation to Previous Work

Several previous investigators measured the fraction of total resistance offered by vessels downstream from the filtration site (R_{Ds}/PVR) at normal or near normal blood flow (1, 18, 19, 32). Two of these studies employed gravimetric techniques (18, 19). Gaar et al. (18) used an isogravimetric technique in an in vitro lobe preparation and found the downstream contribution to be 44%. Gabel and Drake (19) used an isofiltration technique in an intact left lower lobe preparation in which flow was increased by constricting the right pulmonary artery. While flow was not measured, we estimate it was about twice the normal blood flow to the LLL.[5] At this flow R_{Ds} was ~50% of total. Our results, extrapolated to the corresponding flow rates, indicate that R_{Ds} should contribute 45 and 50%, respectively (Figure 8, *bottom*). There is, accordingly, excellent agreement among all studies that utilized gravimetric techniques and these results indicate a progressive increase in R_{Ds}/PVR with flow, up to a fraction of 83% at the highest physiologically relevant rate. Agostoni and Piiper (1) estimated filtration pressure in subpleural capillaries using an osmometer

and found a slightly higher downstream fraction (60%) at a fairly low flow. It is not clear whether subpleural vessels are representative of parenchymal vessels. Furthermore, the total PVR of their preparation was abnormally high (arteriovenous pressure difference was 11.6 mmHg at a flow rate of 0.14 *l*/min). Parker et al. (32) estimated capillary pressure from the change in alveolar pressure of fluid-filled lung segments. They found that downstream resistance accounted for 40% of total resistance.

The longitudinal distribution of PVR was examined in numerous other studies. With the exception of one (24), these will not be discussed since flow rates used were low and partitioning was not in relation to fluid filtration site (for review see *ref.* 10 and 15). Hyman (24) pump perfused left lung segments of various sizes in intact (close-chested) dogs in whom the left PA was cannulated with a tube introduced via the atrial septum. Measurements were made over a very wide flow range extending to 540% of normal blood flow. The relation between flow and PA pressure observed in our lobe is similar to that found by Hyman (24) and others (16) after allowing for differences in size of perfused segments. Hyman also measured the pressure in 2 to 3 mm veins by use of a 0.9 mm catheter introduced retrogradely via LA. He found that the resistance downstream from this site accounted for ~43% of total resistance. Furthermore, this value was independent of flow at flow rates in excess of normal (Table 1, *ref.* 24). We found that R_{Ds} (relative

to the filtration site) accounts for 61% of PVR at four times normal blood flow ($\dot{Q}_{TH}$) and this contribution increased to 83% at the highest flow (Table 1). Hyman's data would suggest that the major part of our R_{Ds} at $\dot{Q}_{TH}$ (43/61 = 0.7) is contained in large veins and that the increase in R_{Ds}/PVR with flow is primarily the result of increasing contribution from vessels between the filtration site and 2 to 3 mm veins.

4. Relevance to Natural High Flow States

The cardiac output in exercising dogs has been documented to increase up to 800 ml/kg (4). Since the highest exercise in the latter study was not exhausting (4), it is possible that cardiac output increases to even higher levels. The flow range of our observations (corresponding to an output range of 400-1,000 ml/kg, Figure 8) is, accordingly, easily reached during exercise in dogs. The pressure-flow relation in our preparation is also similar to that found in exercising dogs; at a cardiac output of ~300 ml/kg, PA pressure was 25±1 mmHg (26) or 28 (range 20.4-34.6) (13) during exercise, and LA pressure was 2.0 and 3.8 mmHg, respectively. At a comparable flow rate, the PA and LA pressures in our lobes were 24 and 2.5 mmHg, respectively (Figure 8). Pulmonary vascular pressures at higher levels of exercise in dogs are not available. Nonetheless, in view of the similarity in the pressure-flow relation between our preparation and the exercising dog at a flow rate of 300 ml/kg and the

probability that the relation in both cases reflects the response of a passive pulmonary vasculature, it is very likely that the pressure-flow relation at higher levels of exercise will be similar to that found in our preparation.

Our results therefore indicate that, unless other factors operate to reduce the resistance downstream from the filtration site, filtration pressure will exceed threshold for edema formation during heavy exercise. To the extent that vascular smooth muscle tone is normally minimal (15, 21),, it is difficult to see how a reduction in R_{Ds} can be effected by neurally or humorally mediated active dilatation during exercise. Left atrial pressure increases during exercise (22), and this may reduce venous resistance (34). While this may decrease the pressure difference between filtration site and LA, it is not reasonable to expect this decrease to completely offset the increase in LA pressure (so that EFP actually falls) in a fully recruited circulation. Ventilation is markedly increased during heavy exercise and changes in lung volume have complex effects on vascular resistance (for review see *ref.* 5, 10, and 15). The effect of increases in ventilation on EFP during high flow needs to be investigated.

It is also likely that our conclusions apply to exercise in humans as well. As in the dog, the maximum cardiac output in healthy young men is five to eight times the resting value (3), and the overall pressure-flow relation is also similar; at 3.5

times the resting cardiac output (results for maximal exercise also not available), PA pressure is, on average, 29±8 (SD) mmHg (9). At the equivalent flow, PA pressure in our preparation was 27 mmHg (Figure 8, *top*).

Several investigators have documented an increase in extravascular water [by indicator-dilution techniques (20, 29)] or in lung lymph flow (6) during even modest exercise. These findings do not establish water accumulation in the lung, since the techniques used are susceptible to vascular recruitment. On the other hand, Marshall et al. (28) failed to document an increase in lung wet-to-dry weight ratio at the end of exercise in dogs. This negative evidence, however, is not conclusive since no hemodynamic measurements were made (i.e. cardiac output is not known), dogs exercised at a pre set level that was probably far from the dog's maximum ability (as judged from the dog's performance in other studies), and the number of dogs studied (four) was too small in relation to the variability of the wet weight-to-dry weight ratio.

Younes et al. (37, 38) have recently reported that some normal subjects develop relative tachypnea, occasionally severe [e.g. (38)], after maximal exercise. By a process of elimination, they suggested that this may be due to development of mild interstitial edema at very heavy work rates. The present results are consistent with, and lend some support to, this view.

Patients with high permeability pulmonary edema (adult respiratory disease syndrome), particularly those with associated sepsis, often display an elevated cardiac output, sometimes in excess of three times normal (23). It is generally believed that this is beneficial in that it promotes a higher O_2 delivery. Indeed it has been shown that further increases in cardiac output, by short term fluid challenge, do increase O_2 consumption in some patients (23). We have documented the presence of a large pressure gradient between EFP and LA pressure in the presence of high flow. Accordingly, any advantage an elevated cardiac output (spontaneous or induced) may have on O_2 delivery is obtained at the cost of promoting more edema, and possibly worse O_2 delivery, in the long run.

G. FOOTNOTES

Footnote 1.

No more than half of the total weight gain limit (i.e. 30 g) could be allowed during the dynamic measurements to permit a comparable number of static observations to be made later.

Footnote 2.

In a truly static blood column, progressive loss of low protein filtrate should result in progressive increase in intravascular oncotic pressure, thereby counteracting further fluid movement. We had initially intended to establish a small venous leak to ensure renewal of blood at the filtration site. In preliminary experiments, however, we noted no change in rate of weight gain as a step increase in static pressure was maintained. Two factors account for this stability in our preparation. First, lung expansion compresses alveolar vessels and distends extra-alveolar vessels (5, 10, 15). The periodic respiratory movements therefore cause mixing of blood in capillaries with that in neighboring vessels. Second, we found that when the LLL cannula was clamped (in the course of a static measurement) so that the reservoir is disconnected, there was a progressive increase in vascular pressure and lobar weight, signifying an increase in lobar blood volume. This blood could

only come from connections with the bronchial circulation, since left PA pressure was higher than both LA and right PA pressures. Since bronchial vessels communicate with pulmonary vessels at the level of pulmonary veins or capillaries (8), this retrograde flow ensures continuous renewal of blood at the filtration site. With the reservoir connected, however, this retrograde flow does not cause an appreciable change in pressure on account of the reservoir's large area.

Footnote 3.

We attempted several approaches to effect reversible occlusion of lobar veins. These included passage of balloon-tipped catheters via the LA [these have to be sutured to vein wall to prevent their extrusion (19)], or directly through vein wall, as well as placement of the pulmonary vein snares before initiation of dynamic data collection. We found that manipulation of vein wall very frequently results in a largely irreversible change in the pressure-flow relation, signifying an increase in pulmonary venous resistance. This would, of course, defeat the purpose of the experiment.

Footnote 4.

The pressure change (ΔP_{CA}) that results from a change in velocity (V) can be calculated from (5)

$$\Delta P = 0.5 \cdot \Gamma(V_1 - V_2)/133.3$$

where Γ is density (kg/m^3) and 133.3 is the constant to convert newton per square meter (i.e., pascal) to mmHg. At a flow rate of 3.0 *l*/min and a cross -sectional area (where the left PA catheter is located) of 1 cm^2, (based on an estimated diameter of 11 mm), velocity at the site of the catheter (left main PA at exit of LUL artery) is 0.5 m/s. If blood slows down to a standstill (i.e., $V_2 = 0$), lateral pressure will increase by ~1 mmHg.

Footnote 5.

LLL normally receives one-third of cardiac output (7). Gable and Drake (19) increased LLL flow by partially constricting right main PA. With complete occlusion LLL flow should increase no more than threefold. Since only partial constriction was used, and cardiac output decreases as PVR increases, LLL flow must have been less than three times normal. The PA-LA pressure difference in their preparation was, on average, 14.4 mmHg, which corresponds to a flow of ~200 $ml \cdot kg^{-1} \cdot min^{-1}$ (see Fig. 8).

H. REFERENCES

1. Agostoni, E., and J. Piper. Capillary pressure and distribution of vascular resistance in isolated lung. *Am. J. Physiol.* 202:1033-1036, 1962.
2. Albert, R.K., S. Lakshminarayan, N.B. Charon, W. Kirk, and J. Butler. Extra-alveolar vessel contribution to hydrostatic pulmonary edema in *in situ* dog lungs. *J. Appl. Physiol.* 54:1010-1017, 1983.
3. Asmussen, E. Muscular exercise. In: *Handbook of Physiology. Respiration.* Washington, DC:Am. Physiol. Soc., 1965, sect. 3, vol. II, chapt. 36, p. 939-978.
4. Bailie, M.D., S. Robinson, H.H. Rostorfer, and J.L. Newton. Effects of exercise on heart output of the dog. *J. Appl. Physiol.* 16:107-111, 1961.
5. Caro, C.G., T.J. Pedley, R.C. Schroter, and W.A. Seed. *The Mechanics of the Circulation.* New York: Oxford Univ. Press, 1978.
6. Coates, G., H. O'Brodovich, and A.L. Jefferies. The effect of exercise on lung fluid and protein exchange in sheep (Abstract). *Am. Rev. Respir. Dis.* 127:305, 1983.
7. Craven, K.D., L. Oppenheimer, and L.D.H. Wood. Effects of contusion and flail chest on pulmonary perfusion and oxygen exchange. *J. Appl. Physiol.* 47:729-737, 1979.

8. Cudkowicz, L. Bronchial arterial circulation in man: normal anatomy and responses to disease. In: *Pulmonary Vascular Diseases*, edited by K.M. Moser. New York: Dekker, 1979, chapt. 2, p. 111-232 (Lung Biol. Health Dis. Ser.)

9. Damato, A.N., J.G. Galante, and W.M. Smith. Hemodynamic response to treadmill exercise in normal subjects. *J. Appl. Physiol.* 21:959-966, 1966.

10. Dawson, C. Role of pulmonary vasomotion in physiology of the lung. *Physiol. Rev.* 64:544-616, 1984.

11. Drake, R., K.A. Gaar, and A.E. Taylor. Estimation of the filtration coefficient of pulmonary exchange vessels. *Am. J. Physiol.* 234 (*Heart Circ. Physiol. 3)*: H266-H274, 1978.

12. Drake, R.E., J.H. Smith, and J.C. Gabel. Estimation of the filtration coefficient in intact dog lung. *Am. J. Physiol.* 238 *(Heart Circ. Physiol. 7)*:H430-H438, 1980.

13. Elkins, R.C., and W.R. Milnor. Pulmonary vascular response to exercise in the dog. *Circ. Res.* 29:591-599, 1971.

14. Erdmann, A.J., T.R. Vaughan, K.L. Brigham, W.C. Woolverton, and N.C. Staub. Effects of increased vascular pressure on lung fluid balance in unanesthetized sheep. *Circ. Res.* 37:271-284, 1975.

15. Fishman, A.P. Pulmonary circulation. In: *Handbook of Physiology. The Respiratory System. Circulation and Nonrespiratory Functions.* Bethesda, MD: Am. Physiol. Soc., 1985, sect. 3, vol. I, chapt. 3, p. 93-166.

16. Fowler, N.O., and J.C. Holmes. Pulmonary arterial pressures of high pulmonary flow. *J. Clin. Invest.* 4:2040-2050, 1965.

17. Frasher, W.G., Jr., and S.S. Sobin. Pressure-volume response of isolated living main pulmonary artery in dogs. *J. Appl. Physiol.* 20:675-682, 1965.

18. Gaar, K.A., Jr., A.E. Taylor, L.J. Owens, and A.C. Guyton. Pulmonary capillary pressure and filtration coefficient in the isolated perfused lung. *Am. J. Physiol.* 213:910-914, 1967.

19. Gabel, J.C., and R.E. Drake. Pulmonary capillary pressure in intact dog lungs. *Am. J. Physiol.* 235 (*Heart Circ. Physiol. 4*):H569-H573, 1978.

20. Goresky, C.A., R.F.P. Cronin, and B.E. Wangel. Indicator dilution measurements of extravascular water in the lungs. *J. Clin. Invest* 48:487-501, 1969.

21. Grover, R.F., W.W. Wagner, Jr., I.F. McMurty, and J.T. Reeves. Pulmonary circulation. In: *Handbook of Physiology. The Circulatory System. Peripheral Circulation and Organ Blood Flow.* Bethesda, MD: Am. Physiol. Soc., 1984, sect. 2., vol. III, chapt. 4, p. 103-136.

22. Gurtner, H.P., P. Walser, and B. Fassler. Normal values for pulmonary hemodynamics at rest and during exercise in man. *Prog. Respir. Res.* 9:295-315, 1975.

23. Haupt, M.T., E.M. Gilbert, and R.W. Carlson. Fluid loading increases oxygen consumption in septic patients with lactic acidosis. *Am. Rev. Respir. Dis.* 131:912-916, 1985.

24. Hyman, A.L. Effects of large increases in pulmonary blood flow on pulmonary venous pressure. *J. Appl. Physiol.* 27:179-185, 1969.

25. Iliff, L.D. Extra-alveolar vessels and edema development in excised dog lungs. *Circ. Res.* 28:524-532, 1971.

26. Lindenfeld, J., J.T. Reeves, and L.D. Horwitz. Low exercise pulmonary resistance is not dependent on vasodilator prostaglandins. *J. Appl. Physiol.* 55:558-561, 1983.

27. Maloney, J.E., S.A. Rooholamini, and L. Wexler. Pressure-diameter relations of small blood vessels in isolated dog lung. *Microvasc. Res.* 2:1-12, 1970.

28. Marshall, B.E., L.R. Soma, and G.R. Neufeld. Lung water volume at rest and exercise in dogs. *J. Appl. Physiol.* 39:7-8, 1975.

29. Marshall, B.E., R.L. Teichner, T. Kallos, H.J. Sugerman, M.Q. Wyche, and K.R. Tantum. Effects of posture and exercise on the pulmonary extravascular water volume in man. *J. Appl. Physiol.* 31:375-379, 1971.

30. Morriss, A.W., R.E. Drake, and J.C. Gabel. Comparison of microvascular filtration characteristics in isolated and intact lungs. *J. Appl. Physiol.* 48:438-443, 1980.

31. Oppenheimer, L., W.H. Unruh, C. Skoog, and H.S. Goldberg. Transvascular fluid flux measured from intravascular water concentration changes. *J. Appl. Physiol.* 54:64-72, 1983.

32. Parker, J.C., A.C. Guyton, and A.E. Taylor. Pulmonary interstitial and capillary pressures estimated from intra-alveolar fluid pressures. *J. Appl. Physiol.* 44:267-276, 1978.

33. Patel, J., F.M. De Freitas, and A.J. Mallos. Mechanical function of the main pulmonary artery. *J. Appl. Physiol.* 17:205-208, 1962.

34. Takahashi, S., and J. Butler. A vascular waterfall in extra-alveolar vessels of the excised dog lung. *J. Appl. Physiol.* 26:578-584, 1969.

35. Taylor, A.E., and J.C. Parker. Pulmonary interstitial spaces and lymphatics. In: *Handbook of Physiology. The Respiratory System. Circulation and Nonrespiratory Functions.* Bethesda, MD: Am. Physiol. Soc., 1985, sect. 3, vol. I, chapt. 4, p. 16-230.

36. Townsend, E.R., J. Duffin, M. Ali, J.W.D. McDonald, J.J. Thiesson, J. Masterson, P. Klement, and J.D. Cooper. Preservation of platelets during extracorporeal circulation in sheep. *Circ. Res.* 49:452-457, 1981.

37. Younes, M., and J. Burks. Breathing pattern during and after exercise of different intensities. *J. Appl. Physiol.* 59:898-908, 1985.

38. Younes, M., and G. Kivinen. Respiratory mechanics and breathing pattern during and following maximal exercise. *J. Appl. Physiol.* 57:1773-1782, 1984.

III. CHAPTER 2

EFFECT OF TIDAL VOLUME AND PEEP ON RATE OF EDEMA FORMATION IN IN SITU PERFUSED CANINE LOBES

A. BACKGROUND

The effect of lung volume on fluid dynamics has been a subject of considerable interest over the past few decades (e.g., *ref.* 4, 5, 9, 12, 13, 15, 19, 30). It has become clear that lung volume effects are complex and involve almost all factors that govern fluid filtration and removal. It is well known that changes in mean (i.e. operating) lung volume alter both extravascular and intravascular pressures (and, hence, the net hydrostatic filtration gradient) because of mechanical interdependence between vascular walls and lung parenchyma (16, 27; for review see *ref.* 8, 24, 26, 28). Furthermore, it has been recently shown that permeability of both alveolar epithelium (11) and microvascular endothelium (22) increase with lung inflation.

The main function of the lung is to exchange gases between blood and atmosphere brought about by <u>oscillatory</u> changes in lung volume. Studies, so far, have been primarily concerned with the effects of sustained elevation in lung volume produced either by positive end-expiratory pressure (PEEP) or by continuous lung inflation. As opposed to the extensive literature on the effects of sustained changes in lung volume on pulmonary fluid dynamics, there is little information about the effects of changing V_T.

B. HYPOTHESIS

Changes in V_T can influence filtration because of the associated changes in operating lung volume. However, there are reasons to believe that changes in V_T may have effects on filtration that are independent of those related to changes in operating lung volume. Although oscillating around a similar mean alveolar pressure (P_{a1}), a major difference between large V_T and PEEP is that large V_T is associated with a higher P_{a1} during one part of the respiratory cycle (inspiration) and a lower P_{a1} during another (expiration). The relation between lung volume and each of the filtration and clearance factors has not been established. If it were linear, then any extra effect accrued when P_{a1} is higher would be offset by opposite effects when P_{a1} is lower, and there should be no net difference in rate of edema formation between large V_T and PEEP.

C. METHODS

Preparation similar to that described in CHAPTER 1.

D. PROTOCOL

Twelve dogs were used in this study. The LUL was ventilated, on a randomized basis, with two different tidal volumes (V_1 and V_2), generating static end-inspiratory airway pressures (EIP) of 7.5 and 17.5 cmH_2O, respectively, with a *base*

line end-expiratory pressure (EEP) of 2.5 cmH_2O. At each level of V_T, edema was induced dynamically as described in CHAPTER 1. A minimum of 2 observations at each of two different flow rates was made at each level of V_T.

In 6 dogs, at the end of the dynamic measurements, edema was induced statically (as described in CHAPTER 1). Static measurements were obtained at levels of V_T equivalent to those used in the dynamic measurements (i.e. EIP of 7.5 and 17.5 cmH_2O). Four to eight different pulmonary vascular pressures were selected at each level of ventilation.

In the other 6 dogs, rate of edema formation was measured in a third condition (V_3) in which V_T was similar to V_1 but PEEP level was increased so that mean airway pressure was approximately the same as in V_2 conditions. Chart speed was increased to 25 mm/sec towards the end of each 4 min period of high flow, and the inflow tubing to the LUL was occluded for 1-2 seconds. During this period pump flow was temporarily diverted to a reservoir. Occlusions were carried out near end-inspiration and near end-expiration. In this group of dogs, only dynamic measurements (i.e. in the presence of high blood flow) were obtained as the total weight gain during the 3 sets of dynamic measurements precluded reliable static measurements. In this series V_1 was tested first but the order of testing V_2 and V_3 was randomized.

In the first group of 6 dogs effective filtration pressure (EFP), at the various levels of ventilation and flow rates was estimated using the gravimetric technique described in CHAPTER 1.

Estimation of middle compartment pressure (P_M). In the second group of 6 dogs, filtration pressure in the dynamic state was estimated using the arterial occlusion technique as static measurements were not available. Following occlusion, PA pressure drops rapidly, followed by a slow decline in pressure that plateaus. The plateau level approximates either LA pressure or alveolar pressure (whichever is higher). The best fit exponential curve for the slow phase, sampled at 50 Hz, was obtained according to the following equation:

$$Y = A \cdot e^{-BX} + C$$

where Y and X are PA pressure and time, respectively; "A" is a constant; "B" is the reciprocal of the time constant; and "C is the asymptote pressure value. "C" was obtained directly by using the lowest flat portion of the curve. P_M, pressure in the compliant middle compartment, at the time of occlusion (t=0) was taken as the sum of "A" and "C". A more elaborate description of this technique and justification for its use under very high flow conditions is provided in CHAPTER 4.

E. RESULTS

Measured and calculated data, obtained in 12 dogs, comparing rate of edema formation with smaller tidal volumes (V_1) versus larger tidal volumes (V_2) are summarized in Table 1. Blood flow to the LUL (mean±SD) was 2.32±0.99 *l*/min. Inflow pressure to the LUL was slightly affected by ventilation. Oscillations in inflow pressure ranged between 2 and 6 mmHg from end-inspiration to end-expiration. Mean inflow pressure to the LUL (LPAP) with smaller tidal volumes was not different from that with larger tidal volumes (42.3 in both cases). Pressure at the filtration site (EFP) estimated by the isofiltration technique in the first 6 dogs and by the occlusion technique in dogs 7 to 12 was also not different (31.4±7.6 vs. 31.3±7.1, respectively). Despite equivalent filtration pressures, rate of edema formation ($\Delta W/\Delta t$) with larger tidal volumes was significantly ($P<0.001$) higher than that obtained with smaller tidal volumes (0.73±0.29 g/min versus 0.58±0.30 g/min, respectively).

TABLE 1. *Vascular pressures and rate of weight gain with small and large tidal volumes*

Dog No.	Wt, kg	Flow, l/min	V_1				V_2			
			LPAP, mmHg	EFP, mmHg	LAP, mmHg	$\Delta W/\Delta t$, g/min	LPAP, mmHg	EFP, mmHg	LAP, mmHg	$\Delta W/\Delta t$, g/min
1	19.0	2.10	45.0	27.5	0.0	0.13	46.0	33.8	0.0	0.24
		2.40	50.0	27.5	0.0	0.13	51.5	33.8	0.0	0.24
2	37.0	3.50	35.5	28.5	7.0	0.60	38.5	28.5	7.0	0.77
		4.00	39.5	31.3	7.0	0.73	42.5	31.4	7.0	0.97
3	25.0	3.00	42.0	33.3	1.5	0.40	42.5	33.3	1.5	0.50
		3.50	47.0	41.8	1.5	0.63	47.5	40.3	1.5	0.75
4	32.0	3.50	32.0	25.5	3.3	0.48	32.5	25.5	3.3	0.56
		4.00	34.0	29.3	3.3	0.58	35.0	30.0	3.5	0.75
5	23.0	3.00	50.5	36.0	0.0	0.42	53.3	34.3	0.0	0.62
		3.50	60.5	52.0	0.0	0.72	61.0	48.3	0.0	1.02
6	20.0	2.50	46.0	42.1	3.0	0.76	45.0	39.5	2.3	0.83
		3.00	49.0	48.0	3.0	0.96	50.0	49.0	1.8	1.17
7	23.0	1.25	40.0	31.7	3.9	0.75	40.5	29.5	8.0	0.75
		1.50	45.5	31.1	3.5	0.88	43.0	32.7	6.5	0.88
8	19.0	1.00	46.0	28.2	6.0	1.00	40.0	25.3	7.0	1.13
		1.25	52.0	29.5	5.9	1.30	50.0	28.6	6.7	1.38
9	21.0	1.50	32.5	25.9	1.0	0.25	35.5	28.1	1.2	0.54
		1.75	36.5	28.5	1.1	0.75	40.0	30.1	0.8	1.00
10	26.0	1.00	30.0	22.5	0.6	0.13	34.0	21.5	0.0	0.38
		1.50	39.0	26.9	0.5	0.38	43.0	26.8	0.0	0.75
11	19.5	1.50	38.5	21.6	3.3	0.50	38.0	24.3	0.5	0.50
		2.00	47.5	28.1	2.8	0.75	46.5	26.6	0.6	0.75
12	22.5	1.50	36.0	26.8	3.6	0.25	27.0	22.5	1.8	0.38
		2.00	40.0	28.9	4.1	0.50	33.0	26.3	2.1	0.63
Mean ± SD	23.9 ±5.5	2.32 ±0.99	42.3 ±7.4	31.4 ±7.6	2.7 ±2.2	0.58 ±0.30	42.3 ±7.7	31.3 ±7.1	2.6 ±2.8	0.73* ±0.29

V_1, small tidal volumes {end-expiratory pressure (EEP) = 2.5 cmH_2O; end-inspiratory pressure (EIP) = 7.5 cmH_2O]; V_2, large tidal volumes (EEP = 2.5 cmH_2O; EIP = 17.5 cmH_2O); LPAP, inflow pressure to the left upper lobe; EFP, effective filtration pressure; LAP, left atrial pressure; $\Delta W/\Delta t$, rate of edema formation. * Significantly different from V_1 ($P < 0.001$) by two-way analysis of variance for repeated measures. No significant difference in other parameters.

TABLE 2. *Pressure intercepts and slopes of the relation between static vascular pressure and rate of edema formation with small and large tidal volumes*

Dog No.	V_1			V_2		
	I, mmHg	S, $g \cdot min^{-1} \cdot mmHg^{-1} \cdot 100\ g^{-1}$	r	I, mmHg	S, $g \cdot min^{-1} \cdot mmHg^{-1} \cdot 100\ g^{-1}$	r
1	20.5	0.072	0.99	20.6	0.078	1.00
2	15.1	0.091	0.95	17.5	0.141	0.99
3	18.0	0.078	0.98	19.2	0.106	0.99
4	8.4	0.064	0.98	10.2	0.087	0.99
5	13.4	0.061	0.99	12.6	0.092	0.98
6	18.7	0.120	0.98	16.6	0.133	0.99
Mean ±SE	15.7±1.8	0.081±0.009		16.1±1.6	0.106±0.010*	

Pressure intercepts (I = P_{crit}) and slopes (S) [normalized to 100 g wet wt of a normal left upper lobe estimated from the dog's body weight (7)] of linear regressions of the relation between static and vascular pressure and rate of edema formation. V_1, small tidal volumes; V_2, large tidal volumes; r, correlation coefficient. * Significantly different from V_1 ($P < 0.01$) by pared t test. Intercepts not significantly different.

TABLE 3. *Airway pressures, vascular pressures, and rate of edema formation with small tidal volumes, large tidal volumes, and small tidal volumes plus PEEP*

Dog No.	V_1					V_2					V_3				
	$\bar{P}aw$, cmH_2O	LPAP, mmHg	EFP, mmHg	LAP, mmHg	$\Delta W/\Delta t$, g/min	$\bar{P}aw$, cmH_2O	LPAP, mmHg	EFP, mmHg	LAP, mmHg	$\Delta W/\Delta t$, g/min	$\bar{P}aw$, cmH_2O	LPAP, mmHg	EFP, mmHg	LAP, mmHg	$\Delta W/\Delta t$, g/min
7	4.6	40.0	31.7	3.9	0.75	7.5	40.5	29.5	8.0	0.75	6.9	39.0	29.7	5.3	0.25
	4.8	45.5	31.1	3.5	0.88	7.7	43.0	32.7	6.5	0.88	7.1	45.0	32.2	5.0	0.50
8	4.0	46.0	28.2	6.0	1.00	7.1	40.0	25.3	7.0	1.13	6.6	45.0	29.1	7.3	0.75
	4.2	52.0	29.5	5.9	1.30	7.3	50.0	28.6	6.7	1.38	6.8	53.0	30.8	7.5	1.50
9	5.3	32.5	25.9	1.0	0.25	7.6	35.5	28.1	1.2	0.54	6.3	36.0	—	0.8	0.25
	5.5	36.5	28.5	1.1	0.75	7.8	40.0	30.1	0.8	1.00	6.5	39.0	—	1.0	0.50
10	4.0	30.0	22.8	0.6	0.13	7.0	34.0	21.5	0.0	0.38	7.1	32.5	21.7	0.0	0.13
	4.2	39.0	26.9	0.5	0.38	7.2	43.0	26.8	0.0	0.75	7.3	41.0	27.0	0.0	0.38
11	4.5	38.5	21.6	3.3	0.50	7.5	38.0	24.3	0.5	0.50	6.5	40.5	26.2	0.0	0.50
	4.7	47.5	28.1	2.8	0.75	7.7	46.5	26.6	0.6	0.75	6.7	48.5	31.0	0.0	0.75
12	5.0	36.0	26.8	3.6	0.25	7.5	27.0	22.5	1.8	0.38	7.7	30.0	23.9	0.3	0.13
	5.2	40.0	28.9	4.1	0.50	7.7	33.0	26.3	2.1	0.63	7.9	40.0	30.3	0.5	0.38
Mean ±SD	4.7 ±0.5	40.3 ±6.4	27.5 ±3.0	3.0 ±1.9	0.62 ±0.35	7.5† ±0.3	39.2 ±6.3	26.9 ±3.2	2.9 ±3.1	0.76* ±0.30	7.0† ±0.5	40.8 ±6.5	28.2 ±3.4	2.3 ±3.0	0.50 ±0.38

V_3, small tidal volume plus positive end-expiratory pressure (EEP = 5.0 cmH_2O; EIP, 11.0 cmH_2O); P_{aw}, mean airway pressure; EFP, effective filtration pressure. For definitions of other abbreviations, see Table 1 legend. * Significantly higher than $\Delta W/\Delta t$ with V_3 ($P < 0.005$) by two-way analysis of variance (ANOVA) for repeated measures. Significantly higher than P_{aw} in V_1 ($P < 0.001$) by two-way ANOVA for repeated measures. No significant difference between V_2 and V_3.

Table 2 shows results of the static measurements which were used to estimate the filtration pressure in the dynamic state in dogs 1 to 6. An excellent linear correlation ($r \geq 0.95$) was obtained between static vascular pressures and $\Delta W/\Delta t$ in each dog under the two V_T conditions. With smaller tidal volumes (V_1), the pressure intercept (P_{crit}) averaged (mean±SE) 15.7±1.8 mmHg and the slope (S) 0.081±0.009 $g \cdot min^{-1} \cdot mmHg^{-1} \cdot 100g^{-1}$. This latter value is comparable to previously reported values in intact lobes (e.g. 20). The slope was higher in all dogs during ventilation with larger tidal volumes (V_2), the average being 131% (0.106±0.010) of the smaller tidal volumes ($P<0.01$). The intercepts were not different.

As mentioned in METHODS, in dogs 7 to 12, $\Delta W/\Delta t$ was measured in a third situation (V_3) in which mean airway pressure (P_{aw}) was increased by introducing additional EEP to the *base line* EEP of 2.5 cmH_2O. A summary of the measured and calculated results under the three different forms of ventilation is shown in Table 3. Comparison between the three conditions was done using analysis of variance for repeated measures. Tukey's test was used to identify the groups that were significantly different. In the third condition substitution for the two missing data was undertaken and the total degrees of freedom were reduced by 2. Despite slightly lower (not significant statistically) filtration pressures (EFP) under V_2 conditions as compared to V_3, $\Delta W/\Delta t$ under V_2 was significantly higher ($P<0.005$). Although the

difference between V_1 and V_3 failed to exceed the significance level (P=0.20) a trend towards a lower $\Delta W/\Delta t$ using higher EEP was evident.

F. DISCUSSION

In CHAPTER 1 we have shown that the fraction of total pulmonary vascular resistance (PVR) contributed by vessels downstream (DS) from the filtration site (i.e. R_{DS}/PVR) increases progressively with increasing pulmonary blood flow. At 4 and 8 times normal blood flow the fractions are 60% and 80%, respectively. As a result, the lung routinely accumulates water at flow rates in excess of four times normal despite low (2-5 mmHg) outflow pressures. Some factor must surely operate to prevent the lung from developing pulmonary edema since flow rates of this order are easily reached during exercise (e.g. 2, 3) and significant pulmonary edema is not known to develop even after very heavy exercise (e.g. 18). Since tidal volume (V_T) increases substantially during exercise, and lung volume affects almost all factors that govern fluid filtration and removal, we reasoned that an increase in V_T may reduce edema formation under conditions of high pulmonary blood flow. To our surprise we observed the opposite; $\Delta W/\Delta t$ increased significantly with larger V_T, at equivalent blood flows (Table 1).

The increase in $\Delta W/\Delta t$ was not the result of higher hydrostatic pressures at the filtration site (EFP); estimated filtration pressures were comparable at both tidal volumes (Table 1). Furthermore, the increase in $\Delta W/\Delta t$ was also observed under static conditions in which case EFP is known with certainty (Table 2).

$\Delta W/\Delta t$ represents the balance between rate of fluid filtration and removal (by lymphatics and lung surface). Therefore, an increase in $\Delta W/\Delta t$, at a given microvascular pressure, implies an increase in filtration, a decrease in clearance, or both. A decrease in fluid removal with large V_T can be discounted; lymph flow is known to increase with larger tidal volumes (1) and there is no reason to expect a reduction in fluid clearance at the pleural surface under these conditions. It follows that the observed increase in $\Delta W/\Delta t$ is primarily the result of an increase in fluid filtration. In fact, due to increased lymphatic drainage (1), the observed increase in $\Delta W/\Delta t$ likely underestimates the increase in rate of fluid filtration.

The rate of fluid filtration from the pulmonary microvasculature ($\dot{Q}_{v,c}$) is governed by the Starling equation (28):

$$\dot{Q}_{v,c} = L_p \cdot A \cdot [(P_c - P_{ti,f}) - \sigma \cdot (\pi_c - \pi_{ti})] \quad . \quad . \quad . \quad . \quad (2)$$

where L_p is the filtration constant per unit area (i.e. index of permeability), A is the membrane area available for filtration, P_c is the hydrostatic pressure within the lumen, $P_{ti,f}$ is the hydrostatic pressure in the tissue fluid surrounding the vessel, σ is the reflection coefficient for proteins, and π_c and π_{ti} are the plasma and tissue fluid oncotic pressures, respectively. Rearranging equation 2:

$$\dot{Q}_{v,c} = L_p \cdot A \cdot P_c - L_p \cdot A \cdot [P_{ti,f} + \sigma \cdot (\pi_c - \pi_{ti})] \quad . \quad . \quad . \quad (3)$$

If one assumes that $P_{ti,f}$, σ, π_c, π_{ti}, are independent of P_c (but see below), a plot of $\dot{Q}_{v,c}$ vs. P_c should be linear with a slope = $L_p \cdot A$ and a pressure intercept = $P_{ti,f} + \sigma(\pi_c - \pi_{ti})$. This type of analysis is routinely applied to identify possible mechanisms of a change in rate of fluid filtration (e.g. 22, 28). According to this interpretation, our data, shown in Table 2 [increased slope (S) without a change in intercept (P_{crit})], would imply that larger V_T acted by increasing permeability (L_p), area (A), or both without a change in $P_{ti,f}$, σ, π_c and π_{ti} (since P_{crit} was unaffected). An increase in surface area is consistent with anatomic and physiologic data which show that both length and circumference (and hence surface area) of extra-alveolar vessels increase with lung volume (16, 27). It is also consistent with the expected increase in surface area of alveolar vessels under the conditions of our experiment[1].

Changes in surface area undoubtedly contribute to the observed response. However, we believe that this conventional interpretation (of changes in slope and intercept) cannot be defended when a change in lung volume is the variable under study for the following reasons:

1) This interpretation leads to the conclusion that $P_{ti,f}$ does not change with increasing lung volume. This is totally inconsistent with the well established effects of changes in lung volume on extravascular pressures. It is well known that alveolar vessels are compressed as lung volume increases (8, 14, 24, 25, 28). This suggests an increase in extravascular pressure (17). It is also well known that, at a given intravascular pressure, extra-alveolar vessels distend as lung volume increases (8, 14, 16, 24, 25, 27, 28), indicating an increase in the net radial forces applied to the exterior of the vessels (P_x, *ref.* 16, 27). Admittedly, the extent to which fluid pressure participates in this overall change in extravascular forces is not known. However, it would be unreasonable to assume that $P_{ti,f}$ does not change under conditions which undoubtedly promote expansion of the extravascular space.

2) The opposite effects of lung volume on $P_{ti,f}$ surrounding alveolar and extra-alveolar vessels dictates that, at a given P_c, alveolar vessels should contribute less whereas extra-alveolar vessels should contribute more to fluid filtration as lung volume increases. It follows that as lung volume increases the overall

behavior of the lobe (relation between $\Delta W/\Delta t$ and P_c) should become progressively more dominated by the fluid filtration and clearance characteristics of extra-alveolar vessels (i.e. $P_{ti,f}$, L_p, A, σ, π_{ti}, and ease of fluid clearance by lymphatics and lung surface). Considering the differences in structure and location of alveolar and extra-alveolar vessels, it would be unreasonable to assume uniformity in these characteristics among the two types of vessels. Thus, it would be surprising if a shift in the predominant site of filtration to extra-alveolar vessels were not associated with a change in the effective values of one or more of these parameters.

3) Implicit in the use of the slope as an index of the filtration coefficient is the assumption that $P_{ti,f}$ is independent of intravascular pressure. While this may be justified at small lung volumes, it is not tenable at large volumes. At least two studies have shown that extravascular pressure increases as intravascular pressure is raised. The change being fairly small at low transpulmonary pressure (P_{TP}) and increases as P_{TP} is increased (16, 27).

4) The fact that the lymphatic drainage (J_l) was not interrupted in our preparation (at least not deliberately so) further complicates the interpretation. An increase in J_l, as a result of large V_T, should increase P_{crit}. If the increase in J_l is proportional to P_c, a decrease in slope is also expected. It

follows that rather than reflecting no change in the product $P_{ti,f}+\sigma(\pi_c-\pi_{ti})$, the lack of change in P_{crit} may be the result of a reduction in this product that was offset by an increase in J_1. It is evident that the complex effects of lung volume precludes a conventional interpretation of our results, and that the data in Table 2 are consistent with a wide range of possibilities. To further narrow these possibilities we compared, in the last 6 dogs, the effects of increasing V_T with that of increasing PEEP. The rationale for this comparison is as follows: A large V_T (i.e. V_2) differs from control (i.e. V_1) in two respects. First, operating (i.e. mean) lung volume is higher. Second, the pressure oscillations are larger. It was conceivable that the size of oscillations, per se, may have independent effects due to dynamic phenomena or non-linearities in the relation between lung volume and any of the various filtration and clearance variables that are affected by lung volume. The results in Table 3 clearly show that the two types of volume manipulation had different effects on $\Delta W/\Delta t$; compared to *base line* (V_1), $\Delta W/\Delta t$ increased significantly with large V_T and tended (NS) to decrease with PEEP despite the fact that EFP was, on average, slightly lower with large V_T and slightly higher with PEEP. The difference in $\Delta W/\Delta t$ between large V_T and PEEP was highly significant ($P<0.005$). Since operating lung volume [as reflected by mean airway pressure (P_{aw}) and hence alveolar pressure (P_{a1})][2] increased from *base*

line in both cases, and the changes in $\Delta W/\Delta t$ were opposite in direction, the difference in $\Delta W/\Delta t$ between the two cases cannot be attributed to differences in microvascular surface area.

Although oscillating around a similar mean P_{a1}, a major difference between large V_T and PEEP is the fact that large V_T is associated with a higher P_{a1} during one part of the cycle and a lower P_{a1} during another. End-inspiratory plateau pressure (EIP) was 6.5 cmH_2O higher while end-expiratory pressure (EEP) was 2.5 cmH_2O lower (Table 3).[3] If the relation between lung volume and each of the filtration and clearance factors were linear, then any extra effect accrued when P_{a1} is higher would be offset by opposite effects when P_{a1} is lower, and there should have been no net difference in $\Delta W/\Delta t$. Our results, therefore, clearly suggest the presence of substantial non-linearities, and these can operate in various ways.

Lung volume and permeability. If the membrane permeability (L_p) were unaffected by lung volume up to a critical inflation pressure, but increased with further inflation, and if that critical inflation pressure happens to fall between EIP of V_2 and V_3 (i.e. between 11.0 and 17.5 cmH_2O, Table 3), then an increase in L_p could have occurred with large V_T and not with PEEP. Permeability of both capillary endothelium and alveolar epithelium have been shown to increase when a critical inflation pressure is exceeded (10, 11, 22). However, this critical

pressure is much higher (>30 cmH_2O) (10, 11, 22) than the peak inflation pressures of our study (<20 cmH_2O). Therefore, this possibility is very unlikely.

Lung volume and $P_{ti,f}$. There is no evidence of non-linearity between P_{TP} and P_x over the range of P_{TP} used in this study (16, 27). However, as indicated earlier, whether the response of $P_{ti,f}$ is similarly linear has not been established, and it is $P_{ti,f}$ that is relevant to filtration. Our observations could be explained if the relation between P_{TP} and $P_{ti,f}$ over the P_{TP} range 11.0-17.5 cmH_2O is steeper (i.e. more $P_{ti,f}$ change per unit change in P_{TP}) than in the range 2.5-5.0 cmH_2O. Alternatively, the change in $P_{ti,f}$ with lung inflation may be time dependent; $P_{ti,f}$ decreasing acutely and returning to *base line* when inflation is sustained. Sustained increases in lung volume (i.e with PEEP) may, therefore, have either a lesser or no effect on $P_{ti,f}$ as compared to increases in the amplitude of volume oscillations. Although direct measurements of liquid pressure outside alveolar vessels have been made at different lung volumes (17) the published data is insufficient to make a firm conclusion about the linearity of the relation between P_{TP} and $P_{ti,f}$ under the conditions of our experiments.

Lung volume and P_{crit} at alveolar and extra-alveolar vessels. Because of the opposite effects of lung volume on $P_{ti,f}$ (relative to pleural pressure) of alveolar and extra-alveolar vessels, increasing lung volume should promote lesser fluid

filtration from alveolar vessels and greater filtration from extra-alveolar vessels. The net effect on filtration is the sum of both actions. Increasing $P_{ti,f}$ should decrease filtration from alveolar vessels up to the point where $(P_c - P_{ti,f})$ equals $\sigma(\pi_c - \pi_{ti})$. Since at this point net filtration should become trivial or cease, additional reduction in the hydrostatic pressure gradient of alveolar vessels (by increasing lung volume and $P_{ti,f}$) should have no further reducing effect on filtration from alveolar vessels. On the other hand, as $P_{ti,f}$ of extra-alveolar vessels continues to decrease with lung inflation, filtration from these vessels would continue to increase. It is evident that in the P_{TP} range 2.5-11.0 cmH_2O of our experiments the opposing effects on filtration from alveolar and extra-alveolar vessels nearly canceled each other out (since $\Delta W/\Delta t$ did not change or decreased slightly as alveolar pressure was varied in this range; V_1 vs. V_3, Table 3). It is possible that the critical $P_{ti,f}$ of alveolar vessels (i.e. the tissue fluid pressure at which filtration ceases) was reached in our experiments at P_{TP} slightly above 11.0 cmH_2O. In this case, when P_{TP} of large V_T (V_2) exceeds that of PEEP (V_3) that part of the respiratory cycle will be associated with a higher net filtration. This difference cannot be offset during the period when P_{TP} with V_2 is lower than that with V_3 since at the lower P_{TP} range differences in P_{TP} have little net effect on filtration (see above).

Lung volume and interstitial fluid movement. It is generally accepted that fluid filters from the microvasculature into the immediate extravascular interstitium and subsequently flows into more proximal sites in the interstitium (28, 29). The resistance to flow between the immediate and the more proximal compartments necessarily influences the back pressure (i.e. $P_{ti,f}$ in the vicinity of the filtration site). Thus, with a higher resistance, $P_{ti,f}$ at the filtration site should be higher, other factors being equal (28, 29). A lower mean resistance with larger V_T, on account of non-linearities in the relation between lung volume and resistance to tissue flow, could result in a lower mean $P_{ti,f}$ and therefore, greater filtration rate.

Very recently, Albelda et al. (1) have shown, in unanesthetized spontaneously breathing sheep, that increasing V_T (produced by increasing dead space), is associated with an increase in pulmonary lymph flow. Under steady state conditions, this increase in lymph flow must reflect a concomitant increase in transvascular fluid filtration. It was not possible to ascertain whether the increase in filtration is a consequence of a primary (pumping) action of ventilation on lymphatic drainage, or the opposite (i.e. higher tidal volumes independently increase filtration and the associated increase in lymph flow is a secondary phenomenon). Since the rate of pulmonary lymph flow (J_l) is normally very small, and the increase in J_l produced by higher tidal volumes was also relatively small (27%), the

associated increase in fluid filtration, assuming a primary effect on lymphatic pumping, would be trivial and the lung would not be expected to gain weight (in fact some loss of weight is to be expected). On the other hand, if the primary effect is on filtration, the increase in J_l may represent only the "tip of the iceberg," and lung water is expected to increase. The distinction is, therefore, important as it establishes whether increases in V_T (or ventilation) would have a net beneficial or deleterious effect on lung water. Our results indicate that the increase in J_l with increasing ventilation is a secondary phenomenon.

Our results suggest that patients with pulmonary edema are better off ventilated with small tidal volumes. Several considerations, however, mitigate against such a recommendation at present. First, a smaller V_T may have negative effects on the lung (e.g. atelectasis) or on gas exchange. Second, the effects of large V_T observed here were based on 4-5 min periods of observations. Whether the effects of a large V_T on edema formation are sustained over longer periods of time is not known. Third, if V_T is decreased, frequency must be increased to maintain ventilation. The independent effects of respiratory frequency on fluid dynamics have not been thoroughly investigated. In isolated sheep lung, Patterson et al. (23) have recently shown a direct relation between lymph flow and respiratory frequency over the range 0-30 min^{-1}. However, it was

not possible to determine whether this effect was due to changes in filtration rate, redistribution of interstitial fluid, or to augmentation in lymphatic transport. Finally, the majority of patients with pulmonary edema on ventilators suffer from high permeability edema, as opposed to the hydrostatic edema studied here. Because the pathogenesis of the two types of edema is entirely different, it cannot be assumed that the V_T effects will be similar.

In summary, we have shown that under edematogenic conditions produced by high pulmonary intravascular pressures, larger tidal volumes promote greater water accumulation, and that increasing operating lung volume by increasing V_T or by increasing end-expiratory pressure have qualitatively opposite effects on rate of edema formation. It is of interest to note that when faced with spontaneous pulmonary edema, the intact organism breathes in a shallow manner and that the reflex effects of receptors which are naturally responsive to pulmonary congestion and edema [pulmonary *J* receptors (6, 21)] are shallow breathing and an elevation of end-expiratory volume (6, 21). The natural response seems to be correct on both counts.

G. FOOTNOTES

Footnote 1.

Although pulmonary capillaries are compressed with lung expansion, reducing capillary blood volume (8, 14, 24, 25, 28), their area should increase in concert with alveolar surface area unless, of course, derecruitment occurs. Derecruitment was not a factor in our experiments since capillary pressure was much higher than peak alveolar pressure (compare EFP and EIP, Tables 1 and 3).

Footnote 2.

Airway pressure (P_{aw}) during inspiration overestimates alveolar pressure (P_{a1}) on account of the pressure expended against flow resistance of the airways, as given by:

$$P_{aw} - P_{a1} = V_I \cdot R_I$$

where V_I is inspiratory flow and R_I is airway resistance during inspiration. During expiration the opposite occurs, P_{aw} underestimates P_{a1} by the product $V_E \cdot R_E$ where V_E and R_E are flow and resistance during expiration, respectively.

During inspiration the total area under the P_{aw} waveform ($\int_0^{Ti} P_{aw} \cdot dt$) overestimates the area under the inspiratory P_{a1} waveform ($\int_0^{Ti} P_{a1} \cdot dt$) by the product $\int_0^{Ti} V_I \cdot R_I \cdot dt$. During expiration the area under the P_{aw} waveform ($\int_0^{Te} P_{aw} \cdot dt$)

underestimates the alveolar counterpart ($\int_0^{Te} P_{al} \cdot dt$) by the product $\int_0^{Te} V_E \cdot R_E \cdot dt$.

If $\int_0^{Ti} V_I \cdot R_I \cdot dt$ equaled $\int_0^{Te} V_E \cdot R_E \cdot dt$, the total area under P_{aw} would equal the total area under P_{al} and mean P_{aw} would then equal mean P_{al}.

In our preparation the lobe does not participate in gas exchange so that $\int_0^{Ti} V_I \cdot dt = \int_0^{Te} V_E \cdot dt$. It follows that if R_I and R_E were equal, mean P_{aw} would equal mean P_{al}.

We calculated R_I and R_E in several lobes from the difference between P_{aw} and P_{al} at different points during inspiration and expiration and by relating that difference to instantaneous flow. The time course of P_{al} was estimated from end-inspiratory plateau pressure (i.e. end-inspiratory P_{al}) and the time course of volume (i.e. integrated flow). We found that R_E is, on average, 60% higher than R_I (20.0 vs. 12.5 $cmH_2O/l/sec$). It follows that $\int_0^{Te} V_E \cdot R_E \cdot dt$ is 60% higher than $\int_0^{Ti} V_I \cdot R_I \cdot dt$ and mean P_{aw} must, therefore, underestimate mean P_{al}.

However, we also found that $\int_0^{Ti} V_I \cdot R_I \cdot dt$ is less than 10% of the total area under inspiratory P_{aw} waveform. The difference between R_I and R_E would thus cause mean P_{aw} to underestimate mean P_{al} by less than 6% or, in absolute terms, less than 0.5 cmH_2O. We believe this is an acceptable error in view of the ease of obtaining mean P_{aw} (low pass filter).

Footnote 3.

The differences in peak and nadir pressures are not similar because of the non-symmetrical alveolar pressure waveform. Because of the relatively slow frequency, EEP is reached early in expiration and is thus maintained for a larger fraction of the respiratory cycle than peak pressure.

H. REFERENCES

1. Albelda, S. M., J. H. Hansen-Flaschen, P. N. Lanken, and A. P. Fishman. Effects of increased ventilation on lung lymph flow in unanesthetized sheep. *J. Appl. Physiol.* 60(6):2063-2070, 1986.
2. Asmussen, E. Muscular exercise. In: Handbook of Physiology. Respiration. Washington, DC: Am. Physiol. Soc., 1964, sect. 3, vol. II, chapt. 36, p. 939-978.
3. Bailie, M. D., S. Robinson, H. H. Rostorfer, and J. L. Newton. Effects of exercise on heart output of the dog. *J. Appl. Physiol.* 16:107-111, 1961.
4. Bø, G., A. Hauge, and G. Nicolaysen. Alveolar pressure and lung volume as determinants of net transvascular fluid filtration. *J. Appl. Physiol.* 42:476-482, 1977.
5. Caldini, P., J. D. Leith, and M. J. Brennan. Effect of continuous positive-pressure ventilation (CPPV) on edema formation in dog lung. *J. Appl. Physiol.* 39:672-679, 1975.
6. Coleridge, H. M. and J. C. G. Coleridge. Reflexes evoked from tracheobronchial tree and lungs. In: Handbook of Physiology. Respiration. Bethesda, MD. Am. Physiol. Soc. 1986, sect. 3, vol. II, chapt. 12, p. 395-430.
7. Craven, K. D., L. Oppenheimer, and L. D. H. Wood. Effects of contusion and flail chest on pulmonary perfusion and oxygen exchange. *J. Appl. Physiol.* 47(4):729-737, 1979.

8. Dawson, C. Role of pulmonary vasomotion in physiology of the lung. *Physiol. Rev.* 64:544-616, 1984.

9. Demling, R. H., N. C. Staub, and L. H. Edmunds, JR. Effect of end-expiratory airway pressure on accumulation of extravascular lung water. *J. Appl. Physiol.* 38:907-912, 1975.

10. Egan, E. A. Fluid balance in air filled alveolar space. *Am. Rev. Resp. Dis.* 127:(5) part 2:537-539, 1983.

11. Egan, E. A., R. M. Nelson, and R. E. Olver. Lung inflation and alveolar permeability to non-electrolytes in the adult sheep in vivo. *J. Physiol. (Lond.)* 60:409-424, 1976.

12. Goldberg, H. S., W. Mitzner, and G. Batra. Effect of transpulmonary and vascular pressures on rate of pulmonary edema formation. *J. Appl. Physiol.* 43:14-19, 1977.

13. Hopewell, P. C., and J. F. Murray. Effects of continuous positive-pressure ventilation in experimental pulmonary edema. *J. Appl. Physiol.* 40:568-574, 1976.

14. Howell, J. B. L., S. Permutt, D. F. Proctor, and R. L. Riley. Effect of inflation of the lung on different parts of the pulmonary vascular bed. *J. Appl. Physiol.* 16:71-76, 1961.

15. Iliff, L. D. Extra-alveolar vessels and edema development in excised dog lungs. *Circ. Res.* 28:524-532, 1971.

16. Lai-Fook, S. J. A continuum mechanics analysis of pulmonary vascular interdependence in isolated dog lobes. *J. Appl. Physiol.* 46:419-429, 1979.

17. Lai-Fook, S. J., K. C. Beck. Alveolar liquid pressure measured by micropipets in isolated dog lung. *J. Appl. Physiol.* 53(3):737-743, 1982.

18. Marshall, B. E., L. R. Soma, and G. R. Neufeld. Lung water volume at rest and exercise in dogs. *J. Appl. Physiol.* 39:7-8, 1975.

19. Mellins, R. B., O. R. Levine, R. Skalak, and A. P. Fishman. Interstitial pressure of the lung. *Circ. Res.* 24:197-212, 1969.

20. Morriss, A. W., R. E. Drake, and J. C. Gabel. Comparison of microvascular filtration characteristics in isolated and intact lungs. *J. Appl. Physiol.* 48:438-443, 1980.

21. Paintal, A. S. Vagal sensory receptors and their reflex effects. *Physiol. Rev.* 53:159-227, 1973.

22. Parker, J. C., M. I. Townsley, B. Rippe, A. E. Taylor, and J. Thigpen. Increased microvascular permeability in dog lungs due to high peak airway pressures. *J. Appl. Physiol.* 57(6):1809-1816, 1984.

23. Patterson, G. A., W. A. Mitzner, and J. T. Sylvester. Assessment of fluid balance in isolated sheep lungs. *J. Appl. Physiol.* 58(3):882-891, 1985.

24. Permutt, S. Mechanical influences on water accumulation in the lungs. In: Pulmonary edema, edited by A. P. Fishman and E. M. Renkin. Bethesda, MD: Am. Physiol. Soc., 1979, chapt. 13, p.175-193.

25. Permutt, S., J. B. L. Howell, D. F. Proctor, and R. L. Riley. Effect of lung inflation on static pressure-volume characteristics of pulmonary vessels. *J. Appl. Physiol.* 16:64-70, 1961.

26. Permutt, S., R. A. Wise, and J. T. Sylvester. Interaction between the circulatory and ventilatory pumps. In: The Thorax. Lung Bio. In Health and Dis. series. Dekker 1985. Vol. 29, part B, chapt. 4, p. 95-124.

27. Smith, J. C. and W. Mitzner. Analysis of pulmonary vascular interdependence in dog lobes. *J. Appl. Physiol.* 48:450-467, 1980.

28. Taylor, A. E., J. C. Parker. Pulmonary interstitial spaces and lymphatics. In: Handbook of Physiology - The Respiratory System, edited by A. P. Fishman and A. B. Fisher, Bethesda, MD: Am. Physiol. Soc., 1986, sect. 3, vol. I, chapt. 4, p.167-230.

29. Taylor, A. E. and B. Rippe. Pulmonary edema. In: Physiology of Membrane disorders. Ed.: Andreoli, T. E. and others. Plenum 1986. Chapt. 56, p. 1025-1039.

30. Wagner, E., P. A. Riebens, K. Katsukara, and P. Salisbury. Influence of airway pressures on edema in the isolated dog's lung. *Circ. Res.* 9:382-386, 1961.

IV. CHAPTER 3

EFFECT OF ALVEOLAR HYPOXIA ON PULMONARY FLUID FILTRATION IN IN SITU DOG LUNGS

A. BACKGROUND

Alveolar hypoxia is widely believed to promote pulmonary edema formation. The mechanism by which this phenomenon occurs is not settled, yet it is crucial to our understanding of high altitude pulmonary edema and may relate to many pathological conditions that result in regional alveolar hypoxia. Suggested mechanisms by which alveolar hypoxia could contribute to increased fluid flux include: 1) An increase in intravascular pressure at the filtration site (EFP), 2) an increase in pulmonary microvascular permeability, or 3) a combination of both. Since hypoxia is known to result in pulmonary vascular constriction, it is not unreasonable to expect it to have an effect on EFP and therefore on pulmonary fluid flux. Whether fluid flux would increase or decrease depends on the degree and location of the constriction in relation to the major site of fluid transudation.

There is both animal (7, 22) and human (27, 28) evidence of constriction of the pulmonary vascular bed during hypoxia. There are also animal experimental data (10) and clinical reports (11, 14) to support the contention that excessive perfusion of a restricted vascular bed can result in pulmonary edema. In contrast, studies of the possible effect of alveolar hypoxia on microvascular permeability have produced conflicting results with some (notably lymph flow and gravimetric studies in dogs)

suggesting an increase in permeability (4, 17, 20, 26) while others (lymph flow studies in sheep) failing to show such an effect (3, 16). These studies have so far used lymph flow and gravimetric techniques, but for these techniques to provide reliable information about permeability, it was necessary to control hydrostatic pressure at the filtration site. This pressure is an important determinant not only of the pressure gradient for fluid movement but also of the filtration surface area. Because of the complex and somewhat uncertain effects of alveolar hypoxia on the parallel and longitudinal distributions of pulmonary vascular resistance (for review see *ref.* 6), it is not possible to obtain an accurate estimate of microvascular filtration pressure during hypoxia in the presence of even modest levels of blood flow. Accordingly, we intend to study the effect of alveolar hypoxia on fluid flux in dog lungs under conditions of very low flow rates, where hydrostatic filtration pressure can be controlled and estimated with certainty.

B. METHODS

An isolated *in situ* perfused left upper lobe (LUL) preparation was used (Figure 1). Thirteen mongrel dogs were anesthetized with sodium pentobarbital and intubated. The animals were ventilated with a dual Harvard pump at a rate of 10/min and a tidal volume of 10-15 ml/kg.

After inserting a catheter in the right carotid artery to monitor systemic blood pressure (BP) and a Swan-Ganz catheter to monitor right pulmonary artery (RPA) pressure, a thoracotomy was performed in the left fifth intercostal space and opened widely. A cannula was inserted through the left lower lobe (LLL) vein into the left atrium (LA). The LLL artery was ligated and a ringed cannula (7 mm I.D., 8 mm O.D.) was inserted immediately proximal to the ligature and secured. The LLL bronchus was cannulated with a Y-tube. One arm of the Y-tube was connected to the second barrel of the dual Harvard pump while the other arm was used to introduce a Fogarty balloon catheter to the level of the left main stem bronchus. When the balloon was inflated it was possible to ventilate the LUL separately from the right lung. The LUL was ventilated with a tidal volume (TV) of 150-200 ml.

A cannula was inserted into the left femoral artery (FA). At this point the animal was fully heparinized. The stem of a Y-cannula was attached to the cannula in the LLL artery. One arm of the Y-cannula was connected to the FA cannula using Tygon tubing primed with saline and mounted on a Cobe-Stöckert roller pump. This system was used to draw femoral arterial blood to perfuse the LUL. The other arm of the Y-cannula contained a catheter equipped with an intravascular occlusive device (OD) (for details see CHAPTER 1). This catheter was advanced to the level of the left main pulmonary artery (LPA), upstream from the LUL artery and the LPA was occluded. At this point perfusion to

the LUL was initiated at a very low flow of 20 ml/min. Inflow pressure was monitored through an orifice in the LPA catheter located proximal to the OD.

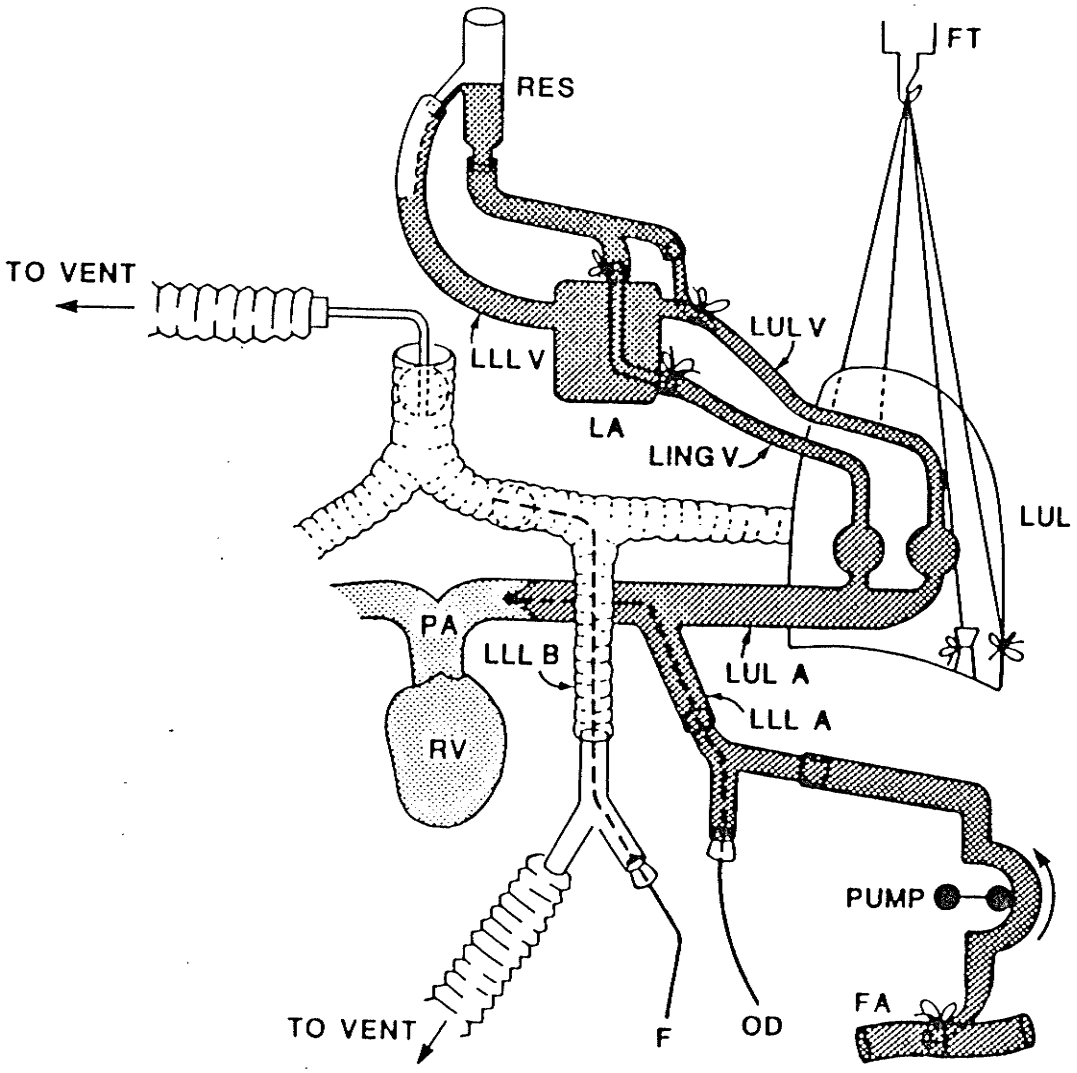

FIGURE 1. Preparation. F, Fogarty catheter; FA, femoral artery; FT, force transducer; LA, left atrium; LING V, lingular vein; LLL A, left lower lobe artery; LLL B, left lower lobe bronchus; LLL V, left lower lobe vein; LUL, left upper lobe; LUL A, left upper lobe artery; LUL V, left upper lobe vein; OD, occlusive device; PA, main pulmonary artery; RES, reservoir; RV, right ventricle.

The LUL veins were then cannulated. A J-shaped cannula was inserted through the left atrial appendage. The short end was inserted 1 cm into the LUL vein via the LA and secured to the vein with silk thread. The cannula was then attached via Tygon tubing to the bottom of a reservoir. The reservoir was constructed with an overflow which was drained to the LA via the cannula in the LLL vein (Figure 1). The lingular vein was ligated at the LA and cannulated with small flexible tubing. This was connected to the reservoir after anastomosis with the tubing from the other pulmonary vein.

The LUL was suspended from a force transducer for continuous monitoring of lobar weight (for details of suspension see CHAPTER 1). Lobar weight was always measured at end expiration.

All pressure lines (systemic BP, LPA, RPA) were connected to appropriate pressure transducers and zeroed at the level of the LUL pulmonary veins as they enter the LA.

Rate of edema formation ($\Delta W/\Delta t$) was determined gravimetrically. Following a step increase in vascular pressure (raising the reservoir) there was an initial fast phase of weight gain (Figure 2). When vascular pressure exceeded a critical value this fast phase was followed by a phase of slow weight gain. The rate of weight gain during this period was constant as long as vascular pressure remained constant (9, see also

CHAPTER 1). Rate of edema formation was derived from the slope of this slow weight gain segment over a period of 3 minutes (Figure 2).

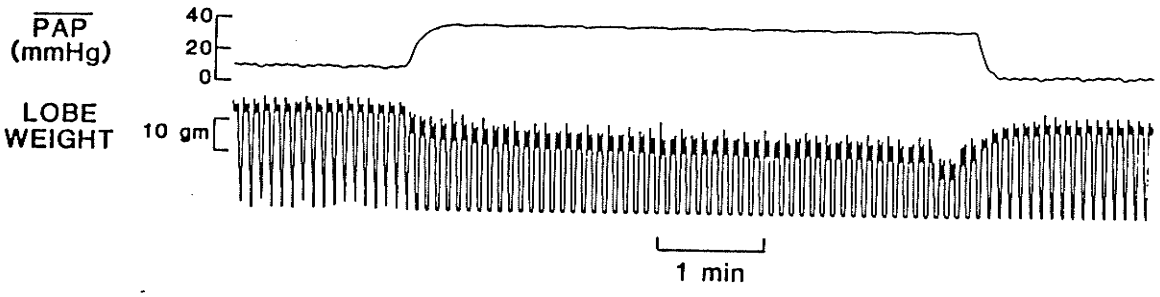

FIGURE 2. Upward deflection of mean left pulmonary arterial pressure (PAP) tracing reflects time at which reservoir was raised (*left*) and then returned to *base line* (*right*). Downward deflection in weight tracing signifies weight gain. Note that end-expiratory lobe weight (thick segment) is progressively increasing. Toward the end of the slow phase of weight gain, 5 g of weight were placed on the lobe to check consistency of weight calibration (downward deflection).

C. PROTOCOL

In the first 6 dogs (Group I) the LUL was ventilated under 2 conditions: 1) 95% O_2 and 5% CO_2. 2) 0% O_2, 5% CO_2, balance N_2. Under each condition the reservoir was elevated from a *base line* of 10 mmHg to various heights corresponding to vascular inflow pressures of up to 54 mmHg in order to produce edema. The reservoir remained elevated for 4 minutes at each point and then returned to *base line*. Two to three points of edema formation were acquired at one F_IO_2. F_IO_2 was then changed to the other level and measurements repeated. This sequence of alternating F_IO_2 was repeated until an average of 7 points with edema formation were acquired for each condition. For each dog and each condition, $\Delta W/\Delta t$, was plotted against inflow pressure and a best fit linear regression was obtained. The slope of the regression line was expressed per 100 g of lung tissue wet weight. The latter was obtained by multiplying the dog's weight (in kg) by 1.36 (5). The pressure threshold for edema formation (P_{crit}) was determined as the x-intercept of the regression line.

In the final 7 dogs (Group II) the LUL was ventilated under 4 conditions: 1) 95% O_2, 2) 21% O_2, 3) 5% O_2, 4) 0% O_2. Each gas mixture also contained 5% CO_2, balance N_2. In this set of dogs all points were acquired at one level of microvascular pressure. The reservoir was raised to a point that corresponded to 40 mmHg inflow pressure. The reservoir level was marked and returned to the same level for each measurement in order to fix

outflow pressure. F_IO_2 conditions were alternated in random order and one point of edema formation was acquired at each F_IO_2. The sequence was then repeated until an average of 3 points were accumulated with each F_IO_2. The points were averaged to give 1 measurement of edema formation per condition per dog.

The final 3 dogs of Group II were prepared differently in order to potentiate hypoxic vasoconstriction. Two maneuvers were used. First, mixed venous blood was drawn from the right atrium (instead of femoral artery) via the right external jugular vein to perfuse the LUL with hypoxic blood and, second, indomethacin 2 mg/kg I.V. was administered prior to experimentation.

In each experiment we periodically stopped pump flow for a few seconds. Pressure in the LPA decreased to a plateau which in the absence of flow reflected reservoir pressure. The difference between LPA pressure with and without flow reflected the total pressure gradient between LPA and reservoir in the presence of flow. This testing was done under all conditions of F_IO_2. In no case was this gradient greater than 2 mmHg. We also measured the pressure drop along the outflow tubing at the experimental flow of 20 ml/min and this was 1 mmHg. It follows that the total pressure gradient across the lobe (i.e. total gradient minus tubing pressure gradient) was always less than 1 mmHg.

The slope and P_{crit} values from Group I (n=6) were compared between the two conditions using paired t-test. Rates of edema formation at the 4 F_IO_2 levels in Group II (n=7) were compared using ANOVA for repeated measures.

D. RESULTS

An example of the relation between $\Delta W/\Delta t$ and inflow pressure, for both hypoxic and hyperoxic conditions (Group I), is shown in Figure 3. Individual as well as mean values for slope, P_{crit} and r are shown in Table 1. Mean (±SE) for slope during hyperoxia and hypoxia were 0.067 ± 0.008 and 0.073 ± 0.017 $g \cdot min^{-1} \cdot mmHg^{-1} \cdot 100g^{-1}$ wet weight, respectively. No significant difference was found between the two conditions (P=0.47).

Mean (±SE) P_{crit} for hyperoxia and hypoxia were 18.3 ± 1.8 and 17.1 ± 1.2 mmHg, respectively. The difference between the two conditions was again not significant (P=0.70).

Figure 4 shows both individual as well as mean values of $\Delta W/\Delta t$ under each of the 4 F_IO_2 conditions (Group II). Mean $\Delta W/\Delta t$ was 0.61 g/min for severe hypoxia, moderate hypoxia and normoxia, and 0.60 g/min for hyperoxia. No significant differences were noted between conditions.

The final 3 dogs, in which indomethacin was added and in which the LUL was perfused with venous blood, are separately identified in Figure 4. When examined separately these dogs showed no significant difference in $\Delta W/\Delta t$ between conditions.

The results (mean±SE) were as follows: 1) severe hypoxia 0.70 ± 0.13, 2) moderate hypoxia 0.71 ± 0.19, 3) normoxia 0.67 ± 0.12, 4) hyperoxia 0.72 ± 0.19 g/min. In these dogs we also tested for the presence of pulmonary vasoconstrictor response to hypoxia. A vigorous response was found in each case. An example is shown in Figure 5.

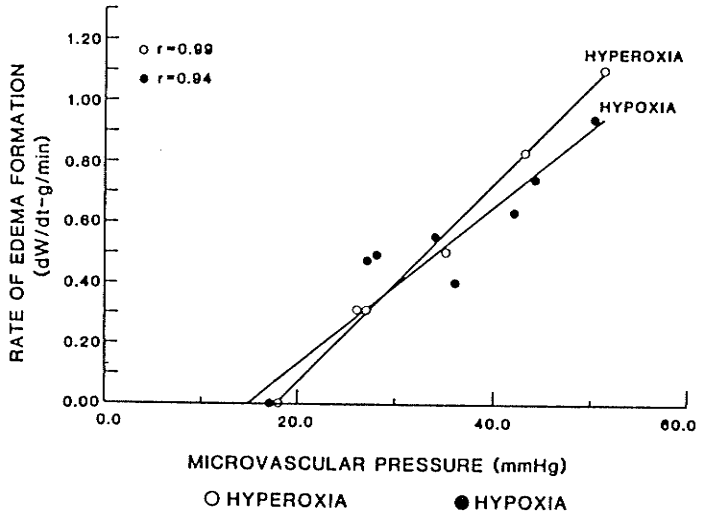

FIGURE 3. Relation between inflow pressure and rate of edema formation during both hypoxia and hyperoxia in *dog 4* (group I).

TABLE 1. *Relation between $\Delta W/\Delta t$ and EFP (group 1)*

Dog No.	Hyperoxia			Hypoxia		
	Slope, $g \cdot min^{-1} \cdot mmHg^{-1} \cdot 100\ g^{-1}$	Pcrit, mmHg	r	Slope, $g \cdot min^{-1} \cdot mmHg^{-1} \cdot 100\ g^{-1}$	Pcrit, mmHg	r
1	0.071	25.9	0.97	0.048	15.4	0.97
2	0.050	15.6	0.94	0.058	15.9	0.92
3	0.099	12.4	0.95	0.157	18.1	0.95
4	0.074	17.8	1.00	0.058	14.9	0.94
5	0.061	18.6	0.93	0.066	15.5	0.94
6	0.047	19.4	0.94	0.051	22.5	0.97
Mean ± SE	0.067±0.008	18.3±1.8	0.96	0.073±0.017	17.1±1.2	0.95

$\Delta W/\Delta t$, rate of edema formation; EFP, effective filtration pressure; Pcrit, critical capillary pressure, obtained from pressure intercept of above relation; r, correlation coefficient of best linear fit.

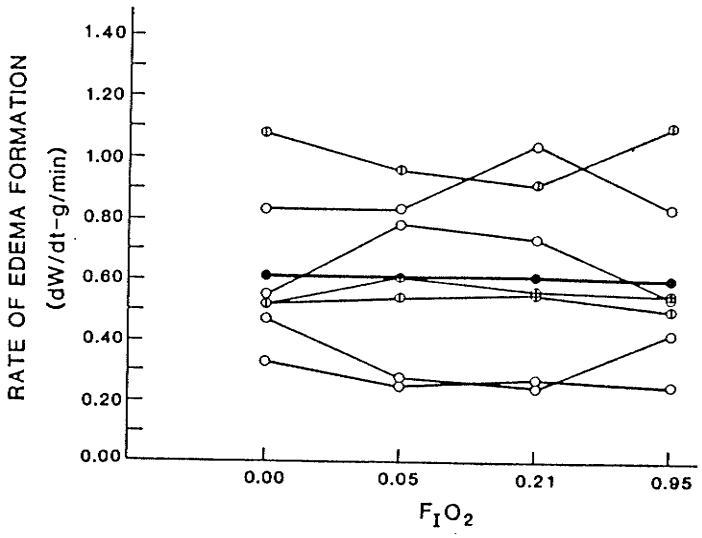

FIGURE 4. Rate of edema formation at 4 different levels of inspired O_2 fraction (F_IO_2). O, Individual dogs; ◍, dogs receiving indomethacin and perfused with venous blood; ●, mean values for all dogs.

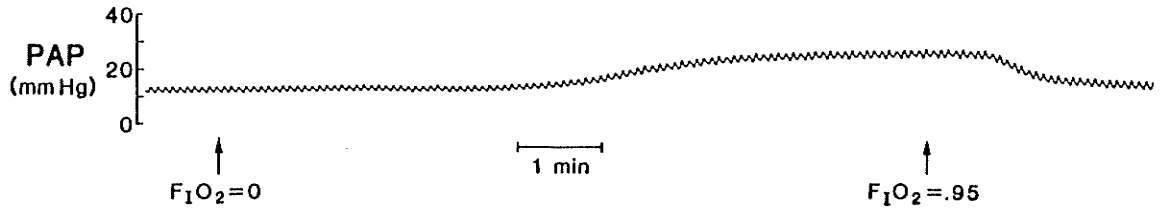

FIGURE 5. Response to hypoxia. PAP, left pulmonary artery pressure. arrow, start of each inspired O_2 fraction (F_IO_2) applied.

E. DISCUSSION

High altitude pulmonary edema is commonly attributed to alveolar hypoxia. Suggested mechanisms by which alveolar hypoxia could contribute to increased fluid flux include: 1) An increase in intravascular pressure at the filtration site (effective filtration pressure, EFP), 2) an increase in pulmonary microvascular permeability, or 3) a combination of both. Since hypoxia is known to result in pulmonary vascular constriction, it is not unreasonable to expect it to have an effect on EFP and therefore on pulmonary fluid flux. Whether fluid flux would increase or decrease would in turn depend on the degree and location, among other factors, of the constriction in relation to the major site of fluid transudation. This fact, that alveolar hypoxia is likely to change EFP, complicates experimental attempts to address the separate question of whether hypoxia increases microvascular permeability, since accurate control and determination of EFP is a minimum requirement for attributing fluid flux changes to permeability changes.

Previous studies have attempted to examine the effect of alveolar hypoxia on the filtration characteristics of the lung in several animal species. In dogs exposed to 10% F_IO_2, Warren et al. (25) observed an increase in lung lymph flow with no significant change in lymph/plasma protein ratio. Similar results were obtained by Beznák and Liljestrand (2) in one dog

and four cats. Despite these observations, one cannot conclude that hypoxia causes an increase in microvascular permeability because adequate measurements of pulmonary hemodynamics were not made in either of these studies. Boonyaprakob et al. (4) and Martin et al. (17) also found increased lymph flow in dogs exposed to hypoxia. However, the concomitant increase in pulmonary artery pressure and cardiac output in their studies may have increased both EFP and surface area for fluid filtration and could have accounted for their results.

In anesthetized sheep, Bland et al. (3) observed no increase in lung lymph flow during hypoxia in spite of increased pulmonary artery pressure. On the other hand, when alveolar hypoxia was produced in sheep with significant lung resections and elevated cardiac output Landolt et al. (16) obtained an increase in lung lymph flow with a decrease in lymph/plasma protein ratio in 3 out of 6 animals. This result is consistent with a change in EFP.

The effect of hypoxia on fluid filtration in the adult animal has also been studied in isolated lung lobe preparations. Mitzner and Sylvester (18), using a gravimetric technique, studied pig lungs (*ex vivo*) exposed to P_IO_2 of 50 mmHg. Hypoxia increased filtration rate at all examined flow rates. However, EFP was not known. In a recent study Kinazewitz et al. (15) documented an increase in fluid filtered from pleural surface of isolated dog lungs in response to severe hypoxia (F_IO_2=0.0). Although EFP was not known with certainty, it was very likely

comparable in the two states since the authors used Verapamil to block hypoxic vasoconstriction and inflow and outflow pressures were comparable. Whether filtration through the pleural surface is representative of deeper structures is not clear, however. Furthermore, the preparation used by these authors was recently found to display pleural inflammation (29). The response observed may thus represent a greater sensitivity of the inflamed pleura to hypoxia.

We are aware of only one study on the effect of hypoxia on fluid filtration in which EFP was directly estimated (20). In this study, utilizing the isogravimetric technique in isolated dog lungs, Parker et al. (20) showed a two fold increase in $K_{f,c}$ during severe alveolar hypoxia (F_IO_2=0.0) as compared to hyperoxia (F_IO_2=0.95). Changes in surface area were unlikely as microvascular pressures were comparable under both conditions, thus suggesting a true change in permeability.

Our *in situ* lung lobe preparation incorporates many of the advantageous features of isolated lobe preparations without sacrificing the major advantages of intact animal studies. Blood flow could be precisely controlled and the transition from natural to pump flow is instantaneous eliminating any period of non-perfusion. In addition, as outlined in CHAPTER 1, use of the LUL lends many advantages including preservation of important *in situ* systems (such as lymphatics, nerves, bronchial circulation), ease of vascular access via LLL artery and ease of suspension.

Also as indicated earlier the fluid filtration characteristics in this preparation are similar to those of intact lungs. Edema formation does not occur until a critical microvascular pressure (P_{crit}) is reached. P_{crit} (±SE) in our experiments (17.7 ± 1.1 mmHg, for all dogs under both hypoxic and hyperoxic conditions) is quite comparable to those reported by Drake et al. (9) (19.7 ± 1.8 mmHg) and Morris et al. (19) (20.1 ± 1.5 mmHg) in intact animals. Furthermore, our slope values (0.070 ± 0.009), though somewhat lower, are also comparable to those reported by Drake et al. (9) (0.11 ± 0.02) and Morris et al.(19) (0.09 ± 0.01 $g \cdot min^{-1} \cdot mmHg^{-1} \cdot 100g^{-1}$).

Another major advantage of this preparation is the precision in estimating true filtration pressure. The maximum pressure drop across the system (pulmonary artery to reservoir) was always less than 2 mmHg. The tubing from the pulmonary veins to the reservoir accounted for 1.0 mmHg of the total pressure drop at the utilized flow (20 ml/min). Thus the pressure drop across the LUL was less than 1.0 mmHg. Differences in longitudinal or parallel distribution of resistance as a result of hypoxia would, accordingly, have no appreciable effect on EFP.

In Group I, F_IO_2 was alternated between 0.95 and 0.0. These conditions have been used previously and were chosen for the experiment in an attempt to maximize any differential effect PO_2 may have on permeability. However, this approach does have drawbacks. First, the process leading to increased permeability

may be an active one (i.e. requiring energy). A maximal effect may occur with a given degree of moderate hypoxia which may be lost with severe hypoxia. Such an effect has been shown to occur with hypoxic pulmonary vasoconstriction (21, 24). Alternatively, hyperoxia, a known physical toxin, may cause equal endothelial permeability changes resulting in an apparent lack of effect of hypoxia. To overcome these problems, Group II experiments were undertaken comparing 4 levels of F_IO_2. These included normoxia and moderate hypoxia (F_IO_2=0.05) as well as the two extremes. By this method any deviation from normal could be detected as might any trends for a gradient or peak effect associated with progressive hypoxia. Our results still showed no significant difference between the 4 conditions.

The dog may have a blunt pulmonary vasoconstrictive response to hypoxia relative to other species (21). People susceptible to high altitude pulmonary edema have been shown to have an exaggerated hypoxic pulmonary vasoconstrictor response (14, 23, 26). Should the mechanism for changes in permeability be related to vasoconstriction, then maximizing hypoxic vasoconstriction might enhance hypoxic induced changes in permeability. After the first 4 dogs in Group II it became apparent that changes in permeability could not be demonstrated. In an attempt to promote permeability changes in the final 3 dogs, we used two methods to enhance pulmonary vasoconstriction. First, since O_2 content of mixed venous blood is known to affect (albeit much less than

alveolar O_2) pulmonary vasomotion, venous blood was used to perfuse the lobe. Second, indomethacin was injected into the dogs prior to the experiment to counter circulating vasodilator prostaglandins (12). This resulted in enhanced hypoxic vasoconstriction (Figure 5). However, no change in edema formation could be demonstrated between the 4 conditions even when the last 3 dogs were examined alone.

The lack of effect of alveolar PO_2 (P_AO_2) on rate of edema formation ($\Delta W/\Delta t$), at a given EFP, may be most simply attributed to the absence of an independent effect of P_AO_2 on microvascular permeability. $\Delta W/\Delta t$, however, is not related exclusively to EFP and permeability. Since $\Delta W/\Delta t$ represents the balance between rates of fluid filtration and removal, it is possible that an increase in fluid filtration rate with hypoxia (secondary to increased permeability) is offset by a concomitant increase in lymphatic clearance (J_l). We are unaware of any studies, in the literature, that examined the effect of hypoxia on lymph flow at fixed microvascular pressures and lung volume history. Accordingly, this possibility cannot be discounted (but see below). We also cannot exclude the possibility that an increase in permeability is offset by opposing changes in other factors that affect fluid filtration rate (such as tissue hydrostatic pressure (P_{ti}), protein reflection coefficient (σ), or tissue oncotic pressure (π_{ti})). We feel, however, that these possibilities are quite remote. First, for the results of Group

II (Figure 4) to be explained on the opposing effect of some other variable (e.g. J_1, P_{ti}, σ, and/or π_{ti}), the two effects must bear the same relation, both qualitatively and quantitatively, to P_AO_2. Otherwise, the effects would not have canceled out at all 4 levels. Second, for hypoxic effects on any of these variables to explain an unchanged slope and intercept, of the relation between $\Delta W/\Delta t$ and EFP (Table 1, Group I), the effect of hypoxia on these variables must also vary with EFP.

It may also be argued that an unchanged slope may have resulted from an increase in permeability that was offset by a concomitant decrease in effective surface area brought about by derecruitment; the latter being the result of hypoxic induced vasoconstriction. It is to be noted, however, that vascular pressures were increased to 40 mmHg (Group II) or more (Group I). For derecruitment to occur with hypoxia, vasomotor tone must increase to an extent that would keep vessels closed despite these very high distending pressures. This is highly unlikely given the rather weak hypoxic vasoconstriction in anesthetized dogs (21). Furthermore, because hydrostatic pressure, in our preparation, is increased to the same extent both upstream and downstream from the filtration site, for derecruitment to occur vasoconstriction of this extent must involve both arteries and veins.

Consequently, with the exception of the study of Parker et al. (20), our results suggest that the reported increases in lung lymph flow or $\Delta W/\Delta t$ with hypoxia were likely the result of changes in microvascular pressure. There are several potential explanations for the difference between our results (no apparent change in permeability) and those of Parker et al. (20), obtained in isolated (*ex vivo*) lobes. First, in using near static conditions our preparation lends itself to a more precise estimate of true filtration pressure regardless of hypoxic induced shifts in vascular tone. Second, Drake et al. (9) have demonstrated major differences in the filtration characteristics between *in situ* and isolated lobes. Isolated lobes begin to accumulate edema at much lower vascular pressures than *in situ* lobes. As well the pattern of edema formation in isolated lobes, at a given pressure, is exponential rather than constant as in *in situ* lobes. It is thus possible that isolated lobes are more susceptible to hypoxia. Third, in our preparation the lobe was perfused with blood that was withdrawn from the animal continuously and pulmonary venous blood was returned to the animal. In the study of Parker et al. (20) the blood used for perfusion recirculated. It is possible, therefore, that accumulating metabolites render the lobe more sensitive to hypoxia. Finally, our lobes had an intact bronchial circulation, perfused with well oxygenated blood, whereas isolated lobes are devoid of bronchial flow. It is possible that

bronchial-pulmonary collateral flow precluded the attainment of sufficiently low P_{O_2} at the microcirculation level in our preparation. This possibility can be discounted for several reasons. First, it is well established (and confirmed in our preparation) that bronchial-pulmonary collateral flow is abolished or reversed at the pulmonary vascular pressures used in the present study (1, 8). Second, the extremely high ventilation/perfusion ratio used in our preparation (≈100:1) dictates that $P_{A}O_2$ and microvascular blood P_{O_2} must be almost equal to inspired P_{O_2}. The addition of a small amount of bronchial flow (≈5 ml/min at the most) upstream from the microcirculation would not materially alter the ventilation/perfusion ratio or P_{O_2} at the microcirculation level. This has been confirmed directly in several dogs by measuring a P_{O_2} of 2-3 mmHg in pulmonary vein blood when the lobe was ventilated with $F_{I}O_2$ of zero. On the other hand, if the increased permeability in the study of Parker et al. (20) occurred at the airway epithelium level (as opposed to microcirculation) then the persistence of O_2 supply to airway walls, in our preparation, might have prevented this from happening. Further studies are needed to identify the reasons for the different responses of *in situ* and isolated dog lungs.

We conclude that alveolar hypoxia has no effect on either the threshold pressure for edema formation or on the relationship between rate of edema formation and microvascular pressure in canine lung lobes studied *in situ*.

F. REFERENCES

1. Auld, P.A.M., A.M. Rudolph, and R.J. Golinko. Factors affecting bronchial collateral flow in the dog. *Am. J. Physiol.* 198:1166-70, 1960.

2. Beznák, A.B.L., and G. Liljestrand. The effect of variations in oxygen tension on the lymph flow. *Acta Physiol. Scand.* 19:170-186, 1949.

3. Bland, R.D., R.H. Demling, S.L. Selinger, and N.C. Staub. Effects of alveolar hypoxia on lung fluid and protein transport in unanesthetized sheep. *Circ. Res.* 40:269-274, 1977.

4. Boonyaprakob, U., P.M. Taylor, D.W. Watson, V. Waterman, and E. Lopata. Hypoxia and protein clearance from the vascular beds of adult dogs and pups. *Am. J. Physiol.* 216:1013-1019, 1969.

5. Craven, K.D., L. Oppenheimer, and L.D.H. Wood. Effects of contusion and flail chest on pulmonary perfusion and oxygen exchange. *J. Appl. Physiol.* 47:729-737, 1979.

6. Dawson, C.A. Role of vasomotion in physiology of the lung. *Physiol. Rev.* 64(2):544-616, 1984.

7. Dawson, C.A., D.J. Grimm and H.J. Linehan. Influence of hypoxia on the longitudinal distribution of vascular resistance. *J. Appl. Physiol.* 44:493-498, 1978.

8. Deffebach, M.E., N.B. Charan, S. Lakshminarayan, and J. Butler. The bronchial circulation, small, but a vital attribute of the lung. *Am. Rev. Respir. Dis.* 135:463-481, 1987.

9. Drake, R.E., J.H. Smith, and J.C. Gabel. Estimation of the filtration coefficient in intact dog lungs. *Am. J. Physiol.* 283(Heart Circ. Physiol. 7):H430-H438, 1980.

10. Gibbon, J.H. Jr., and M. H. Gibbon. Experimental pulmonary edema following lobectomy and plasma infusion. *Surgery.* 12:694-704, 1942.

11. Hackett, P.H., C.E. Creagh, and R.F. Grover. High altitude pulmonary edema in persons without the right pulmonary artery. *N. Engl. J. Med.* 302:1070-1073, 1980.

12. Hales, C.A., E.T. Rouse, J.L. Slate. Influence of aspirin and indomethacin on variability of alveolar hypoxic vasoconstriction. *J. Appl. Physiol.* 45:33-39, 1978.

13. Hultgren, H.N. High altitude pulmonary edema in: Staub N.C. ed. lung water and solute exchange. New York: Marcel Dekker, 437-469, 1978.

14. Hultgren, H.N., R.F. Grover, and L.H. Hartly. Abnormal circulatory response to high altitude in subjects with a previous history of high altitude pulmonary edema. *Circulation.* 44:759-770, 1971.

15. Kinazewitz, G.T., L.J. Groome, R.P. Marshall, W.K. Leslie, and J.N. Diana. The effect of hypoxia on permeability of pulmonary endothelium of canine visceral pleura. *J. Appl. Physiol.* 61(2):554-560, 1986.

16. Landolt, C.C., M.A. Mathay, K.H. Albertine, P.J. Roos, J.P. Wiener-Kronish, and N.C. Staub. Overperfusion, hypoxia, and increased pressure cause only hydrostatic pulmonary edema in anesthetized sheep. *Circ. Res.* 52:335-341, 1983.

17. Martin, D.J., F.A. Grimbert, P. Baconnier, and G. Benchetrit. Effect of acute hypoxia on lung transvascular filtration in anesthetized dogs. *Clin. Respir. Physiol.* 19:7-11, 1983.

18. Mitzner, W., and J.T. Sylvester. Hypoxic vasoconstriction and fluid filtration in pig lungs. *J. Appl. Physiol.* 51(5):1065-1071, 1981.

19. Morris, A.W., R.E. Drake, and J.C. Gabel. Comparison of microvascular filtration characteristics in isolated and intact lungs. *J. Appl. Physiol.* 48:438-443, 1980.

20. Parker, R.E., D.N. Granger, and A.E. Taylor. Estimates of isogravimetric capillary pressures during alveolar hypoxia. *Am. J. Physiol. (Heart Circ. Physiol.)* 10:H732-H739, 1981.

21. Peak, M.D., A.L. Harabin, N.J. Brennan, and J.T. Sylvester. Steady-state vascular responses to graded hypoxia in isolated lungs of five species. *J. Appl. Physiol.* 51:1214-1219, 1981.

22. Peterson, B.T., R.W. Hyde, M.C. Petrini, V. Lam, and B.F. Shreiner. Effect of acute hypoxia on airway and vascular exchangeable water spaces in dogs. *Am. Rev. Respir. Dis.* 129:772-779, 1984.

23. Roy, S.B., S.B. Guleria, and P.K. Khanna. Haemodynamic studies in high altitude pulmonary edema. *Br. Heart J.* 31:52-58, 1969.

24. Sylvester, J.T., A.L. Harabin, M.D. Peak, and R.S. Frank. Vasodilator and constrictor responses to hypoxia in isolated pig lungs. *J. Appl. Physiol.* 49:820-825, 1980.

25. Warren, M.F., D.K. Peterson, and C.K. Drinker. The effects of heightened negative pressure in the chest, together with further experiments upon anoxia in increasing the flow of lung lymph. *Am. J. Physiol.* 137:641-648, 1942.

26. Viswanathan, R., S. Subramanian, S.T.K. Lodi. Further studies on pulmonary edema of high altitude: Abnormal responses to hypoxia of men who had developed pulmonary edema of high altitude. *Respiration.* 36:216-222, 1978.

27. Weiskopf, R.B., and V.W. Severinghaus. Diffusing capacity of the lung for carbon monoxide in man during acute acclimation to 14,246 ft. *J. Appl. Physiol.* 32:285-289, 1972.

28. West, J.B. Diffusing capacity of the lung for carbon monoxide at high altitude. *J. Appl. Physiol.* 17:421-426, 1962.

29. Wiener-Kronish, J.P., V.C. Broadus, M.A. Gropper, K.A. Albertine, and Staub. Evidence for visceral pleural inflammation using a plastic bag to collect liquid. *Fed. Proc.* 46(4):1424, 1987 (*Abstract*).

V. CHAPTER 4

ARTERIAL OCCLUSION VERSUS ISOFILTRATION PULMONARY CAPILLARY PRESSURES DURING VERY HIGH FLOW

A. BACKGROUND

Vascular occlusion techniques have recently emerged as powerful tools in studying the mechanical properties of the pulmonary circulation (2, 8-15, 18, 19). Results of vascular occlusion have indicated that the pulmonary circulation (at least beyond the origin of lobar arteries) behaves as if it is composed of a middle segment, with relatively high compliance and low resistance, interposed between two low compliance high resistance segments (9). The pressure in the middle compartment can be determined by observing the pressure transients following occlusion of the artery, vein, or both (8, 9). Responses to various pharmacologic and physical manipulations, with known action sites, have indicated that the compliant middle segment is anatomically located somewhere between muscular arteries and muscular veins (9-11, 13). The precise localization of the compliant middle compartment within this broad region is not known.

The anatomical extent of the fluid filtration site has also not been established with certainty. However, it is evident that the fluid filtration site must also be located within the region between muscular arteries and muscular veins.

The anatomic relation between the filtration site and the site of major compliance within this intermediate region is of considerable practical and theoretical interest. There is no

compelling reason, in theory, why sites of major compliance and filtration should be the same. The physical properties that endow a segment with a large share of total compliance (relative volume and wall distensibility) are quite different from those that allow a vascular segment to function as a major site of filtration (surface area and membrane permeability). Yet, studies in which pressures within the middle compliant segment (measured by occlusion) and within the filtration site (measure by gravimetric techniques) were compared have shown good agreement (12, 18, 19).

While agreement between occlusion and gravimetric measurements is consistent with the notion that sites of major compliance and major filtration are the same, other explanations are possible. The filtration site may be anatomically separated from the highly compliant site by a relatively small resistance. At low flow rates, the pressures within the two would, thus, be very similar. It must be pointed out that in all studies in which occlusion and gravimetric techniques were directly compared under the same experimental conditions flow was either normal or below normal (18, 19). Given a normal arterial-venous (A-V) pressure difference of 6 to 10 mmHg, if muscular arteries, muscular veins, and intervening region (containing both high compliance and high filtration sites) contribute equally to total resistance, the pressure drop across the latter segment should be no more than 2 or 3 mmHg. Thus, the finding that occlusion and

gravimetric techniques are different by no more than 1 to 2 mmHg could still be consistent with the sites being located at entirely different points within this region. Furthermore, the small maximal anticipated pressure difference between the two techniques during normal flow (in the event the two sites are anatomically different) would be hard to detect, given the resolution of the two techniques.

B. HYPOTHESIS

We reasoned that if the filtration and the compliance sites are anatomically separate, a finite resistance, and hence a pressure gradient, must exist between them. Under conditions of extremely high flow this pressure gradient should expand sufficiently to be detectable as a difference between the results obtained by techniques that measure effective filtration pressure (EFP) and those that measure pressure in the compliant middle compartment (P_M). The present experiments were accordingly designed to compare P_M, measured by the arterial occlusion technique, and EFP, measured by a gravimetric (isofiltration) technique in an intact lobe preparation under conditions of very high flow (7 to 10 times normal).

C. METHODS

The experimental preparation used is similar to that described in CHAPTER 1. Only a brief description is given here.

Six mongrel dogs (mean weight 27 kg, range 19 to 37 kg) were anesthetized with intravenous sodium pentobarbital and ventilated with a dual Harvard pump (tidal volume 10-15 ml/kg, respiratory rate 10 breaths/min). An arterial line was inserted into the right carotid artery to monitor systemic blood pressure (BP). A 7F Swan-Ganz catheter was introduced into the right external jugular vein and advanced into the main pulmonary artery (PA).

A wide thoracotomy was performed in the left fifth intercostal space. Once the thoracic cavity was entered, 2.5 cmH_2O of positive end-expiratory pressure (PEEP) was added. The left lower lobe (LLL) PA was ligated at its entrance into the lobe and cannulated immediately proximal to the ligature. A catheter was passed through one of the tributaries of the LLL veins into the left atrium (LA) to monitor LA pressure. The LLL was then excised. LLL bronchus was cannulated with a Y tube. One arm of the Y was connected to the second barrel of the dual Harvard pump while the other arm was used to introduce a Fogarty balloon catheter to the level of the left main stem bronchus. When the balloon was inflated, it was possible to ventilate the right lung and the left upper lobe (LUL) separately. In all 6 dogs the LUL was ventilated with tidal volumes generating static

end-inspiratory airway pressures of 7.5 cmH_2O with *base line* end-expiratory pressures of 2.5 cmH_2O. Mean (±SD) airway pressure for all 6 dogs was 4.5 ± 0.5 cmH_2O. The right lung was ventilated with air while the LUL was ventilated with 5% CO_2 in O_2. In this fashion LUL alveolar gas tensions are independent of the level of ventilation or blood flow. PEEP was 2.5 cmH_2O for both sides.

A number 9 endotracheal tube was introduced into the LA through the LA appendage. At this time, the animal was fully heparinized.

The stem of a Y cannula (7 mm I.D.) was attached to the cannula in the LLL artery. One arm of the Y tube was connected to the LA cannula using a tygon tube primed with saline and mounted on a Cobe-Stöckert roller pump. This system was used to perfuse the LUL from the LA. The other arm of the Y cannula contained a catheter equipped with an intravascular occlusive device (for details see CHAPTER 1). This catheter was advanced to the level of the left main PA, upstream from the LUL artery, and the left main PA was occluded. At this point, perfusion to the LUL was initiated at a rate calculated to be equivalent to normal LUL flow (12 ml/min/kg (3)). Inflow PA pressure was monitored through an orifice in the left PA catheter, located proximal to the occlusive device.

The LUL was suspended from a force transducer for continuous monitoring of lobar weight (for details of suspension technique see CHAPTER 1). Lobar weight was always measured at end-expiration.

All pressure lines (systemic BP, left PA pressure, right PA pressure, and LA pressure) were connected to appropriate pressure transducers and zeroed at the level of the LUL pulmonary veins as they enter the LA. Continuous recording to these pressures along with lobar weight, was maintained throughout the study on a 6-channel Gould chart recorder.

D. PROTOCOL

After all variables stabilized, flow was increased, in a step fashion, to a value corresponding to 7-10 times normal blood flow to LUL (2.1 - 4.0 l/min). The increased flow was maintained for 4 minutes. Flow was then returned to *base line*. As shown earlier (CHAPTER 1), when flow is increased to these levels, lobar weight undergoes an immediate step increase, presumably reflecting an increase in blood volume, followed by a progressive weight gain at a constant rate. In four of the animals the response to two flow rates, within the above range was tested. In two more animals a single flow rate was obtained. A minimum of two observations at each flow rate were made.

Following the determination of weight changes, flow was increased to the same levels used earlier and, once vascular pressure stabilized (usually in less than 1 minute), the inflow tubing was suddenly clamped for 1-2 seconds. During this period pump flow was diverted to a reservoir and paper speed was 25 mm/sec. Several occlusions were carried out at each flow rate.

At the end of the dynamic measurements, snares were placed around the two LUL veins as they entered the pericardium. Pump flow was stopped and the snares were tightened. A reservoir, primed with the dog's blood and connected to the left PA inflow tube, was used to produce edema statically. Edema was produced by raising the reservoir level from a *base line* of 7 to 10 mmHg to varying degrees of pulmonary vascular pressure for a period of about 4 minutes. Between observations the reservoir level was returned to *base line*. A minimum of 8 observations were made.

Blood gases and hematocrit were drawn at random throughout the experiment to make sure that no major drop in hematocrit or pH occurred. We have shown earlier that the relation between vascular pressure and $\Delta W/\Delta t$ does not change over the period of static measurements. The possible reasons for this constant behavior in our preparation (despite the anticipated hemoconcentration) have been discussed (see Footnote 2, CHAPTER 1).

Estimation of EFP. The approach used to estimate the hydrostatic pressure at the filtration site, EFP, is a modified approach of that developed by Gabel et al. (7). The rate of weight increase beyond the first minute of step increase in flow ($\Delta W/\Delta t$) was calculated and the average value of all determinations (in the same animal) at the same flow was computed. Next, $\Delta W/\Delta t$ for the various pressures during the static measurements were measured and the data were fitted by linear regression analysis ($\Delta W/\Delta t$ vs. static pressure). EFP, in the presence of flow, was estimated from the static pressure that resulted in the same $\Delta W/\Delta t$ as observed during the dynamic state. An example of this method for one dog is shown in Figure 1. Having obtained EFP, it was possible to calculate the pressure drop upstream of the filtration site (difference between left PA pressure and EFP, ΔP_{us}), downstream pressure drop (difference between EFP and LA pressure, ΔP_{ds}), and the upstream and downstream resistances ($\Delta P_{us}/\dot{Q}$ and $\Delta P_{ds}/\dot{Q}$, R_{us} and R_{ds}, respectively).

Estimation of P_M. As reported previously (9), when the inflow tubing was occluded, PA pressure initially decreased rapidly, followed by a slow decline towards LA pressure. An example of this method is shown in Figure 2. PA pressure was measured at 40 msec intervals beyond the phase of rapid drop. The best fit exponential function (at $p<0.001$) was obtained according to the following equation:

$$Y = A \cdot e^{-BX} + C$$

where Y and X are PA pressure and time, respectively; A is a constant; B is the reciprocal of the time constant; and C is the asymptote pressure value. P_M at time of occlusion (t=0) was taken as the sum of A and C. P_M obtained by this technique represents the pressure at the upstream end of the middle compartment.

All P_M values obtained at a given flow in each experiment were averaged. These values were compared to the EFP values obtained under the same conditions by the paired t-test.

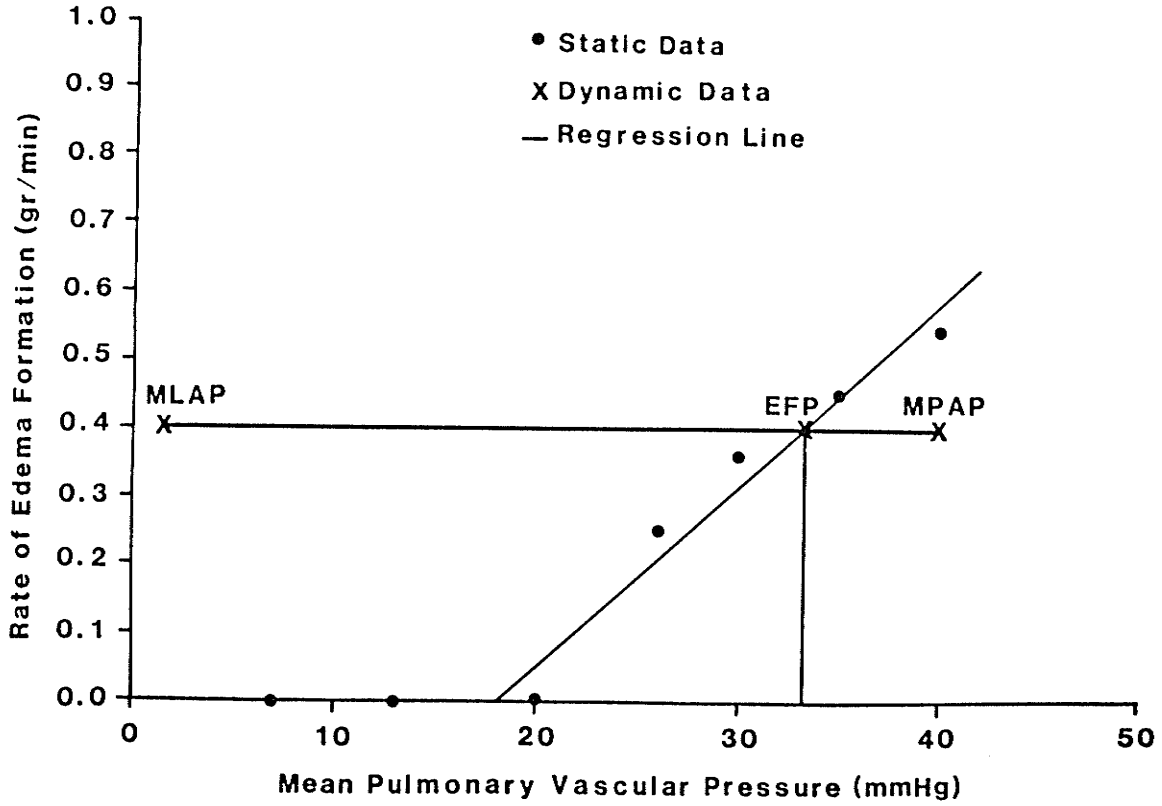

FIGURE 1: Method of EFP estimation. EFP was considered as the point of intersection between the regression line obtained from the static data and a horizontal line drawn between mean pulmonary artery pressure (MPAP) and mean left atrial pressure (MLAP) for a specific flow (at the level of the observed rate of edema formation).

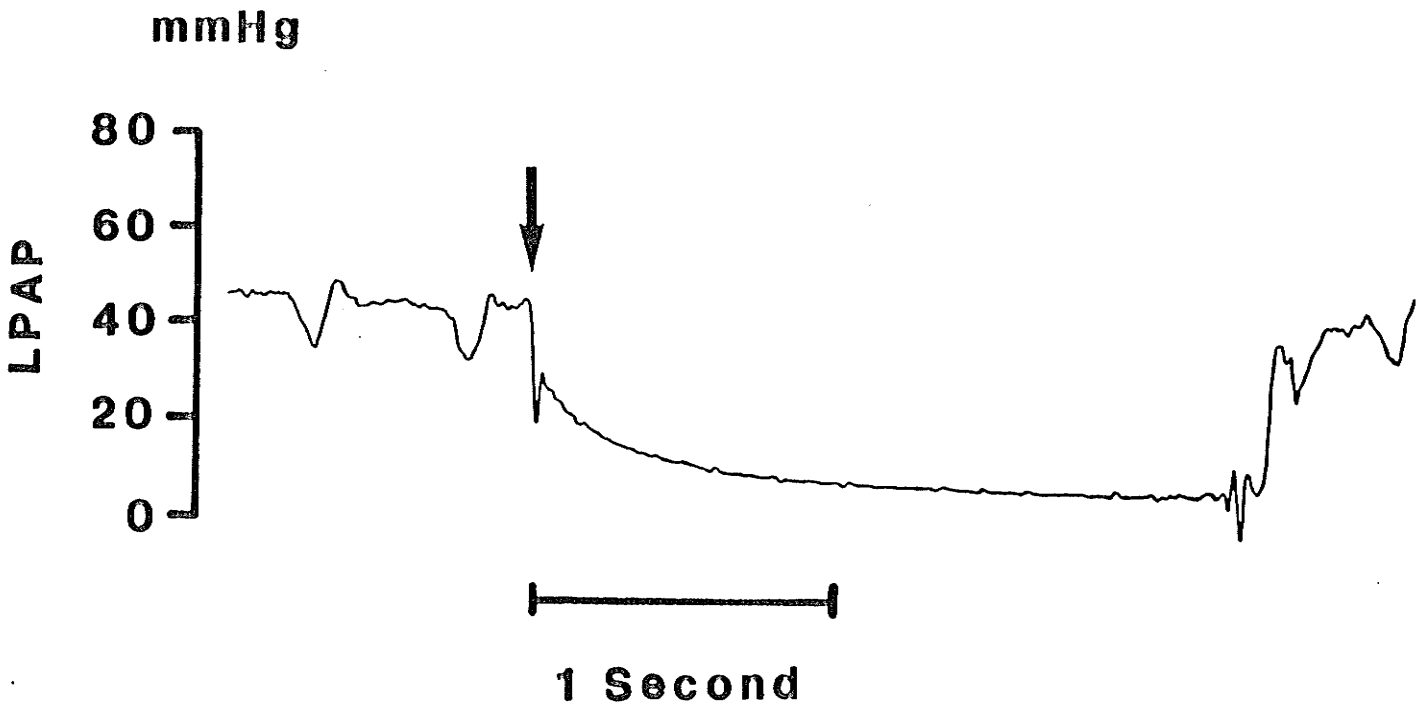

FIGURE 2: An example of changes in left pulmonary artery pressure (LPAP) following arterial occlusion (arrow).

TABLE 1. *Hemodynamic data obtained in six dogs*

Dog No.	Flow, l/min	EFP, mmHg	P_M, mmHg	ΔPus, mmHg		ΔPds, mmHg		Rus, %		Rds, %	
				I	AO	I	AO	I	AO	I	AO
1	2.1	27.5	26.9	17.5	18.1	27.5	26.9	38.9	40.2	61.1	59.8
	2.4	27.5	22.6	22.5	25.4	27.5	22.6	45.0	52.9	55.0	47.1
2	3.5	28.5	31.4	7.5	8.6	21.5	26.9	25.9	24.2	74.1	75.8
	4.0	31.3	34.5	7.7	6.5	24.3	30.0	24.1	17.8	75.9	82.2
3	3.0	33.3	30.0	8.7	9.0	31.8	30.0	21.6	23.1	78.4	76.9
	3.5	41.8	33.5	5.2	8.5	40.3	32.1	11.5	20.9	88.5	79.1
4	3.5	25.5	27.1	6.5	4.9	22.2	25.1	22.6	16.3	77.4	83.7
	4.0	29.3	28.0	5.7	7.0	26.0	26.0	18.0	16.3	82.0	78.8
5	3.0	36.0	34.5	14.0	13.5	36.0	34.5	28.0	28.1	72.0	71.8
6	2.5	42.1	40.1	3.9	5.9	39.1	37.1	9.1	13.7	90.9	86.3
Mean ± SE	3.15±0.21	32.3±1.9	30.9±1.6	9.9±1.9	10.7±2.1	29.6±2.2	29.1±1.4	24.5±3.5	25.4±3.9	75.5±3.5	74.2±3.8

EFP, effective filtration pressure; P_M, pressure obtained by arterial occlusion; ΔP_{us}, upstream pressure drop; ΔP_{ds}, downstream pressure drop; R_{us}, upstream resistance; R_{ds}, downstream resistance; I, determined by the isofiltration technique; AO, determined by the arterial occlusion technique.

E. RESULTS

Table 1 shows the hemodynamic measurements and derived data for all 10 observations (2 flow rates in 4 dogs and one flow rate in two dogs).

The average lobar flow during the comparisons was (mean ± SE) 3.15 ± 0.21 l/min, representing about 10 times normal flow to this lobe. The corresponding PA and LA pressures were 41.9 ± 1.3 and 2.5 ± 0.5 mmHg, respectively. There was no significant difference (P = 0.24) between EFP (32.3 ± 1.9 mmHg) and P_M (30.9 ± 1.6 mmHg) determined by arterial occlusion. As a result, there was also no significant difference between the two methods in estimates of ΔP_{us}, ΔP_{ds}, or the fractions of total resistance contributed by upstream (R_{us}) and downstream (R_{ds}) segments (Table 1).

The phase of rapid decline in PA pressure after occlusion was complete in less than 40 msec in all cases. The time constant of the slow phase of decline averaged (± SE) 0.326 ± 0.067 sec.

F. DISCUSSION

Agreement between pulmonary microvascular pressure measured by occlusion techniques (P_M) and effective filtration pressure (EFP), measured by gravimetric techniques, has been demonstrated in several previous studies (4, 18, 19). The present study differs from previous comparisons in three respects:

1. It is the first study in which results of arterial occlusion were compared to gravimetric measurements done in the same preparation. Of the three occlusion techniques (arterial, venous or double) only arterial occlusion is suitable for use in closed chest preparations, and hence in clinical settings. Previous studies showed agreement with venous or double occlusion techniques (4, 18, 19). In the only study which attempted to evaluate the agreement between filtration pressure and arterial occlusion (12), filtration pressure was not measured. Rather, it was estimated based on an assumed distribution of pulmonary vascular resistance (R_{us}/R_{ds}=60/40) established by Gaar et al. (6) in different experiments. Although the range of pressures was comparable in the two studies, Holloway et al. (12) utilized an intact preparation whereas the equation of Gaar et al. (6) was obtained in isolated (in vitro) lobes.

2. We compared the results of the two techniques in the presence of extremely high flow rates. In all previous studies of this nature blood flow was near normal. As indicated in

"Introduction", comparison under very high flow conditions is a more severe test of the possibility that the filtration and compliance sites may be anatomically separate.

3. This is also the first study in which direct comparisons were made in intact lobes. With the exception of the study of Holloway et al. (12), all previous comparisons were carried out in isolated, in vitro, lobes. The two types of preparations differ considerably, at least in their filtration characteristics (16), and it is not clear whether filtration site is the same under both conditions.

The demonstration that the two techniques continue to provide the same results under these very different conditions provides further support to the notion that the sites of filtration and major relative compliance are intimately related (4, 17-19) and that, as advocated by Townsley et al. (19) and by Cope et al. (2), the occlusion technique can be used for rapid, convenient and accurate estimation of effective filtration pressure under clinical and experimental circumstances.

EFP measured by the isofiltration technique reflects the pressure at the midpoint of the filtration site. In the presence of a significant longitudinal pressure gradient along the filtration site, more than half the filtration must occur upstream from the point where pressure is reflected by EFP. On the other hand, P_M determined by arterial occlusion provides the pressure at the upstream end of the middle compliance segment.

The agreement between EFP and P_M therefore must have implications with respect to the anatomical relation between filtration site and the middle compliant segment. If there is a significant longitudinal pressure gradient along either the filtration site or the site of major compliance, then the filtration site must be astride the upstream end of the middle compliant compartment. On the other hand, if there are no pressure gradients along either site, our data would suggest that filtration takes place entirely within the site of major compliance. Interpretation, accordingly, depends on whether significant longitudinal pressure gradients exist along these segments.

Estimates of the pressure drop along the microvasculature vary greatly depending on the method used and the experimental conditions (for review see 5). Values range from as little as 10% or less (9-11, 13, 15) to as high as 46% (1). The results of Hakim et al. (9-11, 13, 15) are of specific relevance to the present study. These authors measured the pressure drop along the middle compliant segment (ΔP_M) by comparing results of venous and arterial occlusions. At normal flow rates and alveolar pressure, ΔP_M was 1-2 mmHg, representing about 10% of the total pressure drop (9-11, 13, 15). However, and as might be expected from highly compliant vessels, ΔP_M changed little (actually decreased slightly) as flow rate was doubled implying that the decrease in resistance, as a result of dilatation, offsets the increase in flow (9, 15). If this behavior continues into the

very high flow range used in the present study, ΔP_M must have been very small. In this event it would be unlikely that the filtration site is astride the upstream end of the compliant middle segment since, in this case, part of the filtration site would be characterized by high compliance and low resistance while the other part (that upstream from the middle compartment) would be poorly compliant. It is difficult to envision such disparate mechanical properties existing within a vascular segment that subserves a common function, namely filtration. Our data, therefore, suggests that the filtration site lies entirely within the middle compliant compartment.

We have shown in CHAPTER 1 that the fraction of total resistance contributed by the vascular segment downstream from the filtration site (i.e. R_{ds}/R_{tot}) increases progressively as a function of flow. At flow rates comparable to those used in the present study R_{ds} contributed in excess of 75% of total resistance. The present results (Table 1) obtained in a totally different group of animals, are in keeping with those shown earlier. Furthermore, the confirmation of this resistance distribution using an entirely different technique (occlusion) adds more support to the conclusion that at very high flow rates, pressure in the microvasculature is much closer to PA pressure than it is to left atrial pressure. The possible mechanisms underlying this change in resistance distribution with high flow have been already discussed (CHAPTER 1).

G. REFERENCES

1. Bhattacharya, J. and N.C. Staub. Direct measurement of microvascular pressures in isolated perfused dog lung. *Science*, 210:327-328, 1980.

2. Cope, D.K., R.C. Allison, J.L. Parmentier, J.N. Miller and A.E. Taylor. Measurement of effective pulmonary capillary pressure using the pressure profile after pulmonary artery occlusion. *Crit. Care Med.*, 14(1):16-22, 1986.

3. Craven, K.D., L. Oppenheimer and L.D.H. Wood. Effects of contusion and flail chest on pulmonary perfusion and oxygen exchange. *J. Appl. Physiol.* 47:729-737, 1979.

4. Dawson, C.A., J.H. Linehan and D.A. Rickaby. Pulmonary microcirculatory hemodynamics. *Ann. NY Acad. Sci.*, 384:90-106, 1982.

5. Dawson, C.A. Role of pulmonary vasomotion in physiology of the lung. *Physiol. Reviews*, 64(2):544-616, 1984.

6. Gaar, K.A., A.E. Taylor, L.J. Owens and A.C. Guyton. Pulmonary capillary pressure and filtration coefficient in the isolated perfused lung. *Am. J. Physiol.*, 213:910-914, 1967.

7. Gabel, J.C. and R.E. Drake. Pulmonary capillary pressure in intact dog lungs. *Am. J. Physiol.*, 235(4):H569-H573, 1978.

8. Hakim, T.S., C.A. Dawson and J.H. Linehan. Hemodynamic responses of dog lung lobe to lobar venous occlusion. *J. Appl. Physiol.*, 47(1):145-152, 1979.

9. Hakim, T.S., R.P. Michel and H.K. Chang. Partitioning of pulmonary vascular resistance in dogs by arterial and venous occlusion. *J. Appl. Physiol.*, 52(3):710-715, 1982.

10. Hakim, T.S., R.P. Michel and H.K. Chang. Effect of lung inflation on pulmonary vascular resistance by arterial and venous occlusion. *J. Appl. Physiol.*, 53(5):1110-1115, 1982.

11. Hakim, T.S., R.P. Michel, H. Minami and H.K. Chang. Site of pulmonary hypoxic vasoconstriction studied with arterial and venous occlusion. *J. Appl. Physiol.*, 54(5):1298-1302, 1983.

12. Holloway, H., M. Perry, J. Downey, J. Parker and A. Taylor. Estimation of effective pulmonary capillary pressure in intact lungs. *J. Appl. Physiol.*, 54(3):846-851, 1983.

13. Julien, M., T.S. Hakim, R. Vahi and H.K. Chang. Effect of hematocrit on vascular pressure profile in dog lungs. *J. Appl. Physiol.*, 58(3):743-748, 1985.

14. Linehan, J.H., C.A. Dawson and D.A. Rickaby. Distribution of vascular resistance and compliance in a dog lung lobe. *J. Appl. Physiol.*, 53(1):158-168, 1982.

15. Michel, R.P., T.S. Hakim and H.K. Chang. Pulmonary arterial and venous pressures measured with small catheters in dogs. *J. Appl. Physiol.*, 57(2):309-314, 1984.

16. Morriss, A.W., R.E. Drake and J.C. Gabel. Comparison of microvascular filtration characteristics in isolated and intact lungs. *J. Appl. Physiol.*, 48(3):438-443, 1980.

17. Pappenheimer, J.R. and A. Soto-Rivera. Effective osmotic pressure of the plasma proteins and other quantities associated with the capillary circulation in the hindlimbs of cats and dogs. *Am. J. Physiol.*, 152:471-491, 1948.

18. Parker, J.C., P.R. Kvietys, K.P. Ryan and A.E. Taylor. Comparison of isogravimetric and venous occlusion capillary pressures in isolated dog lungs. *J. Appl. Physiol.*, 55(3):964-968, 1983.

19. Townsley, M.I., R.J. Korthuis, B. Rippe, P.C. Parker and A.E. Taylor. Equivalence of isogravimetric capillary pressures obtained by gravimetric and double vascular occlusion methods on lung and skeletal muscle. *J. Appl. Physiol.*, 61(1):127-132, 1986.

VI. CHAPTER 5

DISTENSIBILITY AND PRESSURE-FLOW RELATIONSHIP OF THE PULMONARY CIRCULATION. I. SINGLE VESSEL MODEL.

A. BACKGROUND

The response of the pulmonary circulation to changes in hydrostatic pressure at either end is quite distinctive. At a fixed left atrial pressure (P_{LA}), increases in pulmonary artery pressure (P_{PA}) result in a non-linear increase in flow (F) with the relation (F against P_{PA}) being convex to the P_{PA} axis. Beyond a certain P_{PA}, the pressure-flow (P-F) relationship becomes linear. The extrapolated pressure intercept of this linear segment (termed opening pressure, P_{OP}) is often higher than P_{LA} (1, 6, 8, 12, 22, 27). Also, at a fixed F, raising P_{LA} from a low level initially elicits smaller changes in P_{PA}. Thereafter, the ratio of change in P_{PA} (ΔP_{PA}) over the step change in P_{LA} (ΔP_{LA}), i.e. $\Delta P_{PA}/\Delta P_{LA}$ (Z), increases progressively with increasing P_{LA} approaching unity at higher P_{LA} levels (5, 7, 17, 19, 24, 30).

Two mechanisms have been entertained to account for this characteristic behavior (see *ref.* 21 for discussion). Firstly, a critical opening pressure (P_{crit}) exists at some point along the length of parallel pathways. The site of this critical closure is generally believed to be either alveolar vessels (17, 24, 29) or vessels with high vasomotor tone (12, 20, 22). When P_{LA} is less than P_{crit}, P_{crit} becomes effective downstream pressure [zone 2 of West (31)] and P_{PA} is independent of P_{LA}. The initial non-linearity of the P-F relationship can thus be explained by

progressive opening of parallel channels causing a reduction in total resistance (R_T). That different channels require varying opening pressures (thereby explaining the progressive decrease in R_T over a finite pressure range as opposed to a single pressure point) may be attributed to gravity or non-homogeneous distribution of vascular tone or perivascular forces. The linear segment of the *P-F* relationship is thus the range over which all channels are open and R_T is fixed. By use of this explanation P_{op} is average P_{crit} of the parallel channels, each weighted in proportion to the conductance (% of total conductance) upstream from the sight of P_{crit}. The inverse slope of the linear segment is the fixed resistance of the fully recruited system. According to this analysis, failure of P_{PA} to rise to the same extent as P_{LA} can be attributed to some regions being in zone 2 (where P_{PA} is totally independent of P_{LA}) while others being in zone 3 [$P_{LA} > P_{crit}$ (2, 3, 25), where P_{PA} rises in a one to one relationship with P_{LA}]. In fact, according to this schema, *Z* may be used to ascertain the fraction of parallel channels in the two zones (e.g., *ref.* 3).

Secondly, the same behavior can be explained on the basis of vascular distensibility (21, 33). The linear and non-linear segments of the *P-F* relationship can result from an orderly decrease in vascular resistance (R_V) secondary to a progressive increase in distending pressure. That *Z* at a constant *F*, is less than unity can be explained by a drop in R_V (and hence, $P_{LA}-P_{PA}$)

as P_{LA} (and hence, distending pressure) increases. That Z increases as P_{LA} increases may be due to a non-linear relationship between distending pressure and Rv. For vascular distensibility, independent of P_{crit}, to account for the behavior of the pulmonary circulation, the mechanical behavior of the vessels must quantitatively and qualitatively fit certain criteria.

Since P_{crit} and vascular distensibility are both well documented (e.g. 9, 10, 15, 16, 18, 28), both mechanisms must contribute to the distinctive non-linear behavior of the pulmonary circulation. The extent to which each contributes to this behavior, under normal and pathologic conditions, is not known. This information is crucial to the understanding and interpretation of the response of the pulmonary circulation to various physiologic and pathophysiologic interventions. As it is difficult to isolate the two mechanisms in biologic experiments, it is necessary to rely on theoretical analysis. Fortunately, sufficient information about the mechanical properties of pulmonary vessels has accumulated to permit such analysis. This is the purpose of the next two chapters.

In CHAPTER 5, we give details on the derivation of the mathematical algorithms used to describe the dimensional changes of pulmonary arteries and veins, of the dog, in response to changes in transmural pressure (P_{TM}) and lung volume (V_L). This is based on information that is currently available in the

literature (15, 16, 18, 28). By adopting Poiseuille's law for flow of a Newtonian fluid in rigid tubes, and without other assumptions, we derive a model for steady blood flow in a single elastic vessel having average mechanical properties of pulmonary vessels. We then present and discuss the response of the model to changes in inflow and outflow pressures (P_{in} and P_{out}, respectively) with and without added tone. Since the derived algorithms were based on data obtained in the dog, the current model is representative of the pulmonary circulation in the dog.

In CHAPTER 6, we develop a multibranched model with arterial and venous channels, and intervening capillary sheets [modeled according to Fung and Sobin (9, 10, 11)]. Using the multibranched model, we address issues that could not be addressed with the single vessel model. In the multibranched model, forces acting on individual parallel units of the same generation can be varied independently. Hence, the model has the potential of assessing the effects of gravity and non-homogeneous distribution of vasomotor tone on *P-F* and P_{LA}-P_{PA} relationships of the total system.

B. METHODS

According to Poiseuille's law, resistance (R) of a rigid tube could be described by the following relation:

$$R = (8 \cdot \mu \cdot l)/\pi r^4 \qquad \ldots\ldots (1a)$$

or,

$$R = (8 \cdot \pi \cdot \mu \cdot l)/A^2 \qquad \ldots\ldots (1b)$$

where μ is viscosity, l and r are tube length and radius, respectively, and A is tube cross-sectional area. Justified by the data of Haynes and Burton (13), in the present analysis viscosity was treated as constant (i.e. independent of vessel radius and flow). Therefore, R of any vessel or segment of a vessel was treated as directly proportional to l and inversely proportional to A^2,

$$R = K \cdot (l/A^2) \qquad \ldots\ldots (2)$$

where K is a constant.

When considering an intralobar vessel, l was treated as an exclusive function of lung volume (V_L) which in turn is a function of transpulmonary pressure (P_{TP}) and lung compliance. "A" was modeled as a function of transmural pressure (P_{TM}) and the latter was calculated as:

$$P_{TM} = P_V - P_x \qquad \ldots\ldots (3)$$

where, P_V is intravascular pressure and P_X is perivascular pressure which in turn is a function of P_V and P_{TP} (see below). In the absence of smooth muscle tone, P_{TM} is equal to the passive pressure recoil of the vessel wall (P_{pas}).

In distensible and longitudinally stretchable vessels there is no unique value that can describe the resistance of the vessel under all conditions. Even if the vessel had perfectly uniform mechanical properties, the resistance of successive segments will vary on account of the longitudinal pressure gradient along the lumen. Furthermore, for a given luminal pressure, resistance will vary with the degree to which the vessel is longitudinally stretched. To circumvent this problem in the present analysis each vessel, or segment thereof, was assigned a reference resistance value which is offered by the vessel at a given l and P_{pas}. Resistance under all other conditions is expressed as a fraction of this reference resistance. Reference conditions were chosen to be a P_{pas} of 35 cmH_2O and l at a P_{TP} of zero. Reference resistance, which in our model is an independent input, is henceforth referred to as $R_{0,35}$. The choice of these particular P_{TP} and P_{pas} values as reference conditions was arbitrary and has no effect on the results. Thus,

$$R/R_{0,35} = (l/l_{0,35}) \cdot (A_{0,35}/A)^2 \qquad \ldots\ldots (4)$$

where $l_{0,35}$ and $A_{0,35}$ are the vessel's length and cross-sectional area, respectively, at reference conditions. $R_{0,35}$ is an expression of the basic structural properties of the vessel. A vessel that is small by virtue of its hierarchical position or high passive elasticity of its wall (as opposed to being small by virtue of a small P_{pas} or because of vasomotor tone) would have a large $R_{0,35}$ and vice versa.

1. Calculation of $l/l_{0,35}$

As indicated above, l was exclusively a function of V_L and, hence, P_{TP} and lung compliance. This relation was derived from the data of Smith and Mitzner (28). According to these authors, normalized vessel length [i.e. l/l_{max} = vessel length at any V_L as a fraction of vessel length at maximal (P_{TP} = 30 cmH_2O) lung volume (V_{Lmax})] was linearly related to the cube root of normalized lung volume [i.e. $(V_L/V_{Lmax})^{1/3}$] over the lobe volume interval $0.40 \cdot V_{Lmax}$ to V_{Lmax}, for both arteries and veins (*Ref.* 28, Figures 6A and 6B, respectively). The relationship did not differ from unity and in the present analysis was assumed equal to unity. Thus,

$$l/l_{max} = (V_L/V_{Lmax})^{1/3} \qquad \ldots\ldots (5a)$$

Below $0.40 \cdot V_{Lmax}$, l/l_{max} did not vary considerably and was assumed constant. As a result, normalized vessel length at a P_{TP} of zero (i.e. $l_{0,35}/l_{max}$) is equal to:

$$l_{0,35}/l_{max} = [(0.40 \cdot V_{Lmax})/V_{Lmax}]^{1/3} \quad . \ . \ . \ . \ (5b)$$

or 0.7368.

The relation between (V_L/V_{Lmax}) and P_{TP} can be adequately described by the following relation,

$$V_L/V_{Lmax} = 1-B \cdot e^{-(C_L \cdot P_{TP})} \quad . \ . \ . \ . \ . \ (6)$$

where "B" is the volume decrement below V_{Lmax} at $P_{TP} = 0$ [i.e. 1 minus minimal volume (V_M) as a fraction of V_{Lmax}] and C_L is a constant describing the fractional volume change, of the pressure-volume curve, per unit pressure change (14). Large values for C_L are associated with sharply arched deflation curves (more compliant lungs) and small values for C_L with moderately arched deflation curves (stiffer lungs). Initial values for V_M and C_L of 0.10 and 0.25, respectively, typifying normal lungs were used in this study.

In order to normalize vessel length to $l_{0,35}$, equation 5a was divided by 0.7368. By substituting equation 6, and replacing "B" with $(1-V_M)$ the following relation was derived:

$$l/l_{0,35} = \frac{\left[1-(1-V_M)\cdot e^{-(C_L\cdot P_{TP})}\right]^{1/3}}{0.7368} \quad \ldots\ldots (7)$$

For $l/l_{0,35} < 1$ [i.e. at $(V_L/V_{Lmax}) \leq 0.4$], the ratio was taken as 1.

2. Calculation of $A/A_{0,35}$

Since A is a function of P_{pas} and the latter is importantly determined by P_x, it is necessary to estimate P_x under the various experimental conditions in order to obtain $A/A_{0,35}$.

P_x is influenced by P_v and by P_{TP} (15, 28). The relation between P_x and P_v at various transpulmonary pressures was also derived from data provided by Smith and Mitzner (*Ref.* 28, Figures 11A and 11B). P_x-P_{pl}, P_{pl} being pleural pressure, was re-plotted as a function of P_v-P_{pl} for the various P_{TP} values, for both arteries and veins. The results are shown in Figures 1A and 1B, respectively. The curves appeared to asymptote at higher vascular pressures and therefore, asymptotic regression lines of the form,

$$P_x-P_{pl} = a+b\cdot e^{c\cdot(P_v-P_{pl})} \quad \ldots\ldots (8)$$

were sought. Parameters "a", "b", and "c", on the other hand, varied linearly with P_{TP}. Linear regressions relating these parameters to P_{TP} were therefore obtained ($a = +15.0-0.2\cdot P_{TP}$,

$b = -16.0-0.2 \cdot P_{TP}$, $c = -0.013-0.0003 \cdot P_{TP}$ for arteries, and $a = +12.0-0.1 \cdot P_{TP}$, $b = -12.0-0.2 \cdot P_{TP}$, $c = -0.020-0.0003 \cdot P_{TP}$ for veins). Using this approach, for any P_{TP}, parameters "a", "b", and "c" could be calculated and subsequently P_x at any P_V could be derived. The agreement between these equations and the actual data is shown by the dotted lines in Figures 1A and 1B.

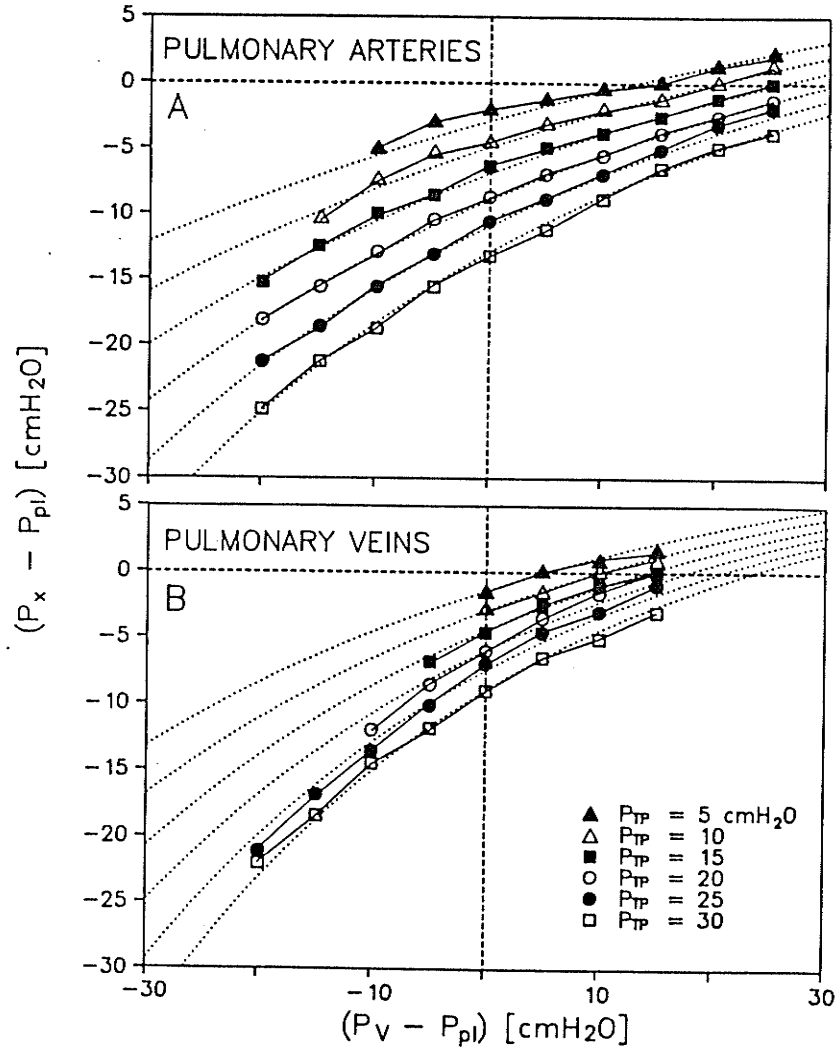

FIGURE 1. Perivascular pressure (P_x) as a function of intravascular pressure P_V at various transpulmonary pressures (P_{TP}), for both arteries (*panel A*) and veins (*panel B*). P_{pl}, is pleural pressure. Dotted lines represent the results of the regression analysis, according to equation 8, using the appropriate values of the constants a, b, and c mentioned in the text.

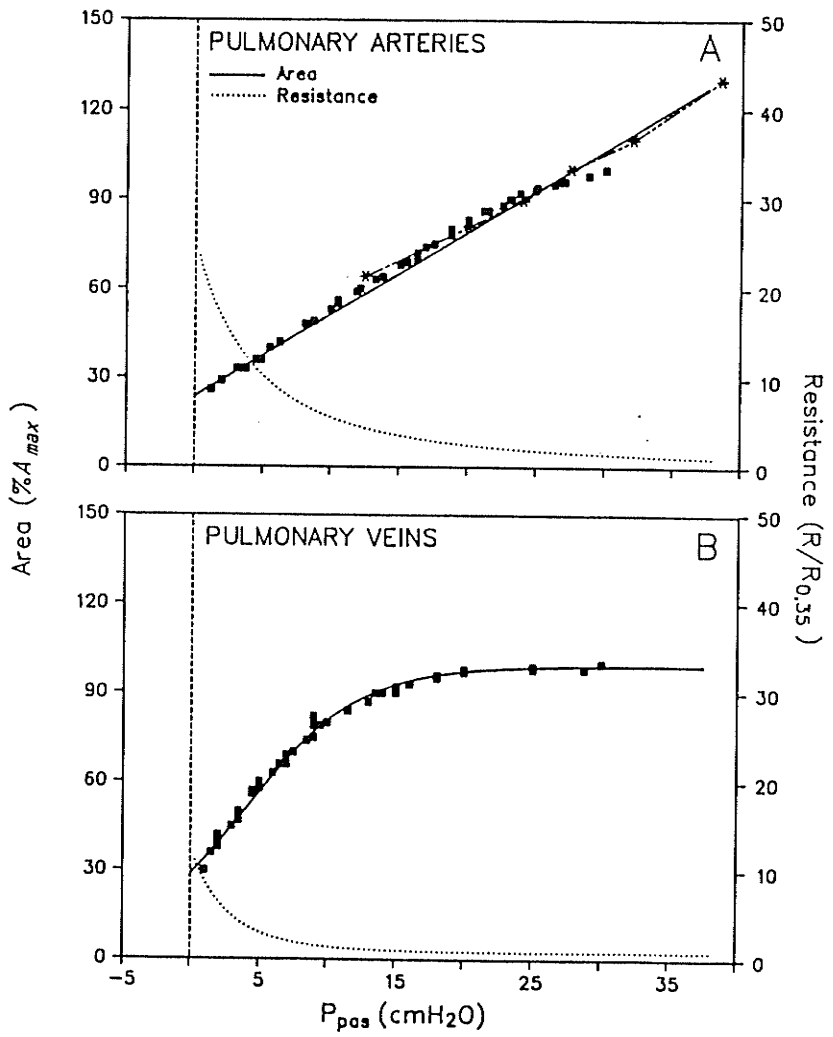

FIGURE 2. Vascular cross-sectional area (*left y-axis*) as a function of passive pressure (P_{pas}) for both arteries (*panel A*) and veins (*panel B*). Solid lines represent predictions according to equation 9a for veins (B_v = 2.43, C_v = 0.236) and equation 11a for arteries (A_a = 0.242, B_a = 0.028). Dotted lines represent vascular resistance (R) calculated relative to a reference resistance ($R_{0,35}$) at P_{pas} equals 35 cmH_2O (*right y-axis*).
■ Smith and Mitzner (28).
* Maloney et al. (18)

The relation between A and P_{pas} was also derived from the study of Smith and Mitzner (28). These authors provided plots of the relation between P_V and normalized vessel cross-sectional area (i.e. A/A_{max}, A_{max} being A at P_V = 30 cmH_2O), for different P_{TP} values (Figures 7A and 7B, *ref.* 28). P_x, for each P_V and P_{TP}, shown in these figures, was calculated using the approach described above and subtracted from P_V to obtain P_{pas}. Their data was then re-plotted, A/A_{max} as a function of P_{pas}, for both arteries and veins and the new plots are shown in Figures 2A and 2B, respectively. As evident from both figures, when expressed as a function of P_{pas}, A/A_{max} is independent of P_{TP}.

At higher P_{pas}, A/A_{max} for veins tended to asymptote (Figure 2B). For $P_{pas} \geq 0$, the data points could be adequately described by a logistic relation of the form,

$$A/A_{max} = 1/\left[1+B_V \cdot e^{-(C_V \cdot P_{pas})}\right] \quad \ldots\ldots (9a)$$

Accordingly, regression lines of this form were obtained for veins. Under specific reference conditions of P_{pas} (i.e P_{pas} = 35 cmH_2O), $A_{0,35}/A_{max}$ is equal to:

$$A_{0,35}/A_{max} = 1/\left[1+B_V \cdot e^{-(C_V \cdot 35)}\right] \quad \ldots\ldots (9b)$$

To normalize A to $A_{0,35}$, equation 9a was divided by equation 9b and the following relation was derived:

$$A/A_{0,35} = \left[1+B_v \cdot e^{-(C_v \cdot 35)}\right] / \left[1+B_v \cdot e^{-(C_v \cdot P_{pas})}\right] \quad . . (10)$$

From Figure 2A, it could be clearly seen that arteries, unlike veins, continued to expand over the pressure range 0 to 30 cmH_2O and did not appear to reach a maximum value. To accommodate for larger P_{pas} values than those provided by Smith and Mitzner (28), additional data points obtained by Maloney et al. (18) at higher vascular pressures were superimposed (after correcting the data for cross-sectional area and expressing it as a function of P_{pas}) over the data obtained by Smith and Mitzner (28). For arteries, the relation between A/A_{max} and P_{pas} appeared linear over the range 0-40 cmH_2O. Accordingly, a best linear fit for arteries of the form,

$$A/A_{max} = A_a + B_a \cdot P_{pas} \quad . . . . . (11a)$$

was obtained. At reference conditions (i.e. $P_{TP} = 0$, and $P_{pas} = 35$ cmH_2O),

$$A_{0,35}/A_{max} = A_a + B_a \cdot 35 \quad . . . . . (11b)$$

Thus, for arteries,

$$A/A_{0,35} = \frac{A_a + B_a \cdot P_{pas}}{A_a + B_a \cdot 35} \qquad \ldots\ldots (12)$$

By substituting the detailed solutions for $l/l_{0,35}$ and $A/A_{0,35}$ for veins in equation 4 and rearranging, the following relation was derived:

$$R_{ve} = \frac{R_{ve0,35} \cdot \left[1-(1-V_M)\cdot e^{-(C_L \cdot P_{TP})}\right]^{1/3}}{0.7368} \cdot \left[\frac{1+B_v \cdot e^{-(C_v \cdot P_{pas})}}{1+B_v \cdot e^{-(C_v \cdot 35)}}\right]^2 \qquad (13)$$

where R_{ve} is venous resistance, and $R_{ve0,35}$ is venous resistance at reference conditions of P_{TP} = 0 and P_{pas} = 35 cmH_2O. Values for the constants B_v (equal 2.4307) and C_v (equal 0.2355) were obtained by regression analysis from average data of Smith and Mitzner (Figure 2B). Given $R_{ve0,35}$, any change in R_{ve} that is due to either a change in P_{TP} or P_{pas} could be calculated using equation 13.

Analysis similar to the one outlined above using the relevant equations for $l/l_{0,35}$ and $A/A_{0,35}$ was used to derive the relation between arterial resistance (R_{ar}) and both P_{TP} and P_{pas}.

$$R_{ar} = \frac{R_{ar0,35} \cdot \left[1-(1-V_M) \cdot e^{-(C_L \cdot P_{TP})} \right]^{1/3}}{0.7368} \cdot \left[\frac{A_a + B_a \cdot 35}{A_a + B_a \cdot P_{pas}} \right]^2 \qquad (14)$$

A_a and B_a (equal to 0.2419 and 0.0275, respectively) were also obtained by regression analysis from average data of Smith and Mitzner (Figure 2A).

3. Modeling of smooth muscle tone

Accurate modeling of the mechanical effects of smooth muscle contraction on the pulmonary circulation is currently not possible because of lack of critical morphologic and functional information about pulmonary vascular smooth muscle. Information obtained from systemic vessels is not readily transferable to pulmonary vessels, at least not in the quantitative sense. Firstly, there is considerable heterogeneity in smooth muscle properties within the systemic circulation (for review see *ref.* 23). Secondly, smooth muscle morphology and function generally reflect adaptation to the mechanical stresses and functional requirements at their specific locale (23). The pulmonary circulation is a low pressure system with different objectives and control from the systemic circulation. Nonetheless, it is feasible to define the range of mechanical effects within the extremes of theoretically possible smooth muscle characteristics in the pulmonary circulation.

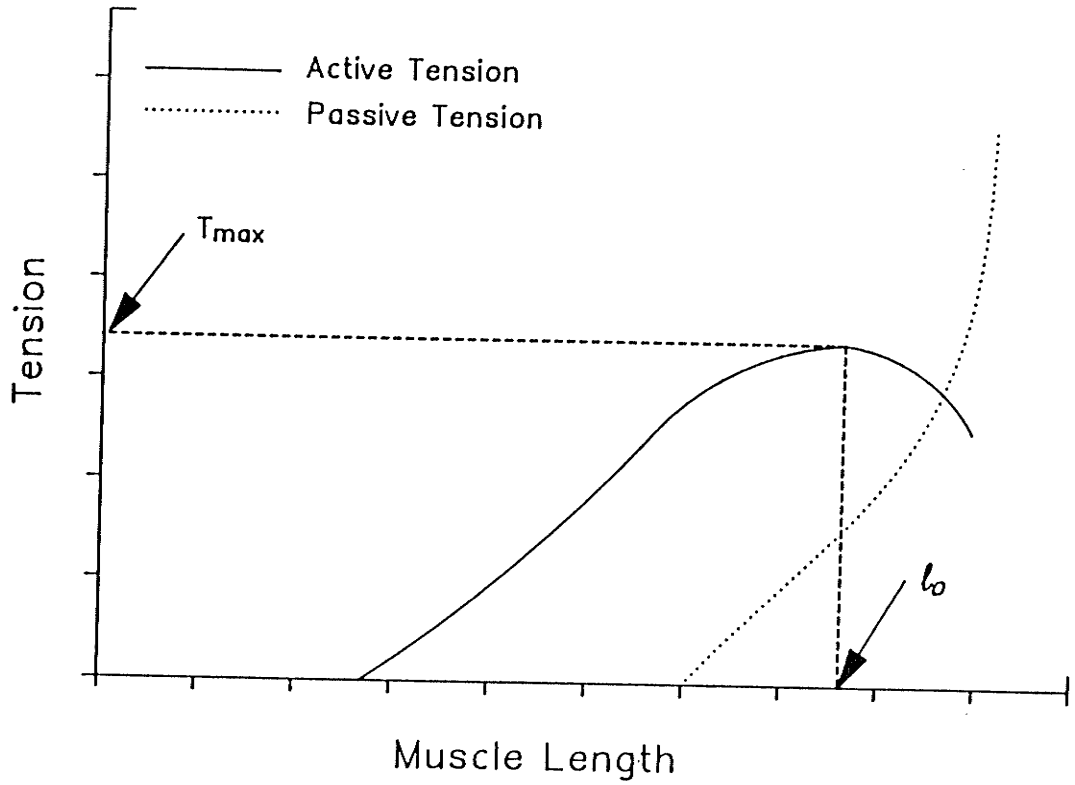

FIGURE 3. Schematic representation of the isometric active tension curve in a maximally stimulated muscle (*solid line*) and passive tension curve in a relaxed muscle (*dotted line*) as a function of muscle length.

All smooth muscle strips, regardless of their source (vascular, airway, intestinal, etc...) display common qualitative properties (Figure 3). Under passive conditions the muscle tissue exerts no tension up to a certain length beyond which tension rises non-linearly as a function of length. Active tension is maximal at a specific length (l_o) and declines above and below this point. There is no reason to believe that pulmonary vascular smooth muscle behaves differently in the qualitative sense. Several features, however, need to be known before this qualitative length-tension relationship can be converted into lumen radius (or area) versus radial active pressure (P_T) relation. The latter is required to predict the effect of active tension on the total *P-F* relationship.

First, how steep is the tension decline above and below l_o? A steep decline below l_o, for example, could decrease the muscle's ability to generate radial (i.e. collapsing) pressure as lumen area decreases, even after allowing for improved mechanical advantage according to Laplace's relation (see below).

Second, what is the relation between lumen area and smooth muscle length? This relation is critically affected by smooth muscle orientation relative to the vessel's longitudinal axis and by the amount of non-muscular tissue contained within the muscle layer. At one extreme (i.e acute angular orientation or a thick non-muscular tissue internal to the muscle layer), smooth muscle length, and hence circumferential tension, may change little over

the entire range of lumen areas. The treatment used by Burton (4) and Permutt (26) in modeling the effect of active tension on *P-F* relations implicitly assumes this extreme behavior (i.e. active tension independent of vessel radius). At the other extreme (i.e. circular orientation and a thin non-muscular layer), muscle length may decrease to the point where no active tension is possible long before the lumen is completely closed. In this case, vessels cannot close completely under the influence of active tension.

Third, what is the relation between lumen radius (r_l) and the radius of the smooth muscle layer (r_m)? This is a function of the amount of non-muscular tissue contained within the muscle layer. Although vascular resistance is related to r_l, it is r_m that critically governs the relation between circumferential active tension (T) and radial collapsing pressure (P_T), according to Laplace's relation ($P_T = T/r_m$). At one extreme (a thick non-muscular layer), r_m changes little with r_l. P_T, in this case, is simply a function of T (which also changes very little). In other words, P_T would be dependent on the level of smooth muscle activation and independent of lumen area. At the other extreme, r_m changes substantially with r_l. In this case, as the vessel distends above its r_o (vessel radius associated with l_o), P_T decreases partly because of larger r_m and partly because of less T. As the vessel lumen decreases below r_o, P_T may increase,

decrease, or remain the same depending on the relative effects on T (as dictated by the first two relations) and r_m (dictated by the third relation).

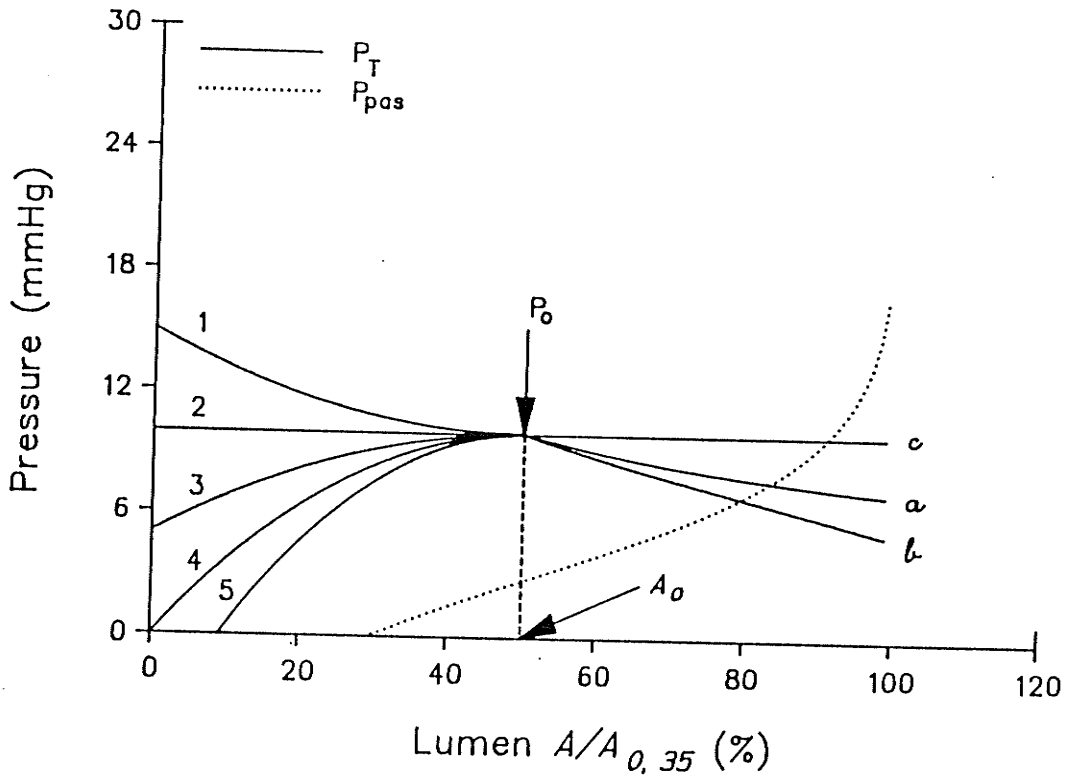

FIGURE 4. Schematic representation of the various P_T treatments above (*curves a, b, and c*) and below (*curves 1 to 5*) A_o. P_{pas} is shown by the dotted line. A_o is area at which maximum active tension is produced. P_o is the pressure produced by active tension at A_o. (See text for explanation)

According to this analysis, for a given level of tone, the relation between lumen area and P_T can follow five different pathways below A_o (lumen area at which muscle is at l_o) and two pathways above A_o (Figure 4). Below A_o as lumen area decreases P_T may increase, remain the same, decrease towards an intercept on the pressure axis, decrease towards zero or decrease towards an intercept on the area axis. The last two possibilities do not permit complete closure of vessels under the influence of active tension. Above A_o, pressure decreases either as a function of radius alone (i.e. constant tension, *line a*, Figure 4) or at a steeper rate (decrease in tension as well, *line b*, Figure 4). By assigning a pressure value at A_o (i.e. P_o) which is a reflection of the level of activity, it is possible to study the effect of these various patterns on the *P-F* relation. Figure 4 shows a third pattern (*line c*) in which P_T is independent of lumen area above A_o. This pattern is physiologically untenable. In the single vessel model we include pattern *c* in the comparisons with other patterns to assess the effect of assuming a constant P_T on the results. The use of P_T independent of lumen area, if inconsequential to the results, would considerably expedite the computations with the multibranched model.

The following equations were used to model the various possible pressure patterns below (equation 15) and above (equation 16) A_o:

$$P_T = P_o \cdot \left[(K_p - 1) \cdot \left[\frac{A/A_{0,35}}{A_o/A_{0,35}} - 1 \right]^2 + 1 \right] \quad \ldots\ldots (15)$$

and,

$$P_T = (P_o) \cdot \left[\frac{A_o/A_{0,35}}{A/A_{0,35}} \right]^{1/2} - L_p \cdot [(A/A_{0,35}) - (A_o/A_{0,35})] \quad \ldots (16)$$

where K_p (equation 15) is the pressure intercept (i.e. at zero lumen cross-sectional area) as a fraction of P_o, and L_p (equation 16) is a factor by which P_T can be forced to drop at a rate greater than that allowed by Laplace's law. For pattern *c*, $P_T = P_o$.

The location of A_o, relative to the physiologic area range, is not known for pulmonary vessels. However, it is known that for all smooth muscle l_o occurs at a length where passive tension is substantial (23). For pulmonary vascular smooth muscle A_o is, therefore, likely well above the resting point of the vessels (area at which relaxation pressure is zero in Figure 2). We carried out calculations assuming two values for A_o, $A_o = 0.50 \cdot A_{0,35}$ and $A_o = 0.70 \cdot A_{0,35}$. These correspond to relaxation pressures of 9.64 and 16.08 mmHg for arteries, and 2.77 and 5.41 mmHg for veins.

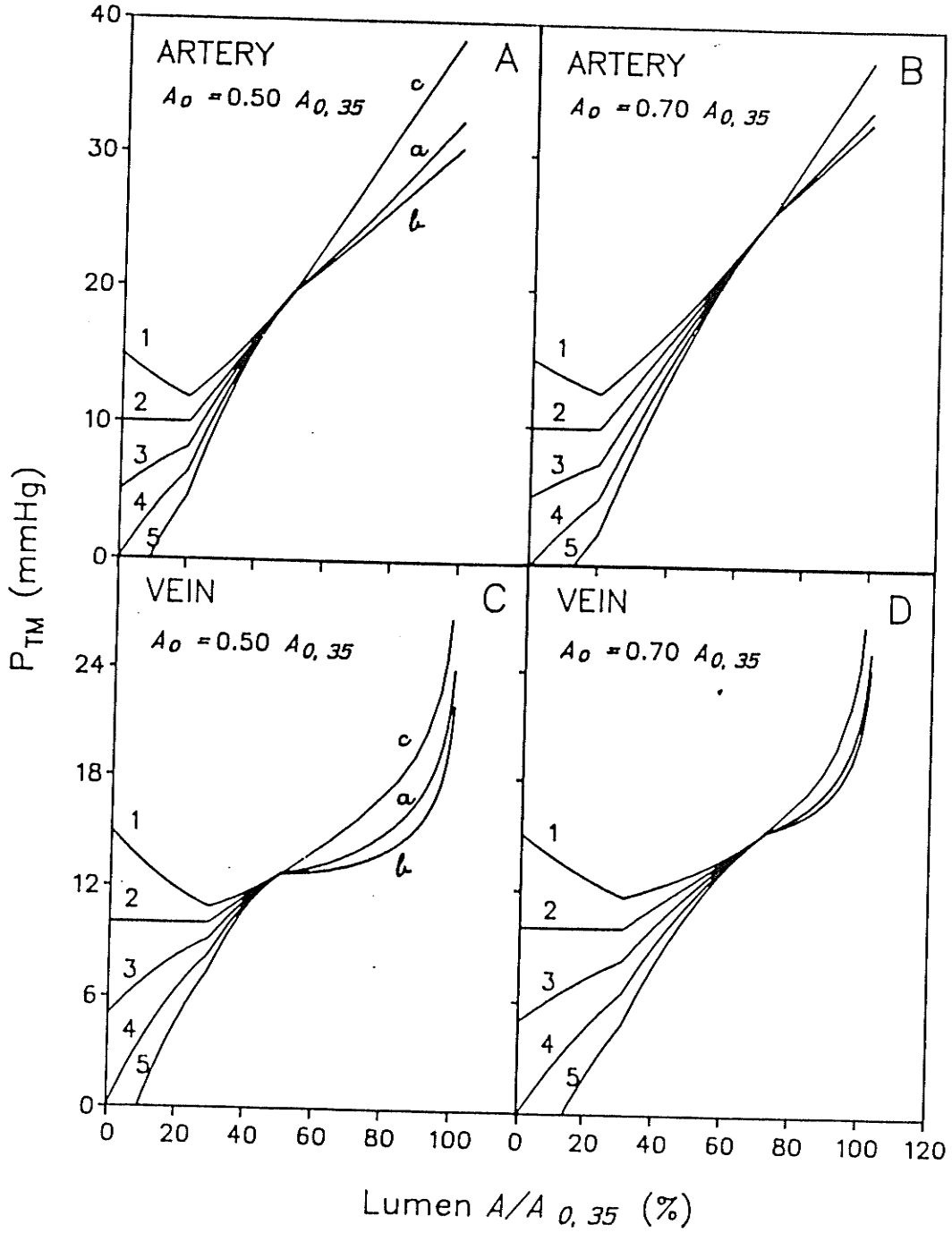

FIGURE 5. Transmural pressure (P_{TM}) (sum of P_{pas} and P_T) as a function of lumen $A/A_{o,35}$ for an average pulmonary artery (*panels A and B*) and vein (*panels C and D*) at two different A_o [$A_o = 0.5 \cdot A_{o,35}$ (*left panels*) and $A_o = 0.7 \cdot A_{o,35}$ (*right panels*)] and for the various P_T treatments shown in Figure 4.

In the presence of smooth muscle tone, the total recoil pressure (P_{TM}) for a vessel is the sum of passive and active pressures: Thus,

$$P_{TM} = P_{pas} + P_T \qquad \ldots\ldots (17)$$

Equations 13 and 14 were rearranged to obtain P_{pas} as a function of R [$P_{pas} = g(R)$] for veins and arteries, respectively. Equations 15 and 16 were rewritten so that P_T is also a function of R [$P_T = h(R)$]. Thus,

$$P_{TM} = g(R) + h(R)$$

$$= f(R) \qquad \ldots\ldots (18)$$

This latter function was used for the iterations to be described below.

Lumen area-P_{TM} relations for arteries and veins are shown in Figure 5. In the left panels, A_o was $0.50 \cdot A_{o,35}$ and in the right panels it was $0.70 \cdot A_{o,35}$. The plots depict the five relations below, and the three relations above A_o, at a P_o of 10 mmHg.

With treatments 1 and 2 there is a minimum pressure (P_{min}) below which vessel compliance becomes negative (treatment 1) or zero (treatment 2). For example, from Figure 5A, P_{min} for treatment 1 is about 11 mmHg and for treatment 2 is 10 mmHg. In

both cases the vessel closes completely once P_{TM} decreases below P_{min}. The main difference between the two treatments is that with treatment 2 the vessel reopens once P_V is returned to P_{min} while in treatment 1 a greater pressure (15 mmHg, Figure 5A) is required to reopen the vessel once it closed. This would produce a hysteresis in the *P-F* relation. In treatments 3 to 5 the compliance below A_o is positive. Hence, graded reductions in vessel cross-sectional area below the point of minimum resting tension are possible.

Above A_o, the slope of the area-pressure relation (i.e. vessel wall elastance, dP/dA) is the sum of the negative P_T relation (decreasing P_T with increasing area in treatments *a* and *b*) and the positive P_{pas} relation (Figure 3). Vessel wall elastance with active tension in this region is, therefore, less than that of the resting vessel. As the slope of the area-active pressure relation above A_o is a function of P_o (equation 16, above), values of P_o greater than a certain limit would result in a zone with negative elastance. The vessel cannot operate in this region since, according to the wave-speed limiting equation[1], flow cannot exist where elastance is zero or negative. The critical P_o above which a negatively sloping segment occurred above A_o with treatment *a*, when A_o was $0.50 \cdot A_{0,35}$, was 30 mmHg for arteries and 10 mmHg for veins. This represents about 300% and 350% of the resting pressure at this point for arteries and veins, respectively. For A_o equal to $0.70 \cdot A_{0,35}$, the critical P_o

values were 50 and 20 mmHg, also representing about 300% and 350% of resting pressure for arteries and veins, respectively. We limited the maximum P_o values to 300% of resting pressure for arteries and 350% for veins to avoid this complication. This is probably well justified since preliminary observations on pulmonary vascular smooth muscle indicate that active tension produced during maximal stimulation at l_o is not much higher than the passive tension exerted at the same length (N.L. Stephens et al., and R.A. Rhoades et al., personal communication). Our treatment, therefore, may overestimate the pressure generating ability of pulmonary vascular smooth muscle.

4. Calculation of resistances

In the present algorithm F and P_{out} for the vessel were independent inputs. To the extent that P_v along the length of vessels decreases and vessels are distensible, resistance along each vessel is not uniform. Because of the non-linear relation between P_{pas} and resistance calculation of effective resistance provided by each vessel based on P_v at some point along the vessel (P_{in}, P_{out}, or some average of the two), especially in the presence of variable P_T, is not precise. Accordingly, to calculate effective resistance, each vessel was considered as composed of a large number (n=100) of short segments connected in series, with each segment having a reference resistance of $R_{0,35}/n$ ($R_{0,35}$ being reference resistance of the whole vessel).

The actual resistance of each segment, beginning with the most downstream segment, was obtained by iteration. Each iteration consisted of two steps. In step one, the resistance obtained at the end of the previous iteration ($R_{0,35}$ for the first iteration) was used to calculate P_{TM} that applies for that resistance according to equation 18. Since for the single vessel P_x was zero, $P_{TM} = P_V$. In the second step a new R was calculated from,

$$R = (P_V - P_{out})/F \qquad \ldots\ldots (19)$$

where P_{out} is P_V of the segment just downstream from the current (or the inputted P_{out} for the most downstream segment). If the second R differed from the R used in the first step, an intermediate value was used in the next iteration. Iteration continued until R values calculated in step one and step two were similar, indicating that the radial and longitudinal pressure gradients are in equilibrium, and P_V ceased to change. P_V was then used as P_{out} for the next upstream segment and the process was repeated for the whole vessel length. Effective resistance for the whole vessel under these conditions is the sum of all calculated segmental resistances.

The derivation of the pressure profile according to the above scheme ignores the possibility of wave-speed (WS) limitation at some point along the vessel. In our standard treatment (equations 13 and 14) absolute area (A) and vessel

elastance (dP/dA) at the prevailing P_{TM} are not considered, and these determine a maximum flow value (F_{max}) which can be transmitted by the segment according to the theory of WS limitation (Footnote 1). It would be of interest to see how the presence of WS limitation would influence the P-F and P_{out}-P_{in} relations. For this purpose an algorithm was developed which calculates F_{max}, at the segment, from the WS equation (Footnote 1) given the steady-state solution for P_V (as above), the area, and dP/dA of the segment at this P_V. Different assumed $A_{0,35}$ were used to force various degrees of flow limitation. In the iterations used to calculate P_V at a given segment, if F_{max} was less than F (which is an independent input), P_V was incremented in steps of 0.01 mmHg. Following each step, P_T, P_{TM}, and R were recalculated and a new F_{max} was computed. Step increases in P_V continued until the condition $F_{max} > F$ was met. This treatment essentially forces a waterfall at the flow limiting segment, the pressure drop along the segment being greater than that predicted by Poiseuillian flow.

C. RESULTS AND DISCUSSION

1. Pressure-flow relations in a single vessel

P-F relationships of a single artery and a single vein are shown in Figure 6. In Figures 6A and 6B, the pressure-area relationships of all segments were assumed similar and equal to

that of an average pulmonary artery (as in Figure 2A). The vessel shown in Figures 6C and 6D consisted of segments with pressure-area characteristics similar to those of an average pulmonary vein (as in Figure 2B). $R_{0,35}$ was the same for all segments of a given vessel and was adjusted so that at a *F* of 2 *l*/min, and P_{out} of 5 mmHg, P_{in} was roughly 15 mmHg, thereby simulating relationships in a "typical" 20 kg dog under anesthesia. Extravascular pressure was zero under all conditions. Figures 6A and 6C were generated with a P_{out} of 5 mmHg and Figures 6B and 6D with a P_{out} of 15 mmHg.

Solid lines in Figure 6 represent the condition without smooth muscle tone (i.e. $P_T = 0$). Since P_{out} is positive and extravascular pressure is zero, P_{TM} is positive and well above the collapsing pressure (i.e. P_{crit}) in all segments. For both vessels, at a low P_{out} (Figures 6A and 6C), the *P-F* relationship is initially convex to the pressure axis. Above a certain *F*, which is vessel type dependent, this relationship becomes nearly linear. Extrapolation of this linear segment results in a pressure intercept (P_{op}) that is well above both P_{out} (5 mmHg) and P_{crit} (zero). Calculated R from this segment (1/slope) is well below the vessel's R when maximally distended. The latter is given by the inverse slope of a line joining P_{out} and the *P-F* point at a very high flow. The particular *P-F* of the pulmonary circulation with an initial convex and a final apparently linear segment is, therefore, obligate and independent of the presence

of P_{crit} along the vessels, or of recruitment. Furthermore, the mechanical properties of the pulmonary vessels are such that the nearly linear segment occurs within the physiologic range (2-8 *l*/min for a 20 kg dog). It is thus evident that using P_{op} and the inverse slope of the linear segment as indices of P_{crit} and the fixed resistance of a fully distended system, in the presence of distensible vessels, is incorrect.

At higher P_{out} (Figures 6B and 6D), the *P-F* relationship of an artery (Figure 6B) is still curvilinear, yet to a smaller extent, whereas that of a vein is linear (Figure 6D). The reason for this behavior in both vessels could be explained by examining the pressure-resistance relationships of Figures 2A and 2B, respectively. In the $P_{pas} \geq 15$ mmHg range, both vessels are operating in the range where resistance drops little (*dots*, Figure 2B) with a step increase in transmural pressure (i.e. the flat portion of the pressure-resistance relationship). Whereas resistance of arteries continues to drop, that of veins remains fairly constant making them behave like rigid tubes.

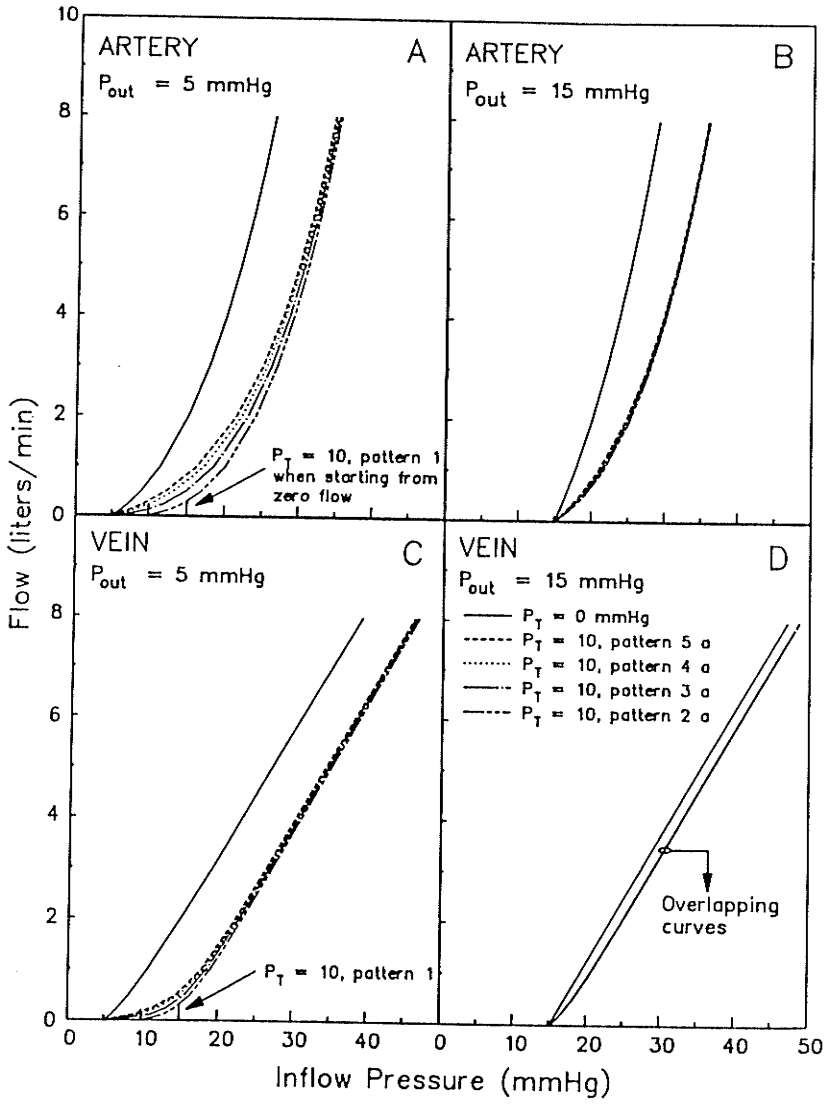

FIGURE 6. *P-F* relationships of a single artery (*panels A and B*) and a single vein (*panels C and D*) at two outflow pressures (P_{out}), P_{out} = 5 mmHg (*left panels*) and P_{out} = 15 mmHg (*right panels*). Solid lines represent the condition without smooth muscle tone. Dashed and dotted lines represent the condition with P_T of 10 mmHg at A_o ($A_o = 0.7 \cdot A_{o,35}$), for treatments 1 to 5 shown in Figure 4 when added uniformly along each vessel.

Effect of added tone. The additional interrupted lines in Figure 6 show the effect of adding tone, equivalent to 10 mmHg at A_o, uniformly along each vessel. The different lines pertain to different assumed patterns of P_T response to lumen area below A_o (Figure 4). In all simulations pattern "*a*" was used to simulate the *A*-P_T relation above A_o. The pattern of tone used does not affect the basic response of the *P-F* relation. In all cases, the relations, with and without tone, diverge until a certain pressure difference is reached above which the lines become essentially parallel. The main differences between the different tone patterns are in the low flow range, particularly P_z, when P_{out} is low (Figures 6A and 6C). The magnitude of the parallel shift is little affected by the tone pattern.

It must be pointed out that the parallel shift occurs regardless of the relation between P_{out} and the amount of added tone (in other words, whether or not a waterfall is established with the addition of tone). Figure 6B, for example, shows the *P-F* relationship for the same artery shown in Figure 6A but with a P_{out} of 15 mmHg. The inflow pressure at which flow just starts (P_z), under these conditions, does not change with the addition of tone since P_{out} is greater than P_{crit}. However, the *P-F* relationships still diverge from each other until a certain ΔP is reached. Thereafter, the two lines become nearly parallel. P_{op},

extrapolated from the linear segment, increases by an amount that is P_{out} and vessel type dependent, and the absolute value of P_{op} still does not represent true opening pressure (i.e. P_{crit}).

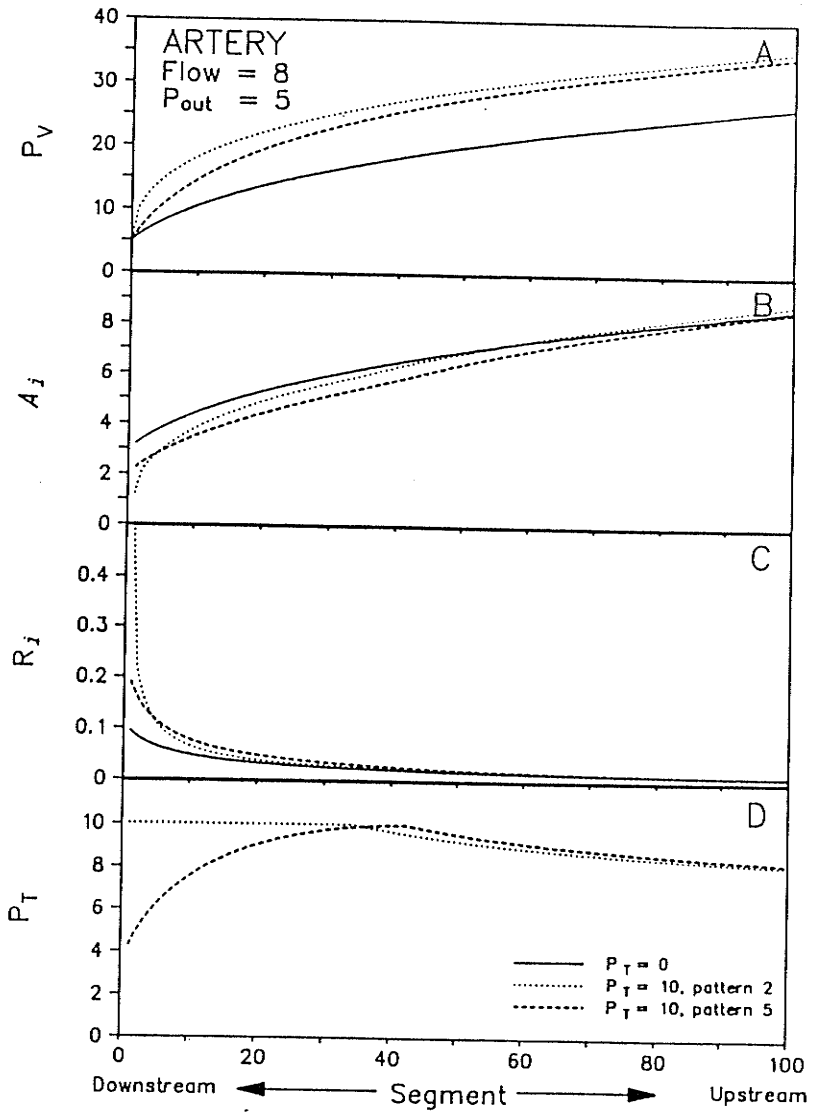

FIGURE 7. Longitudinal profile of P_V (*panel A*), segmental *A* (*panel B*), segmental R (*panel C*), and P_T (*panel D*) at a flow rate of 8 and P_{out} of 5. *Solid lines*, without tone; *dotted lines*, P_T of 10 at A_o, treatment 2; *dashed lines*, P_T of 10 at A_o, treatment 5.

The reason for the relative insensitivity of the magnitude of parallel shift to tone pattern is shown in Figure 7. Figure 7 shows the longitudinal profile of P_V, segmental area (A_i), segmental resistance (R_i), and P_T along an artery at a flow of 8 *l*/min and P_{out} of 5 mmHg (see Figure 6A) under three conditions; no tone and tone of 10 mmHg (at A_o) with patterns 2 (*dotted line*) and 5 (*dashed line*). The difference between the two patterns of tone is most obvious at the most downstream segments, where area is smallest; P_T with pattern 2 is much larger than with pattern 5 (Figure 7D). In fact, with pattern 2 there is a waterfall at segment 1 since P_T (equals 10 mmHg) is greater than P_{out} (Figure 7A, *dotted line*, segment 1). Because resistance increases more with pattern 2 at the most downstream segments, P_V rises at a faster rate (as a function of segment number). This counteracts the effect of the larger P_T. In fact, by segment 5 in this example A_i is larger (Figure 7B) and R_i is lower (Figure 7C) with pattern 2 even though P_T is still higher (Figure 7D). These changes cause the difference in P_V, highest at the most downstream segments, to progressively narrow as a function of vessel length (Figure 7A, *dotted* and *dashed lines*). The rate at which the two longitudinal pressure profiles converge is necessarily a function of flow. In this example (8 *l*/min) inflow pressure (segment 100) is nearly the same. At low flow rates, although the pressure profiles also converge toward the

inflow point, the rate at which the difference narrows is less resulting in some difference in P_{in} (Figure 6A, in the low flow range).

With high P_{out}, the vessel area is near or above A_o even at the most downstream segments. There is little difference in P_T between the different patterns near A_o (Figures 4 and 5). The initial divergence in P_V at the most downstream segments is therefore much less and easily neutralized by the more upstream segments. This explains the lack of any substantive difference between tone patterns in Figures 6B and 6D). With veins (figures not shown), the pressure differential (between the two patterns) developed at the downstream segments results in a more effective compensation in the upstream segments on account of the steeper pressure-area relation. The longitudinal pressure profiles, therefore, converge more readily. Hence, the small dispersion of lines in Figure 6C.

In Figure 6 we used only one pattern of A-P_T relation above A_o (pattern *a*). To assess the effect of other possible behaviors (patterns *b* and *c*, Figure 4), we developed *P-F* relations with the three patterns using pattern 2 for the relation below A_o. The results for a P_o of 10 mmHg are shown in Figure 8. With pattern *b*, where P_T, for a given P_o, decreases both because of Laplace's relation and because of decrease in tension above A_o, the *P-F* relation with tone shows a slight tendency to converge toward the

no-tone line at high flow rates. The differences between pattern *a* (decrease in P_T on account of Laplace's relation only) and pattern *c* (P_T independent of area) are very minor.

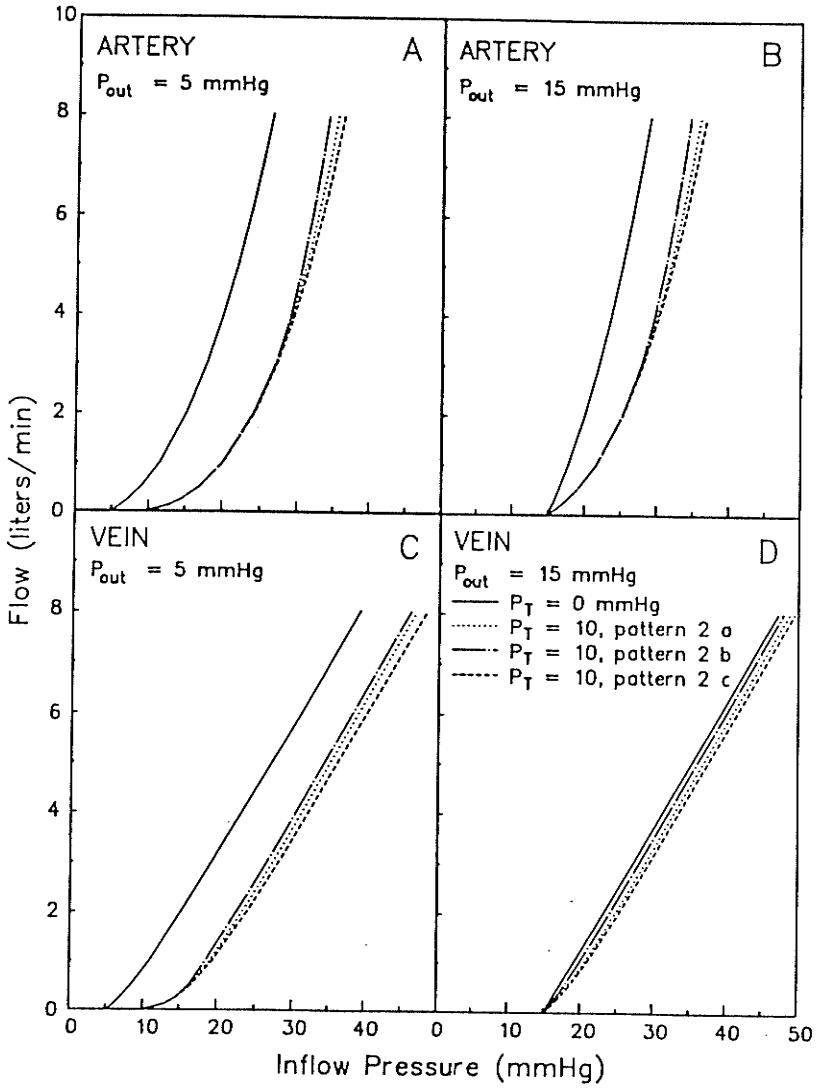

FIGURE 8. *P-F* relations with three patterns (*a*, *b*, and *c*) above A_o using pattern 2 for the relation below A_o. *Upper panels* relations obtained in an average pulmonary artery; *Lower panels* relations in an average pulmonary vein; *Left panels*, P_{out} = 5 mmHg, and *right panels*, P_{out} = 15 mmHg. The results are for a P_o of 10 mmHg.

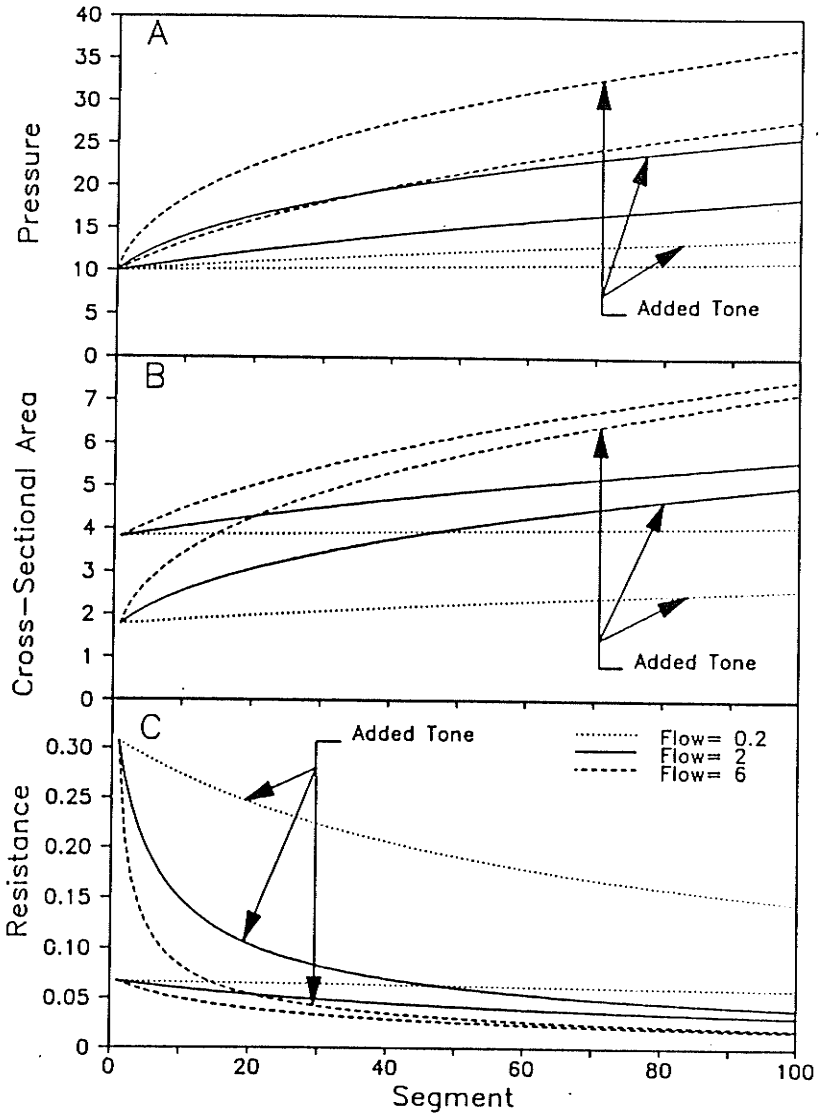

FIGURE 9. Longitudinal profile of Pv (*panel A*), segmental *A* (*panel B*), and segmental R (*panel C*), at below normal, normal, and above normal flow rates with and without an added tone (pattern 2 *c*) of 10 mmHg. Curves pertaining to added tone are marked with arrows.

The considerable insensitivity of the *P-F* relation in the physiologic flow range (2-8 *l*/min) to the pattern chosen to model the *A*-P_T relation above and below A_o makes it possible to get around the uncertainty about the real relation in the pulmonary circulation without risking serious errors. In the absence of any experimental data to favor a particular pattern, we shall use pattern 2 *c* (P_T independent of *A*) in subsequent modeling, if only because it is expeditious.

The reason for the initially divergent and then parallel shift of the *P-F* relationships with added tone is shown in Figure 9. Panels A, B, and C show the longitudinal profile of P_V, segmental cross-sectional area (A_i), and segmental resistance (R_i), respectively, at 3 different flow rates with and without an added tone of 10 mmHg. The units in this figure are relative and, therefore, have been omitted. An artery with a P_{out} of 10 mmHg, to eliminate a Starling resistor effect, is represented. Changes produced by tone at the first (i.e. most downstream) segment are similar under all flow rates. Since P_V for segment #1 (P_{out} here) is the same, the addition of tone reduces P_{TM} by the same amount and hence, cross-sectional area of segment #1 (A_1, panel B) decreases and its resistance (R_1, panel C) increases to the same extent under all flow conditions. P_V for segment #2 with tone increases by ($\Delta R_1 \cdot F$) compared to no tone, where ΔR_1 is the difference in resistances of segment #1 between both conditions (i.e. with and without tone). As a result, A_2

decreases and R_2 increases to a lesser extent than their respective values in segment #1. The increase in P_V as a result of a higher downstream resistance (R_{DS}) with tone causes areas and resistances to progressively approach respective values without tone. Because the increase in P_V for a given segment is a function of F, A_i and R_i with tone approach respective values without tone at a faster rate (as a function of segment number) with higher flows as compared to lower flows (panels B and C, Figure 9). The segment where $\Delta R_{DS} \cdot F$ equals P_T will have equivalent cross-sectional areas and resistances. The pressure drop along this segment will be the same with and without tone and the increase in P_V (as a function of segment number) thereafter will remain unchanged. At low flow rates, $\Delta R_{DS} \cdot F$ does not reach P_T at any point along the vessel because of low F. The vessel will, thus, be constricted throughout its length, albeit more so downstream (panel B). As F increases, R_i with tone approaches that without tone faster, but at the expense of greater P_V. P_{in} with tone compared to without tone increases with increasing F until ΔP_{in} equals P_T. At this point R_{100} (i.e. resistance of the most upstream segment) becomes the same with and without tone. Increasing F further causes the point at which segmental resistances with and without tone are equal to move farther downstream with no further change in ΔP_{in}. The F above which the slope of the P_{in} vs. F relation become similar with and without tone (F_{crit}) depends on the magnitude of P_T (higher F_{crit}

with greater P_T) and the elastic behavior of the vessel wall (and hence, how R_i changes as a function of P_v). For example, in a vein (figures not shown), P_v need not rise to completely match P_T. Rather, once P_v rises to a value that places the vessel on the flat part of its P_{pas}-A relation (Figure 2B), the effect of tone is dissipated. This change in P_v (ΔP_v) then becomes the maximal deviation in the P-F relation and the flow at which this ΔP_v is developed becomes F_{crit}. Hence the smaller parallel shift in Figure 6D.

Figure 9, panel B, also depicts what one might see if vessel dimensions were observed (e.g. by angiography) with and without uniformly added tone. At low F the vessel would appear to constrict rather uniformly (*dotted line* panel B). At the highest F constriction would appear limited to the most downstream segments, thereby giving the false impression that the increase in tone is regional.

Effect of wave-speed limitation. We wished to determine the extent to which the presence of a waterfall due to wave-speed (WS) limitation would alter the P-F relation derived on the basis of distensibility alone. By experimenting with different levels of absolute $A_{0,35}$ we selected a value that results in a step up in pressure of 8 mmHg along a vessel with arterial characteristics at a flow of 8 *l*/min and a P_{out} of 5 mmHg. $A_{0,35}$ that had this effect was 1.1 cm^2. We then generated the P-F

relation for that vessel and compared it with the relation when WS limitation was ignored (see "METHODS"). The results are shown in Figure 10.

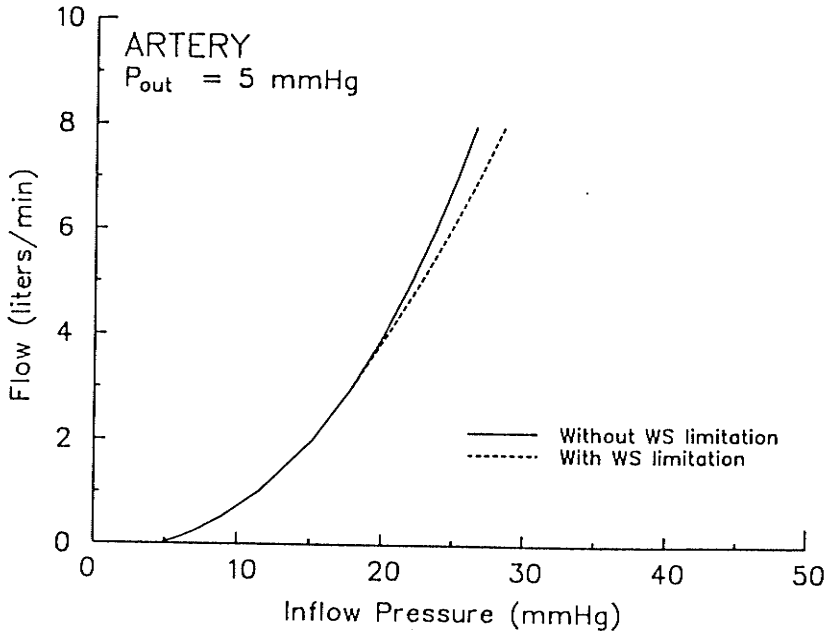

FIGURE 10. *P-F* relationships with (*dashed line*) and without (*solid line*) wave-speed (WS) limitation for an average pulmonary artery with a Pout of 5 mmHg.

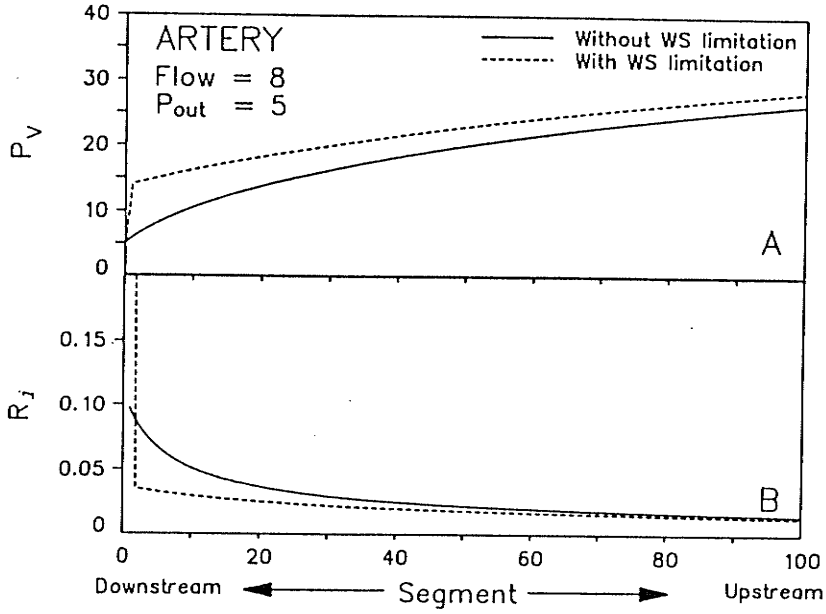

FIGURE 11. Longitudinal profile of Pv (*panel A*) and segmental R (*panel B*) at a flow rate of 8 and Pout of 5. *Solid lines*, represent the case without wave-speed (WS) limitation; *dashed lines*, with WS limitation.

The two curves deviated from each other only above a flow of 3 *l*/min, the lowest level at which a step change in pressure due to WS limitation was present. The general behavior is similar in the two cases showing a gradual change in slope leading to an apparently linear segment. Of interest is the fact that although the waterfall effect within the vessel was 8 mmHg at F = 8 *l*/min (see below), the deviation in P_{in} at the same flow was only 2 mmHg (Figure 10). The reason for this attenuation is shown in Figure 11. Since the vessel properties are uniform, choking will occur at the most downstream segment, when pressure and, hence, A and dP/dA are lowest (Figure 2). By comparison to the case where WS limitation was ignored (*solid line*), there is a step up in pressure at segment #1. This causes all segments upstream to operate at a lower resistance. The pressure difference, therefore, narrows progressively upstream (Figure 11A).

2. Outflow-inflow pressure relationships

Figure 12 shows changes in P_{in} as P_{out} increases at 2 *l*/min (*upper* panels) and 8 *l*/min (*lower* panels). *Left* panels show curves obtained in an average pulmonary artery (as in Figures 6A and 6B). *Right* panels show curves obtained in an average pulmonary vein (as in Figures 6C and 6D). In the passive vessel (*solid line*), as P_{out} rises, Rv drops resulting in a decrease in

(P_{in}-P_{out}). P_{in} does not increase to the same extent as P_{out} except for the vein (solid line, Figures 12B and 12D) at P_{out} > 12 mmHg.

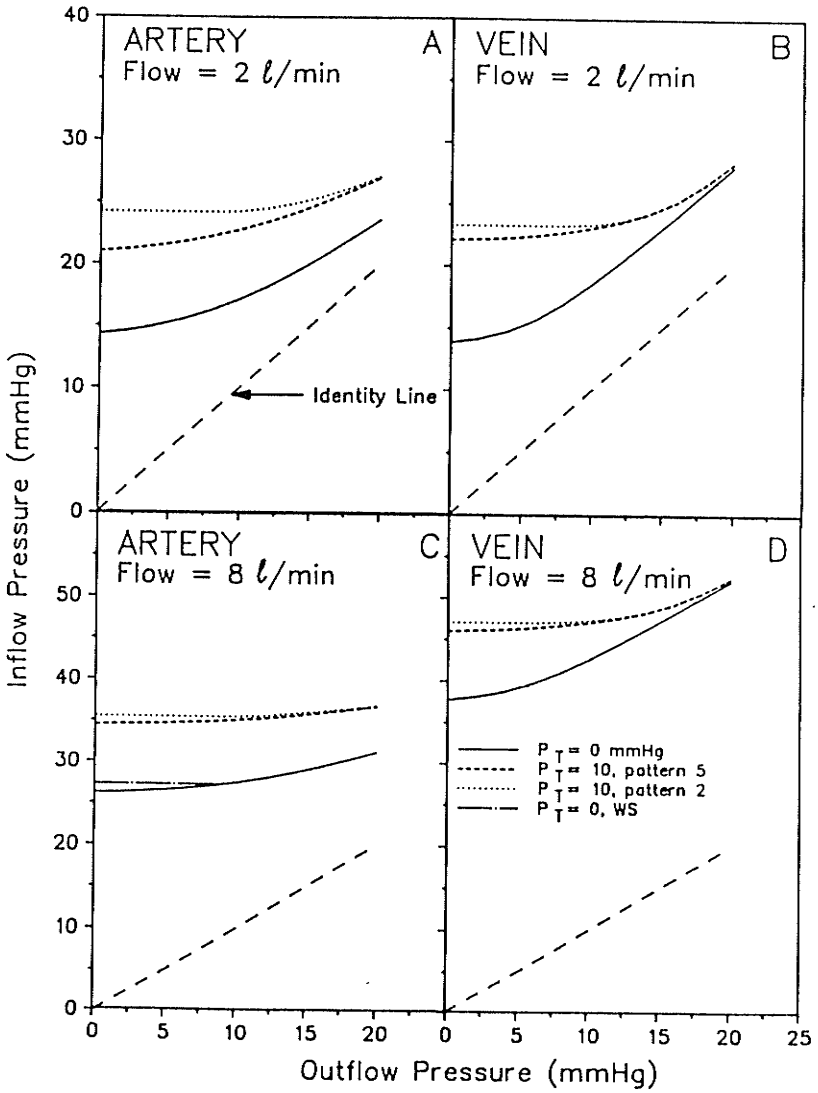

FIGURE 12. P_{out}-P_{in} relations for the same artery (*left panels*) and vein (*right panels*) shown in Figure 6 at two different flows, F = 2 *l*/min (*upper panels*) and F = 8 *l*/min (*lower panels*). *Solid lines* are without smooth muscle tone; *dashed lines* are with a P_T = 10 mmHg, treatment 5; *dotted lines* are with a P_T = 10 mmHg, treatment 2; and *chain-dotted* lines when wave-speed (WS) limitation was imposed on the artery at 8 *l*/min (highest point in Figure 10).

Although this behavior was qualitatively expected, its magnitude was striking. At normal flow (2 *l*/min), *Z* (i.e. $\Delta P_{in}/\Delta P_{out}$) in the P_{out} range 0-5 mmHg was less than 0.23 for both artery and vein. Between 5 and 10 mmHg *Z* was less than 0.45 for the artery and about 0.72 for the vein. For the artery *Z* was still below 0.75 even in the P_{out} range 15 to 20 mmHg. Over the same P_{out} range *Z* becomes even smaller as *F* increases. This is due to a greater reduction in $(P_{in}-P_{out})$ for a step increase in P_{out}, since the decrease in $(P_{in}-P_{out})$ is a function of the change in R (ΔR) and *F*. Under all conditions the change in *Z* as P_{out} increases is gradual, reflecting the progressive decrease in sensitivity of resistance to vascular pressure (Figure 2, *dots*).

Dashed and dotted lines describe the response with added tone of pattern 5 and pattern 2, respectively. With pattern 5 there is no waterfall since P_T decreases to zero before the vessel is closed. With pattern 2 there is a waterfall up to a P_{out} of 10 mmHg and this is evident by a segment with a slope of zero in the P_{out} range 0-10 mmHg. The chain-dotted line in panels C pertain to the case with WS limitation (as illustrated in Figure 11) which, as may be expected, also shows a perfectly flat segment. Although with distensibility alone (no waterfall) *Z* in the low P_{out} range technically is not zero, the difference from the case with waterfall would be difficult to detect experimentally, especially at high flow.

In summary, the elastic properties of pulmonary vessels of the dog are such that the presence of a linear segment in the P_{in}-F relation within the physiologic flow range, and a $\Delta P_{in}/\Delta P_{out}$ ratio of near zero in the low P_{out} range, are to be expected in the absence of critical closure or WS limitation. These relations, therefore, have little value in detecting a waterfall along the circulation. Addition of tone, homogeneously to a vessel, causes a parallel shift in the P_{in}-F relation in the physiologic flow range whether or not a waterfall is established. The magnitude of the parallel shift is P_{out} and vessel type dependent. A parallel shift, therefore, does not necessarily signify the development of a waterfall and its magnitude is not a quantitative reflection of the radial pressure exerted by smooth muscles.

D. FOOTNOTES

Footnote 1.

According to the wave-speed theory of flow limitation the maximum flow that can be conducted by a vessel (F_{max}) is given by the following relation:

$$F_{max} = A \cdot \left[\frac{A}{\delta} \cdot \frac{dP}{dA}\right]^{1/2}$$

where A is cross-sectional area, dP/dA is vascular elastance, and δ is the fluid density flowing in the given tube. (For a comprehensive review of the wave-speed flow-limiting mechanism see *ref.* 32).

For a given reference area ($A_{0,35}$) A and dP/dA, at a given P_{TM}, could be calculated from equation 10 for veins and equation 12 for arteries.

E. GLOSSARY

μ: viscosity of blood.

0,35: when applied as subscript to a statement refers to the value of the statement at reference conditions of P_{TP} = 0 and P_{pas} = 35 cmH_2O.

A: vessel cross-sectional area (lumen).

A_i: cross-sectional area of segment i.

A_{max}: highest lumen cross-sectional area reported by Smith and Mitzner (28) [i.e. at P_{pas} of 30 cmH_2O].

A_o: lumen area at optimal muscle length (l_o).

C_L: a constant describing the fractional lung volume change per unit pressure change.

F: flow.

F_{crit}: critical flow at which the cross-sectional area of the most upstream segment of a vessel is the same with and without added tone.

F_{max}: maximal flow, as allowed by the wave-speed limitation theory, in a given segment and for a given P_v.

F_T: total flow.

l: vessel length

LA: left atrium.

l_{max}: vessel length at maximal (P_{TP} = 30 cmH_2O) lung volume.

l_o: optimal muscle length, length at which muscle produces maximal tension.

P-F: pressure-flow.

PA: pulmonary artery.

P_{art}: intravascular pressure at the arterial end of a capillary sheet.

P_{crit}: critical opening pressure, the minimal pressure required to open an individual vessel.

P_G: pressure produced by gravitational forces.

P_{in}: inflow pressure.

P_{LA}: left atrial pressure.

P_{min}: minimal P_V below which vessel compliance becomes zero or negative with treatments 1 and 2 of P_T (Figure 5).

P_o: pressure produced by active tension when smooth muscle layer is at l_o.

P_{op}: opening pressure, obtained from the extrapolated pressure intercept of the linear segment of a *P-F* relationship.

P_{out}: outflow pressure.

P_{PA}: pulmonary arterial pressure.

P_{pas}: passive pressure (i.e. in the absence of vasomotor tone).

P_{pl}: pleural pressure.

P_T: pressure due to vasomotor tone.

P_{TM}: transmural pressure.

P_{Tot}: total pressure, the sum of P_T and P_{pas}.

P_{TP}: transpulmonary pressure.

P_V: intravascular pressure.

P_X: perivascular pressure.

P_Z: the pressure at which flow commences in a vessel.

r: radius.

R: resistance. When followed by a "'" pertains to venous resistance and when combined with a numerical followed by a lower case letter refer to Figure 1, part II of this communication for exact location of the vessel in the multibranched model.

R_{ar}: resistance of an arterial extraalveolar pulmonary vessel.

R_{DS}: downstream resistance.

R_i: resistance of segment i.

r_l: lumen radius.

r_m: radius of smooth muscle layer.

r_o: lumen radius when smooth muscle layer is at l_o.

R_T: total resistance.

R_V: vascular resistance.

R_{ve}: resistance of a venous extraalveolar pulmonary vessel.

T: tension.

T_{max}: maximal active tension obtained at l_o.

V_L: lung volume.

V_{Lmax}: maximal (i.e. at P_{TP} = 30 cmH_2O) lung volume.

V_M: minimal (i.e. at P_{TP} = 0) lung volume as a fraction of V_{Lmax}.

WS: wave-speed.

Z: the change in P_{PA} (ΔP_{PA}) as a fraction of a step change in P_{LA} (ΔP_{LA}); $\Delta P_{PA}/\Delta P_{LA}$ in the multibranched model and $\Delta P_{in}/\Delta P_{out}$ in the single vessel model.

F. REFERENCES

1. Banister, J., and R.N. Torrance. The effects of the tracheal pressure upon flow: pressure relations in the vascular bed of isolated lungs. *Quart. J. Exptl. Physiol.* 45:352-367, 1960.

2. Brower, R.G., R.A. Wise, C. Hassapoyannes, B. Bromberger-Barnea, and S. Permutt. Effect of lung inflation on lung blood volume and pulmonary venous flow. *J. Appl. Physiol.* 58:954-963, 1985.

3. Brower, R.G., R.A. Wise, C. Hassapoyannes, M. Hausknecht, and S. Permutt. Longitudinal distribution of vascular compliance in the canine lung. *J. Appl. Physiol.* 61(1):240-247, 1986.

4. Burton, A.C. Physical principles of circulatory phenomena: the physical equilibria of the heart and blood vessels. In: *Handbook of Physiology - Circulation.* Washington, D.C.: Am. Physiol. Soc. 1962, sect. 2, vol. I, chapt. 6, p. 85-106.

5. Carlill, S.D., and H.N. Duke. Pulmonary vascular changes in response to variations in left auricular pressure. *J. Physiol.* 133:275-286, 1956.

6. Carlill, S.D., H.N. Duke, and M. Jones. Some observations on pulmonary hemodynamics in the cat. *J. Physiol.* 136:112-121, 1957.

7. Dawson, C. Role of pulmonary vasomotion in physiology of the lung. *Physiol. Rev.* 64:544-616, 1984.

8. Edwards, W.S. The effects of lung inflation and epinephrine on pulmonary vascular resistance. *Am. J. Physiol.* 167:756-762, 1951.

9. Fung, Y.C., and R.T. Yen. A new theory of pulmonary blood flow in zone 2 condition. *J. Appl. Physiol.* 60(5):1638-1650, 1986.

10. Fung, Y.C., and S.S. Sobin. Elasticity of the pulmonary alveolar sheet. *Circ. Res.* 30:451-469, 1972.

11. Fung, Y.C., and S.S. Sobin. Pulmonary alveolar blood flow. *Circ. Res.* 30:470-490, 1972.

12. Graham, R., C. Skoog, L. Oppenheimer, J. Rabson, and H.S. Goldberg. Critical closure in the canine pulmonary vasculature. *Circ. Res.* 50(4):566-572, 1982.

13. Haynes, R.H., and A.C. Burton. Role of non-Newtonian behavior of blood in hemodynamics. *Am. J. Physiol.* 197:943-950, 1959.

14. Hoppin, F.G., JR., J.C. Stothert, JR., I.A. Greaves, Y. Lai, and J. Hildebrandt. Lung recoil: elastic and rheological properties. In: *Handbook of Physiology - The Respiratory System.* Mechanics of Breathing, Part I. Bethesda, MD: Am. Physiol. Soc. 1986, sect. 3, vol. III, chapt. 13, p. 195-215.

15. Lai-Fook, S.J. A continuum mechanics analysis of pulmonary vascular interdependence in isolated dog lobes. *J. Appl. Physiol.* 46(3):419-429, 1979.

16. Lai-Fook, S.J., and R.E. Hyatt. Effect of parenchyma and length changes on vessel pressure-diameter behavior in pig lungs. *J. Appl. Physiol.* 47(4):666-669, 1979.

17. Lopez-Muniz, R., N.L. Stephens, B. Bromberger-Barnea, S. Permutt, and R.L. Riley. Critical closure of pulmonary vessels analyzed in terms of Starling resistor model. *J. Appl. Physiol.* 24(5):625-635, 1968.

18. Maloney, J.E., S.A. Rooholamini, and L. Wexler. Pressure-diameter relations of small blood vessels in isolated dog lung. *Microvasc. Res.* 2:1-12, 1970.

19. McDonald, I.G., and J. Butler. Distribution of vascular resistance in the isolated perfused dog lung. *J. Appl. Physiol.* 23(4):463-474, 1967.

20. Mitzner, W. Resistance of the pulmonary circulation. In: *Clinics in Chest Medicine.* Vol. 4, No. 2, May 1983, p. 127-137.

21. Mitzner, W., and I. Huang. Interpretation of pressure-flow curves in the pulmonary vascular bed. In: *The Pulmonary Circulation in Health and Disease.* Edited by J.A. Will, C.A. Dawson, E. Kenneth Weir, and C.K. Buckner. Academic Press, Inc. 1987. p. 215-230.

22. Mitzner, W., and J.T. Sylvester. Hypoxic vasoconstriction and fluid filtration in pig lungs. *J. Appl. Physiol.* 51:1065-1071, 1981.

23. Murphy, R.A. Mechanics of vascular smooth muscle. In: *Handbook of Physiology - The Cardiovascular System.* Bethesda, MD: Am. Physiol. Soc. 1980, sect. 2, vol. II, chapt. 13, p. 325-351.

24. Permutt, S., B. Bromberger-Barnea, and H.N. Bane. Alveolar pressure, pulmonary venous pressure, and the vascular waterfall. *Med. Thorac.* 19:239-260, 1962.

25. Permutt, S., P. Caldini, A. Maseri, W.H. Palmer, T. Sasamori, and K. Zierler. Recruitment versus distensibility in the pulmonary vascular bed. In: *The Pulmonary Circulation and Interstitial Space*, edited by A.P. Fishman, Chicago, IL:Hecht, 1969, p. 375-390.

26. Permutt, S., and R.L. Riley. Hemodynamics of collapsible vessels with tone: the vascular waterfall. *J. Appl. Physiol.* 18:924-932, 1963.

27. Shoukas, A.A. Pressure-flow and pressure-volume relations in the entire pulmonary vascular bed of the dog determined by two-part analysis. *Circ. Res.* 37:809-818, 1975.

28. Smith, J.C., and W. Mitzner. Analysis of pulmonary vascular interdependence in excised dog lobes. *J. Appl. Physiol.* 48(3):450-467, 1980.

29. Takahashi, S., and J. Butler. A vascular waterfall in extra-alveolar vessels of the excised dog lung. *J. Appl. Physiol.* 26:578-584, 1969.

30. West, J.B., and C.T. Dollery. Distribution of blood flow and the pressure-flow relations of the whole lung. *J. Appl. Physiol.* 20:175-183, 1965.

31. West, J.B., C.T. Dollery, and A. Naimark. Distribution of blood flow in isolated lung relation to vascular and alveolar pressure. *J. Appl. Physiol.* 19:713-724, 1964.

32. Wilson, T.A., J.R. Rodarte, and J.P. Butler. Wave-speed and viscous flow limitation. In: *Handbook of Physiology - The Respiratory System.* Mechanics of Breathing, Part I. Bethesda, MD: Am. Physiol. Soc. 1986, sect. 3, vol. III, chapt. 5, p. 55-61.

33. Zhuang, F.Y., Y.C. Fung, and R.T. Yen. Analysis of blood flow in cat's lung with detailed anatomical and elasticity data. *J. Appl. Physiol.* 55(4):1341-1348, 1983.

VII. CHAPTER 6

DISTENSIBILITY AND PRESSURE-FLOW RELATIONSHIP OF THE PULMONARY CIRCULATION. II. MULTIBRANCHED MODEL.

A. BACKGROUND

In the preceding chapter we developed equations, based on available *in situ* data, which describe the effects of intravascular pressure and lung volume on length and cross-sectional area, and hence resistance, of pulmonary arteries and veins. We then described a method for integrating this information to obtain changes in inflow pressure (P_{in}), for single vessels, as outflow pressure (P_{out}) or flow (F) is changed. The P-F and P_{in}-P_{out} relations obtained for single arteries and veins displayed the fundamental characteristics observed in the intact whole pulmonary circulation. Thus, that the P-F relation is convex to the pressure axis in the low flow range with a distinctly linear segment in the physiologic flow range. Also, P_{in} changed little as P_{out} was increased in the low pressure range, the proportionality ($\Delta P_{in}/\Delta P_{out}$, also termed Z here) then increased gradually toward unity as P_{out} increased.

In the present communication we describe the P-F and P_{in}-P_{out} relations in a multibranched model in which each serial or parallel component behaves according to the behavior of single vessels described earlier (CHAPTER 5) but where the forces acting on individual vessels can be varied. In this fashion we could simulate the effects of factors that act non-uniformly on pulmonary vessels such as gravity, vascular occlusion and

vasomotor tone. This model also incorporates a capillary sheet, modeled according to the sheet-flow theory of Fung and Sobin (10, 11).

B. METHODS

Figure 1 shows an outline of the various components of the model. The arterial system bifurcates sequentially up to 8 parallel channels that converge and reunite at the venous side to end in the left atrium (LA). Separating the arterial and venous beds are 8 capillary beds (shaded rectangles). All extraalveolar vessels were subject to a common transpulmonary pressure (P_{TP}) and all capillaries were subject to a common alveolar pressure (P_A).

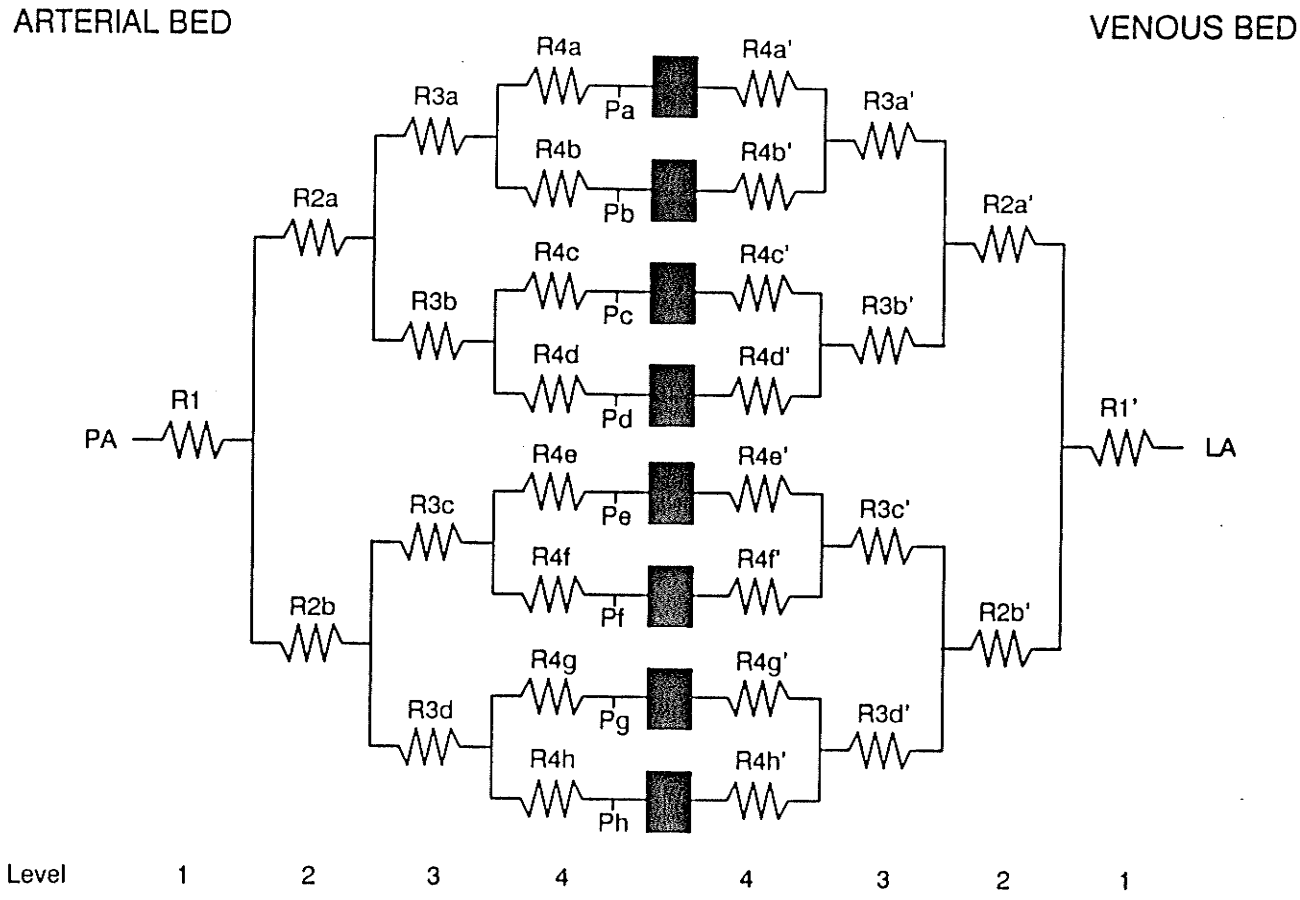

FIGURE 1. Multibranched model - starting at the pulmonary artery side (PA), the arterial vascular bed bifurcates sequentially up to 8 parallel channels that converge and reunite, at the venous side, to end in the left atrium (LA). Separating the two vascular beds are 8 capillary sheets (black areas) representing the capillary bed.

Modeling of the capillary sheet. Fung and Sobin (10, 11) described the pulmonary capillary bed as a sheet of two membranes separated by a set of regularly spaced posts. Both membranes and posts are elastic and respond to changes in intravascular pressure (P_V), P_A, and lung volume (V_L). At a constant P_{TP}, the sheet thickness (H) varies linearly with P_V according to the following relation:

$$H = H_o + \alpha \cdot (P_V - P_A) \qquad \ldots\ldots (1)$$

where H_o is capillary sheet thickness at $P_V = P_A$, and α is compliance (in $\mu m/cmH_2O$) of the capillary sheet. Equation 1 is valid for a $(P_V - P_A)$ range that is between zero and an upper limit $[0 \leq (P_V - P_A) \leq P_{max}]$. P_{max} [25 cmH_2O in the dog (11)] is the pressure at which the sheet reaches maximum thickness (H_{max}) and becomes non-distensible. H_o, in the dog, was estimated by Fung and Sobin (10, 11) to be 2.5 μm. α, on the other hand, is highly dependent on and inversely related to P_{TP} (10, 11). From data available in the literature on the dog lung and in which α was estimated at various P_{TP} (10, 11, 12), given H_o = 2.5 μm, the following relation between α and P_{TP} was derived:

$$\alpha = 0.073 + 0.2 \cdot e^{-(0.141 \cdot P_{TP})} \qquad \ldots\ldots (2)$$

In the pressure range for which equation 1 applies [i.e. $0 \leq (P_V - P_A) \leq 25$ cmH_2O], in combination with equations for blood rheology, conservation of mass, and momentum, Fung and Sobin (10, 11) obtained a basic equation that describes the *P-F* relation in terms of sheet thickness at the arterial (H_{art}) and venous (H_{ven}) ends:

$$F = C \cdot (H_{art}^4 - H_{ven}^4) \qquad \ldots\ldots (3)$$

or,

$$F = C \cdot \{[H_o + \alpha \cdot (P_{art} - P_A)]^4 - [H_o + \alpha \cdot (P_{ven} - P_A)]^4\} \quad \ldots (4)$$

where "C" is a constant that is related to sheet area, length and width, geometry of posts, vascular space-to-tissue ratio, and viscosity (for further details, see *ref.* 10, 11); and P_{art} and P_{ven} are vascular pressures at the arterial and venous ends of the capillary sheet, respectively.

Because the computer algorithm requires the *P-F* relationship to be expressed in terms of resistance (R), equation 4 was rearranged to provide capillary resistance (R_c). Thus, for $0 \leq (P_{art} - P_A) \leq 25$ and $0 \leq (P_{ven} - P_A) \leq 25$,

$$R_c = \frac{(P_{art} - P_{ven})}{C \cdot \{[H_o + \alpha \cdot (P_{art} - P_A)]^4 - [H_o + \alpha \cdot (P_{ven} - P_A)]^4\}} \quad \ldots (5a)$$

or,

$$R_c = \frac{[(P_{art}-P_A)-(P_{ven}-P_A)]}{C\cdot\{[H_o+\alpha\cdot(P_{art}-P_A)]^4-[H_o+\alpha\cdot(P_{ven}-P_A)]^4\}} \quad . . (5b)$$

When $(P_{art}-P_A)$ exceeds 25 cmH_2O, while $0 \leq (P_{ven}-P_A) \leq 25$, H_{art} reaches H_{max} (maximal sheet thickness given by $H_o+\alpha\cdot 25$), and equation 5b becomes:

$$R_c = \frac{[25-(P_{ven}-P_A)]}{C\cdot\{H_{max}^4-[H_o+\alpha\cdot(P_{ven}-P_A)]^4\}} \quad . . . . . (6)$$

When $(P_{ven}-P_A)$ rises towards 25, while $(P_{art}-P_A) > 25$, R_c decreases non-linearly towards an asymptote [minimal capillary resistance (R_{cmin})] which would be obtained when both ends are maximally distended. For a given H_o and α, R_{cmin} is a function of the constant "C" according to the following relation:

$$R_{cmin} = 1/[4\cdot\alpha\cdot C\cdot(H_{max})^3] \quad . . . . . (7)$$

Hence, when both $(P_{art}-P_A)$ and $(P_{ven}-P_A)$ are greater than 25, R_c is treated as constant and equal to R_{cmin}.

The situation becomes more complex when P_{ven} is less than P_A. In this range, R_c consists of two components. The proximal component, R_{c1}, covers the region from the arterial end (where H

is related to P_{art}) to the point where intravascular pressure equals P_A (and $H = H_o$). The resistance of this segment is given by:

$$R_{c1} = \frac{(P_{art}-P_A)}{C\cdot\{[H_o+\alpha\cdot(P_{art}-P_A)]^4-H_o^4\}} \quad \ldots\ldots (8)$$

The more distal segment (R_{c2}) acts as a Starling resistor whose R changes inversely with *F* to absorb the pressure difference between P_A and P_{ven}. Thus,

$$R_{c2} = \frac{(P_A-P_{ven})}{C\cdot\{[H_o+\alpha\cdot(P_{art}-P_A)]^4-H_o^4\}} \quad \ldots\ldots (9)$$

When $0 \leq (P_{art}-P_A) \leq 25$, R_c, the sum of R_{c1} and R_{c2} simplifies to:

$$R_c = \frac{(P_{art}-P_{ven})}{C\cdot\{[H_o+\alpha\cdot(P_{art}-P_A)]^4-H_o^4\}} \quad \ldots\ldots (10)$$

When $(P_{art}-P_A)$ is greater than 25, H_{art} becomes H_{max} and R_{c1} becomes fixed. Thus,

$$R_{c1} = \frac{25}{C\cdot(H_{max}^4-H_o^4)} \quad \ldots\ldots (11)$$

and R_{c2} becomes,

$$R_{c2} = (P_A - P_{ven})/F \qquad \ldots\ldots (12)$$

Since F here is determined by $(P_{art}-P_A)$ and R_{c1}, i.e.

$$F = (P_{art}-P_A)/R_{c1} \qquad \ldots\ldots (13)$$

hence,

$$R_c = R_{c1} + \frac{(P_A - P_{ven})}{[(P_{art}-P_A)/R_{c1}]} \qquad \ldots\ldots (14)$$

or,

$$R_c = \left[\frac{25}{C\cdot(H_{max}^4 - H_o^4)}\right] \cdot \left[\frac{(P_{art}-P_{ven})}{(P_{art}-P_A)}\right] \qquad \ldots\ldots (15)$$

Finally, when $(P_{art}-P_A)$ decreases below zero, F through that segment was assumed to equal zero.

It must be noted that the above analysis, although not contradictory with the sheet-flow theory of Fung and Sobin (10, 11), represents our own concept of their model. Relations between $(P_{in}-P_A)$ and F at various $(P_{out}-P_A)$ for a sheet with R_{cmin} of 0.4 $cmH_2O/l/min$, H_o of 2.5 μm, and α of 0.172 $\mu m/cmH_2O$

(i.e. P_{TP} of approximately 5 cmH_2O) are shown in Figure 2A. Relations between ($P_{out}-P_A$) and F at different ($P_{in}-P_A$) for the same sheet are shown in Figure 2B.

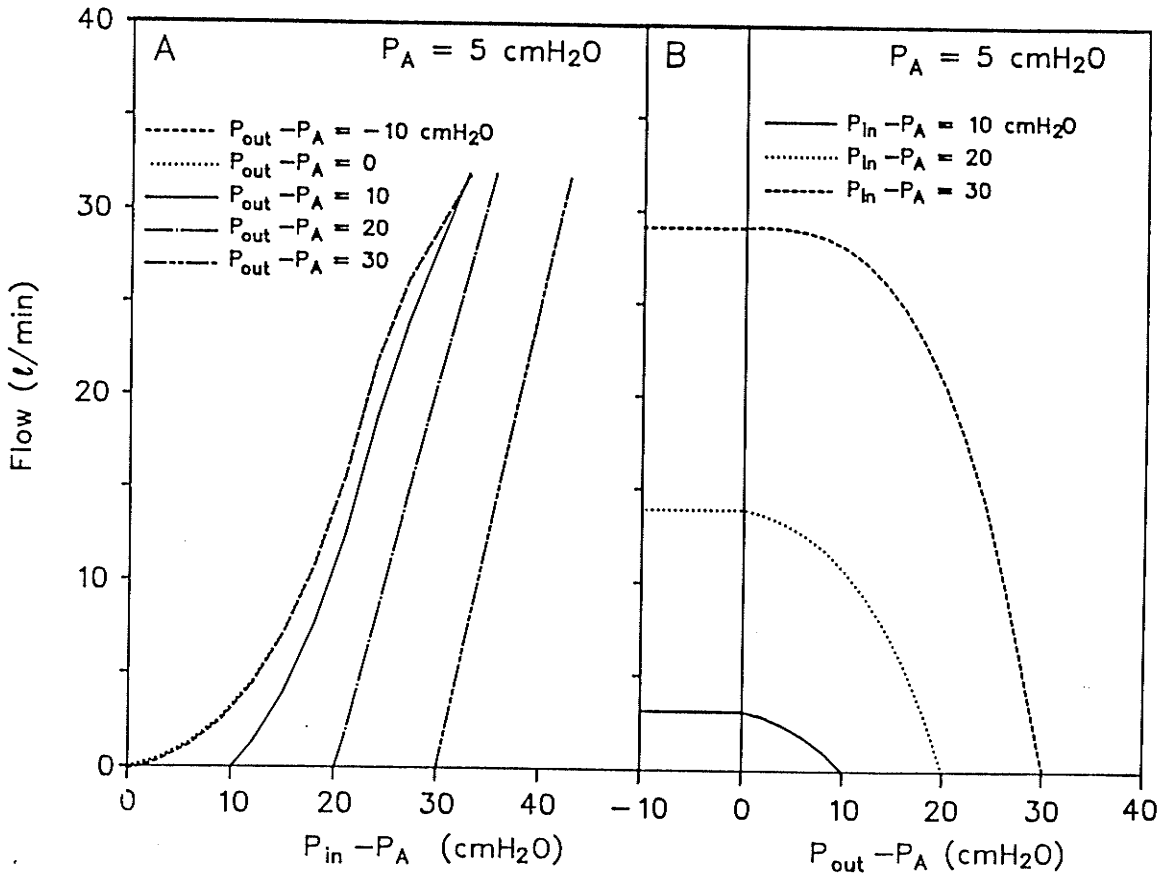

FIGURE 2. Panel A: *P-F* relations of the capillary sheet at various P_{out}. Panel B: *Pout-F* relations showing flow limitation at various levels of P_{in}. P_A is alveolar pressure.

C. PROCEDURE

We used a personal computer (10 MHz, 80286 based IBM-compatible system with an 80287 co-processor) to carry out the calculations. For a given P_{LA} and total blood flow (F_T), the algorithm computes the steady state values for pressure and F at different points in the model under specific conditions of P_{TP}, gravitational effects, mechanical properties, and vasomotor tone in individual vessels.

General inputs are P_A, pleural pressure (P_{pl}), lung height (H_t), P_{LA}, F, and V_M and C_L [the parameters describing the pressure-volume relation of the lung (CHAPTER 5)]. *Branch-specific* inputs are as follows:

1) Mechanical properties of vessels: Each extra-alveolar vessel can be given the properties of an artery or a vein which responds to transmural pressure (P_{TM}) according to equations derived in part I of this communication [equations 13 and 14, respectively (CHAPTER 5)]. In addition, the mechanical properties of each vessel [i.e. cross-sectional area (A) vs. P_{TM} relations] could be individually altered by appropriate selection of the constants "B_v" and "C_v", and "A_a" and "B_a" [part I, equations 13 and 14, respectively (CHAPTER 5)]. For the sake of simplicity, data presented here were generated under the assumption that all precapillary branches behaved like arteries and all post-capillary branches behaved like veins. Values for

the constants were obtained from average data of Smith and Mitzner (28) as specified earlier (CHAPTER 5). These values were kept uniform for each type of vessel.

H_o and α of each capillary sheet could be varied individually. In the present analysis H_o was 2.5 μm and values for α were calculated according to equation 2.

2) **Reference resistance ($R_{o,35}$):** This is the resistance a particular extra-alveolar vessel would have at P_{TM} = 35 cmH_2O and P_{TP} = 0 cmH_2O (CHAPTER 5). For the analysis presented in "Results" total resistance of each arterial generation (i) under reference conditions [$R_{TO,35(i)}$] was assumed similar to that of other arterial generations. Thus,

$$R_{TO,35(1)} = R_{TO,35(2)} = R_{TO,35(3)} = R_{TO,35(4)}$$

or,

$$R_{O,35(1)} = R_{O,35(2)}/2 = R_{O,35(3)}/4 = R_{O,35(4)}/8$$

where $R_{O,35(i)}$ is reference resistance of individual branches within a generation. A similar treatment was used for the venous system. Hence,

$$R_{TO,35(1)}' = R_{TO,35(2)}' = R_{TO,35(3)}' = R_{TO,35(4)}'$$

and,

$$R_{0,35(1)}' = R_{0,35(2)}'/2 = R_{0,35(3)}'/4 = R_{0,35(4)}'/8$$

Furthermore, arteries and veins of the same generation were considered to have equivalent $R_{0,35}$. Maloney et al. (19) found that arteries and veins of the same generation achieved equal diameters in the vascular pressure range of 28 to 40 cmH_2O. We have also found, by trial and error, that when resistances of arteries and veins of same generation are made equal at P_{TM} of 35 cmH_2O, the partition of resistance upstream and downstream from the capillaries under *base line* (normal) conditions (F_T = 2 *l*/min, P_{LA} = 3 mmHg, and P_{TP} = 0 cmH_2O and a normal R_T under these conditions of 6 mmHg/*l*/min) to be about 50:50. This distribution is well within the range described in the literature (9).

R_{cmin} for each capillary sheet was used to derive the constant "C" (equation 7, above). The relation between R_{cmin} for capillary sheets and $R_{0,35}$ for extra-alveolar vessels was somewhat problematic since data for the contribution of capillaries to total resistance (R_T) at P_{TM} = 35 cmH_2O is not available. A fraction of 0.2 was chosen arbitrarily. The effect of errors in this selection for values below (0.05) and above (0.5) 0.2 on the overall response of the system was tested (see "RESULTS").

Values for $R_{0,35}$ and R_{cmin} were obtained by trial and error. R_T of 6 mmHg/*l*/min under the *base line* conditions described above (i.e. F_T = 2 *l*/min, P_{LA} = 3 mmHg and P_{TP} = 0 cmH_2O) was sought. These were (in mmHg/*l*/min): $R_{0,35(1)}$ = 0.2, $R_{0,35(2)}$ = 0.4, $R_{0,35(3)}$ = 0.8, $R_{0,35(4)}$ = 1.6, R_{cmin} = 3.2, $R_{0,35(4)}'$ = 1.6, $R_{0,35(3)}'$ = 0.8, $R_{0,35(2)}'$ = 0.4 and $R_{0,35(1)}'$ = 0.2.

3) Vasomotor tone: For each extra-alveolar vessel a P_T value corresponding to the pressure exerted by smooth muscle tone at A_o was added.

Calculation of pulmonary artery pressure. Iteration proceeded in loops with each loop consisting of the following steps:

1) Calculation of *F* in each branch. As a first step, calculation of *F* in each branch was based on $R_{0,35}$ and R_{cmin} values assigned to the various branches and capillaries, respectively, and F_T. Thus, for R_1, $F = F_T$. For the second generation of arteries (R_{2a} and R_{2b}) F_T was partitioned in inverse proportions to the respective downstream resistance down to the equivalent venous branch, inclusive. Thus, for R_{2a}, the relevant resistance was the sum of all resistances between R_{2a} and R_{2a}', inclusive, taking into account the parallel and serial arrangement of resistors. The same principles were used to partition *F* into subsequent generations. Resistances computed at the end of each iteration (see below) were used for the subsequent iteration.

2) **Calculation of P_V at different points.** Starting with P_{LA}, P_{in} to R_1' was calculated from F_T and the resistance assigned to that vessel. P_{in} for R_1' then served as P_{out} for the next generation. This process was then repeated up to the first arterial generation. Again, for the first iteration $R_{0,35}$ was used. For subsequent iterations the resistance value obtained at the end of the previous iteration, for the particular vessel, was used.

3) **Accounting for gravity.** The model consists of 14 vertical spaces between 15 vascular levels (Figure 1). Each level was assigned a rank [$Rn_{(i)}$]. When referencing pressures to the bottom of the lung, ranks span from 0 (bottom level) to +14 (top). To reference pressures to the "hilum" the ranks were -7 to +7 and to reference pressures to top of lung the ranks were -14 to 0. P_G in cmH_2O was calculated from,

$$P_G = \frac{H_t}{14} \cdot Rn_{(i)} \qquad \ldots\ldots (16)$$

Depending on the vessel rank, P_G, for each vessel, was calculated and subtracted from P_V after converting the latter to cmH_2O.

4) **Allowing for vascular tone.** See section C, CHAPTER 5 for details of handling smooth muscle tone. As indicated earlier (CHAPTER 5), there is little information regarding the change in P_T as a function of lumen area (A) in pulmonary vessels.

However, we have shown that the *P-F* relation of individual vessels is, qualitatively, quite insensitive to the P_T vs. *A* relation. Over the wide range of possible behaviors (see Figures 6 and 8, CHAPTER 5 and related text), the differences between various patterns were primarily in the magnitude of change in P_z for a given active state. The magnitude of parallel shift (in the *P-F* relations) also varied slightly for a given active state depending on the pattern selected (CHAPTER 5). However, these differences are meaningless in the present context. Accordingly, and for simplicity, in the present analysis P_T was assumed constant and does not vary with vessel diameter [i.e. pattern 2 *c* (CHAPTER 5)].

5) **Calculation of P_x.** For all vessels except R_1 and R_1', P_x was calculated according to equation 8 (CHAPTER 5) using the appropriate (i.e considering P_{TP}) constants "a", "b" and "c", and P_v. For R_1 and R_1' extravascular pressure was assumed equal to P_{p1} (i.e. zero in the present analysis).

6) **Calculation of P_{TM}.** For each extra-alveolar vessel, starting with P_{out} as P_v, P_{TM} was calculated as $P_v - P_x$. As each vessel was further divided into 25 serial segments, P_x and hence, P_{TM} for each successive segment was continuously adjusted as a function of P_v for that vessel. For the capillary sheets ($P_{art}-P_A$) and ($P_{ven}-P_A$) were individually calculated.

7) **Calculation of resistances.** Calculation of resistance of extra-alveolar vessels was done using numerical integration as indicated in "Methods" (CHAPTER 5). Each vessel consisted of 25 segments (as opposed to 100 in the preceding communication) to speed up calculations. Results obtained with 25 segments were different from those obtained with 100 segments at the second decimal level. R_c of each capillary sheet was calculated according to the appropriate form of equation 5.

8) **Comparing resistances.** Resistances obtained in step 7 were then compared with the assumed values used in step 1. If the two values were within 0.1% of each other in all vessels, a correct solution was presumed and iteration stopped. If the values differed by more than 0.1% in any vessel a new set of resistances, intermediate between the two values, was selected (for all vessels) for use in step 1 and the cycle was repeated. Intermediate values were calculated as 0.95 of the previous value plus 0.05 of the new value. Although this approach required more iterations to reach a solution, it prevented divergent oscillations. With this routine, the time required to reach a steady-state ranged between 3 and 120 seconds. This time depended on the complexity of the problem (primarily the extent of heterogeneity among branches).

D. RESULTS AND DISCUSSION

1. Response of the multibranched model in physiologic states

P-F relationships at various outflow pressures. *P-F* relationships for P_{LA} of 0, 5, 10, 15, and 20 mmHg at both low (5 cmH_2O) and high (20 cmH_2O) P_A were generated for a H_t of 14 cm (all pressures being referenced to LA). P_{pl} was zero and the circulation was passive (i.e. $P_T = 0$). The results are shown in Figures 3A and 3B, respectively. All curves are initially convex to the pressure axis. Above a certain flow this relationship becomes nearly linear.

At lower P_A (Figure 3A), raising P_{LA} in steps from 0 to 20 mmHg produced equivalent shifts in the pressure intercept at zero flow (P_z). This indicates that P_{LA}, under these conditions, was acting as effective outflow pressure due to the presence of at least one alveolar vessel that was maintained open by gravitational forces at the bottom of the lung. At higher P_A (20 cmH_2O) an increase in P_z did not occur until P_{LA} exceeded 10 mmHg. This is attributed to the collapse of all alveolar vessels thus forcing P_z to be independent of P_{LA} until the first alveolar vessel opens. Raising P_{LA} causes a roughly parallel shift in the linear portion of the *P-F* relationship. The extent

of this shift is typically less than the rise in P_{LA} and it increases with increasing P_{LA} (Figure 3A). Also, for a given change in P_{LA}, the shift is smaller at higher P_A (Figure 3B).

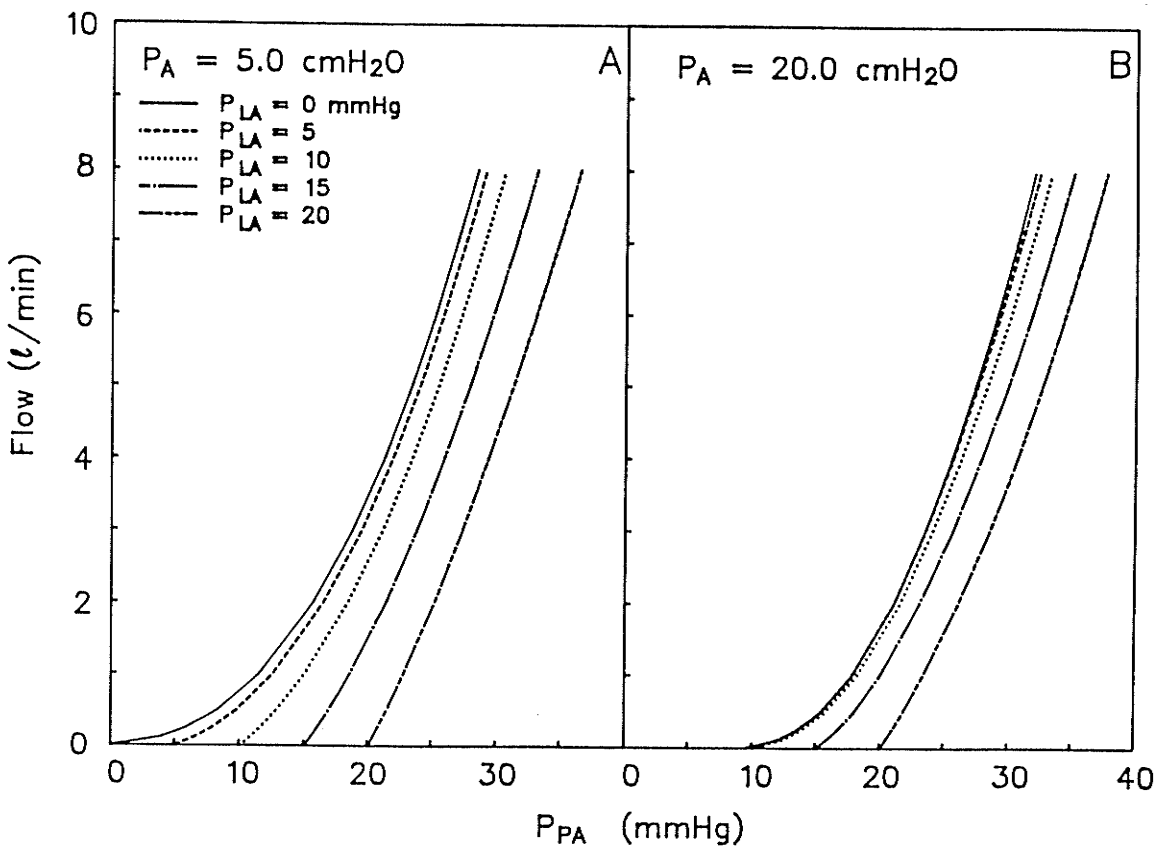

FIGURE 3. *P-F* relations generated with the multibranched model at various left atrial pressures (P_{LA}) for both low (Panel A) and high (Panel B) alveolar pressures (P_A).

The model predictions for *P-F* relations at various P_{LA} are in striking agreement with results reported by Banister and Torrance (1). Their results, obtained in isolated cat lungs, also show that raising venous pressure shifts the *P-F* curves to the right by an amount that is always less than the rise in venous pressure and is markedly affected by P_A.

As indicated in "INTRODUCTION" the progressive reduction in R_T with increasing *F* (implicit from the non-linear behavior of the *P-F* relation) could be due to progressive recruitment, progressive vascular distention, or both. To assess the relative importance of these two factors we compared *P-F* relations generated with and without gravity effects. Figure 4A (*left*) shows *P-F* relationships when P_A is 5 cmH_2O and P_{LA} is 0 mmHg (referenced to LA). Under these conditions, and in the presence of gravity (H_t = 14 cm, *dashed line*), raising P_{PA} just above zero initiates *F* in the lowest segment only [since P_V exceeds P_A only in the lowest capillary sheet]. As P_{PA} is increased more channels are recruited and when P_{PA} exceeds 9 mmHg all channels are recruited. By inputting H_t as zero (*solid line*), gravity effect (no vertical pressure gradient) and progressive recruitment are eliminated. Instead, all vessels open when P_{PA} just exceeds 5 cmH_2O (or 3.6 mmHg). As seen from Figure 4A, apart from the difference near zero *F* the two lines (*solid* and *dashed*) are almost indistinguishable indicating that recruitment

contributes little to the non-linear behavior of the *P-F* relationship. Over most of the *F* range, non-linearity is primarily a function of distensibility of the vascular bed.

To ascertain the extent to which the special mechanical characteristics of the capillary sheet are responsible for the overall behavior, we have generated *P-F* relations using a single vessel in which the 50 most downstream segments have the mechanical properties of extra-alveolar veins and the 50 most upstream segments have the mechanical properties of extra-alveolar arteries (CHAPTER 5) under the same P_{out} (i.e. equal to zero) after adjusting $R_{0,35}$ so that P_{in} at a normal *F* of 2.0 *l*/min was similar to that of the multibranched model. The results are shown by the dotted line in Figure 4A (*left*). Again, there was little difference from the response of the multibranched model with a capillary sheet whether or not gravity (i.e. recruitment) was a factor.

Figure 4B shows *P-F* relationships generated when P_A is 20 cmH_2O and P_{LA} is 0 mmHg (*left*) with (H_t = 14 cm, *dashed line*) and without (H_t = 0, *solid line*) gravity effects. Under these conditions, similar to lower P_A, recruitment affects the *P-F* relationship only over a limited flow range that is below normal. The distinctive behavior (i.e. non-linear followed by linear) of the *P-F* relationship is still dictated by the characteristic static behavior (distensibility) of the pulmonary vessels.

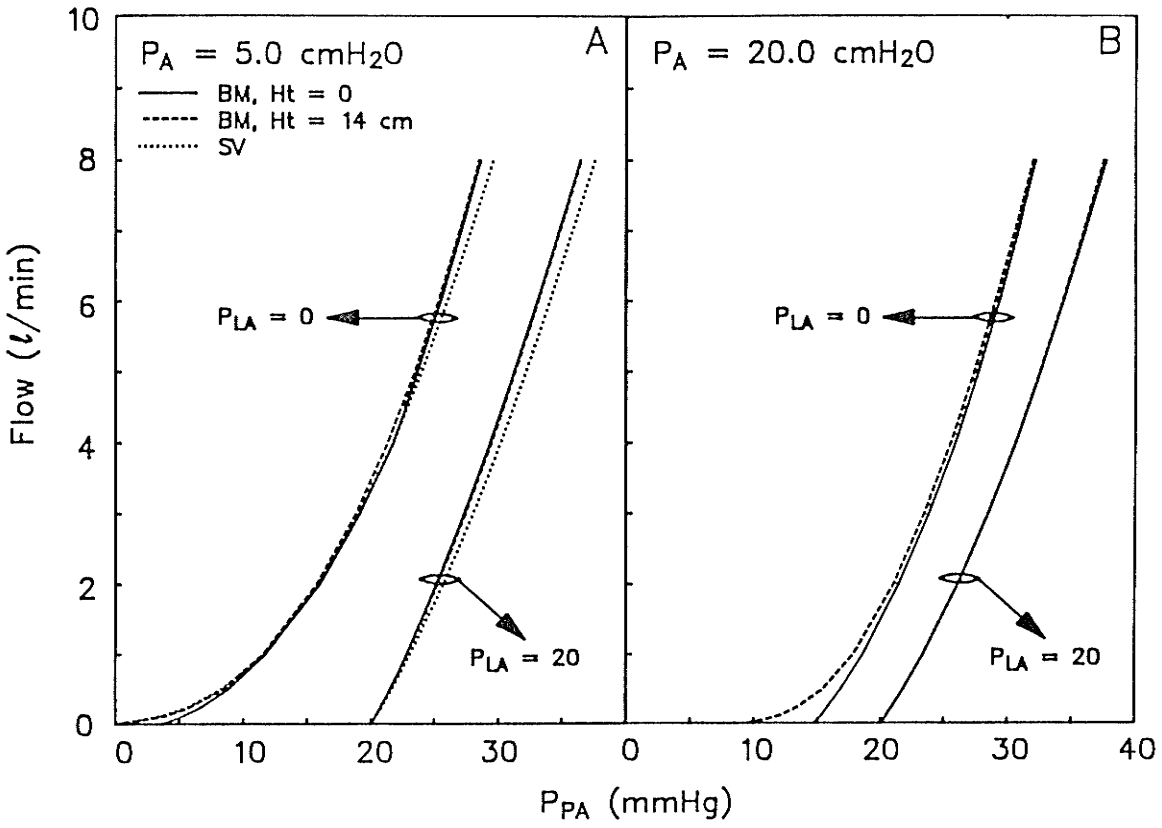

FIGURE 4. *P-F* relations generated with (H_t=14 cm) and without (H_t=0 cm) gravity effects using the multibranched model (BM) and a mixed single vessel (SV) at low (0 mmHg) and high (20 mmHg) outflow pressures. Panel A shows relations generated when P_A is 5 cmH_2O and Panel B when P_A is 20 cmH_2O.

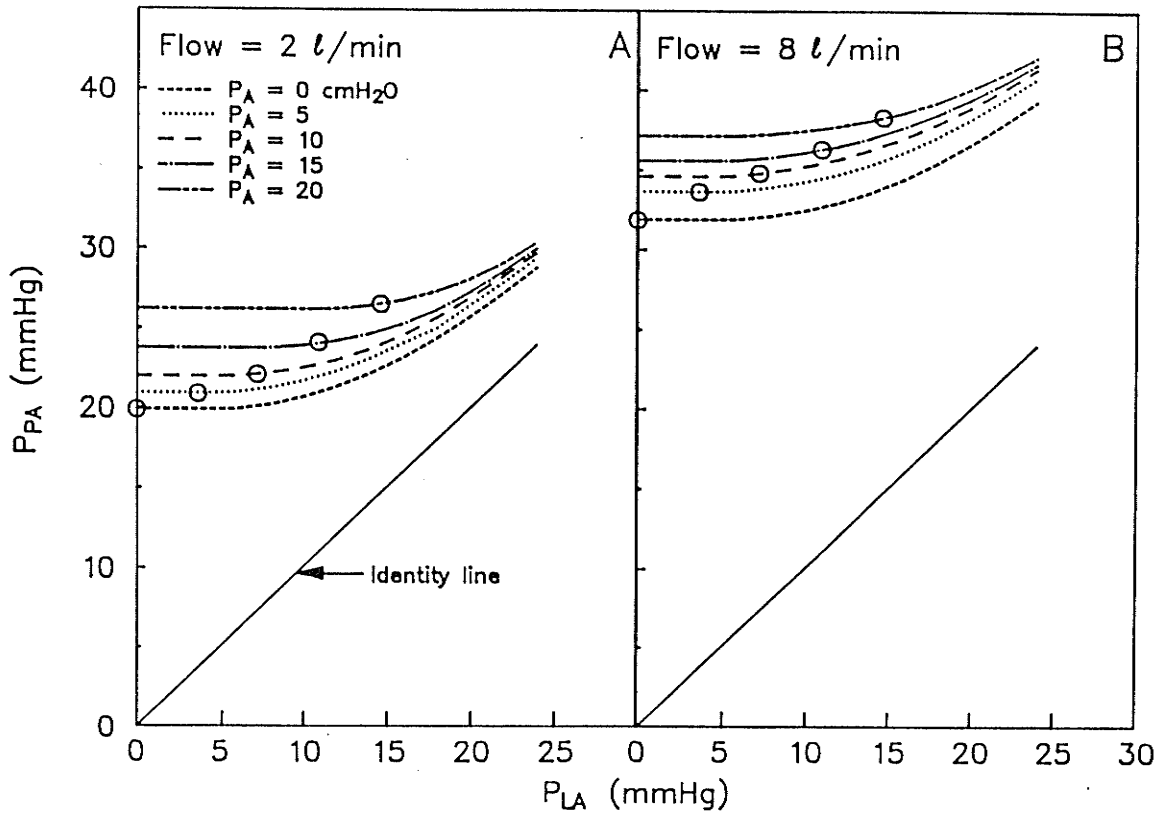

FIGURE 5. P_{LA}-P_{PA} relationships generated with the multibranched model at various alveolar pressures (P_A) for both normal (Panel A) and above normal (Panel B) flow rates. Open circles designate the point at which P_{LA} equals P_A.

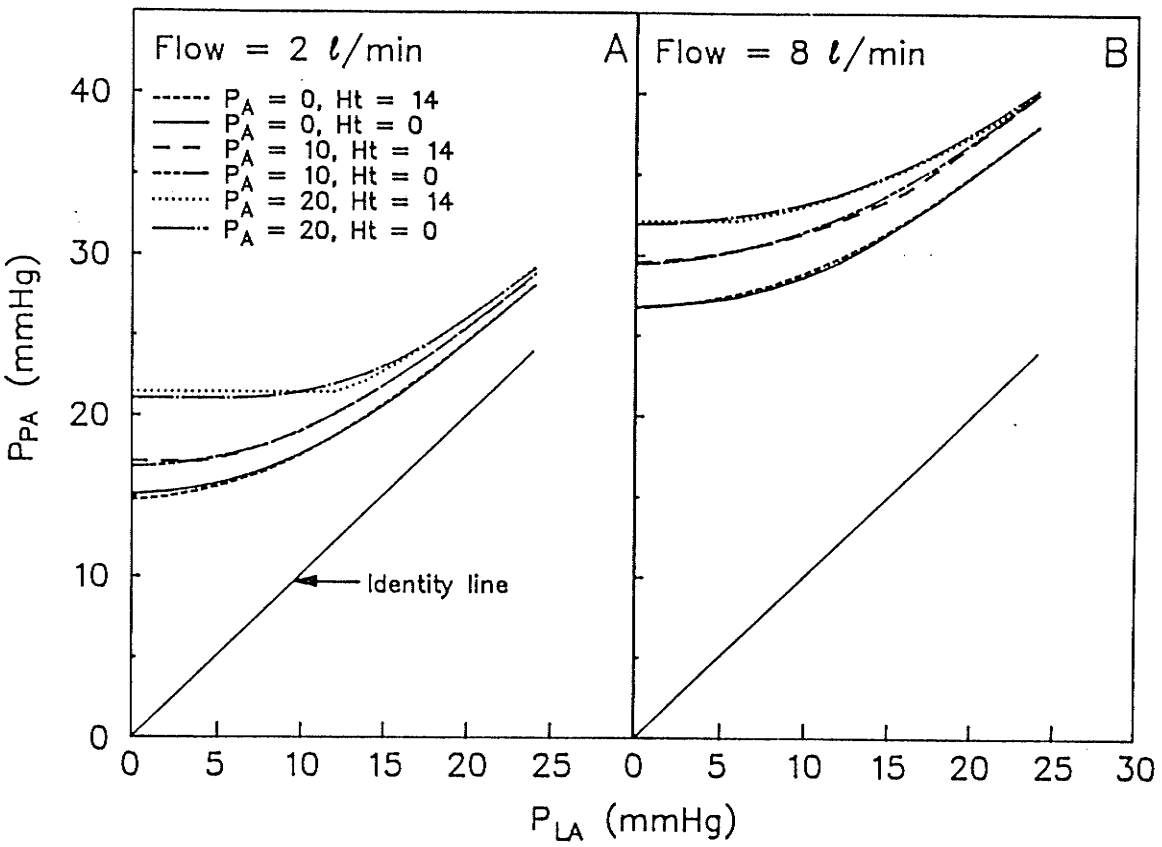

FIGURE 6. P_{LA}-P_{PA} relationships at various alveolar pressures generated with (H_t=14 cm) and without (H_t=0 cm) gravity effects at both normal (Panel A) and above normal (Panel B) flow rates.

As might be expected, when the same three conditions were compared at high P_{LA} [multibranched with and without gravity (Figures 4A and 4B, *right*) and single vessel (Figure 4A, *right*)] little differences were observed.

P_{LA}-P_{PA} relationships at various P_A. P_{LA}-P_{PA} relationships at P_A of 0, 5, 10, 15, and 20 cmH_2O for both normal (2 *l*/min) and above normal (8 *l*/min) pulmonary blood flows are shown in Figures 5A and 5B, respectively. For the sake of comparison with existing animal studies, in these runs pressures were referenced to the bottom of the lung (H_t = 14 cm). At both flow rates and all P_A levels, there is a P_{LA} range over which P_{PA} is independent of P_{LA}. Above this range, the slope of the curve (i.e. $Z = \Delta P_{PA}/\Delta P_{LA}$) increases smoothly toward unity. The point of inflection between a slope of zero and a slope greater than zero appears to coincide with P_A (circles) for P_A greater than 5 cmH_2O.

The model results of P_{LA}-P_{PA} relations are highly consistent with results previously reported by various investigators. Banister and Torrance (1) noted that venous pressure had to rise to values within one cmH_2O of P_A in order to have any influence on P_{PA} at constant *F*. West and Dollery (29) also found that venous pressure had no effect on P_{PA} at constant *F* until it exceeded P_A. Permutt et al. (23) showed that P_{LA} had to be increased to values approximately equal to P_A before there was any decrease in *F* at constant P_{PA}. Our results are also in

striking agreement with results reported by Lopez-Muniz et al. (18). In the range P_{TP} greater than 5 mmHg a near identity between the transition point and P_A was found, whereas in the range P_{TP} less than 5 mmHg the transition point occurred at outflow pressures of about 5 mmHg. The latter value was fixed and independent of P_A at a constant *F*. Lopez-Muniz et al. (18) and Permutt and Riley (25) attributed this phenomenon to smooth muscle tone. While vascular tone can enhance this phenomenon the present model predicts its existence without any vascular tone.

The experimental data quoted above have helped support the notion that a vascular waterfall exists at the capillary level when P_A exceeds P_{LA}. In the region where P_{PA} is independent of P_{LA} (i.e. slope near zero) most of the capillaries are presumed to show this waterfall phenomenon (zone 2 perfusion). Hence, pressure upstream from the capillaries is independent of P_{LA} at all levels. A slope that is intermediate between zero and one would, using the same interpretation, indicates that some units are in zone 2 while others, in more dependent regions, are in zone 3 (on account of gravity). In these, upstream pressure is influenced by P_{LA}. To the extent that a similar behavior is displayed by a single vessel with mechanical properties similar to those of extra-alveolar vessels and where a capillary sheet does not exist and intravascular pressure is greater than perivascular pressure throughout its length [i.e. a waterfall does not exist (CHAPTER 5)], distensibility of the vascular bed,

independent of any vascular waterfall, must account for at least some of this behavior. To evaluate the extent of this contribution we have generated P_{LA}-P_{PA} relations with a H_t of 14 cm (i.e. as in Figure 5) and compared the results with those when H_t was zero. In the latter case all capillary sheets are either in zone 2 or zone 3 depending on P_{LA}. If the explanation for the distinct behavior of this relation is the heterogeneity of flow regime (zone 2 vs. zone 3) in different regions, then when gravity is removed transition from a slope of zero to a slope greater than zero should be very crisp and once the transition pressure is exceeded, the slope of the P_{LA}-P_{PA} relation should be fixed and near unity. The results for selected alveolar pressures of 0, 10 and 20 cmH_2O at the two flow rates (2 and 8 *l*/min) are shown in Figures 6A and 6B, respectively. Notice that pressures in this figure were referenced to LA. This was done to ensure that P_{LA} with and without gravity effects were equal (in absolute terms) without having to correct P_{LA} for lung height when pressures are referenced to the bottom of the lobe. That the transition in all cases is still gradual (in fact the curves are almost indistinguishable) strongly suggests that a waterfall phenomenon at the level of the capillaries is not a significant factor underlying the P_{LA}-P_{PA} behavior. Rather, the explanation is similar to that discussed in relation to the single vessel. Increasing P_A simply forces a segment of the circulation to

operate at low distending pressures where R is highly dependent on distending pressure, thereby accentuating the mechanism (i.e. decrease R_T) that damps the response of P_{PA} to changes in P_{LA} and to which all vascular segments contribute.

P-F relationships at various P_A. *P-F* relationships were generated at P_A of 0, 5, 10, 15, and 20 cmH_2O and P_{LA} of 2 and 15 mmHg (H_t = 14 cm, all pressures referenced to LA). The curves are shown in Figures 7A and 7B, respectively.

At lower P_{LA} (Figure 7A), raising P_A from 0 to 10 cmH_2O produced no effect on P_z. P_z was not affected by lung inflation and was equal to P_{LA} at these levels of P_{TP} due to the presence of at least one alveolar vessel that was maintained open by gravitational forces at the bottom of the lung. At higher P_{TP} (15 and 20 cmH_2O), an increase in P_z with lung inflation is evident. A parallel shift in the rectilinear part of the *P-F* relationship is also evident.

By raising P_{LA} to 15 mmHg, full recruitment of the capillary bed is achieved (Figure 7B). Under these conditions, the increase in P_z is eliminated. The parallel shift of the *P-F* relationship is also diminished.

Our model predictions are highly consistent with results previously reported by various investigators. In 1951, in isolated canine right lower lobes, Edwards (8) first showed that raising P_A causes both an increase in P_z and a shift toward

higher P_{PA} in the *P-F* relationship. A shift in the *P-F* relation, with increasing P_A has been shown by other investigators in both dog (14, 26) and cat preparations (1, 2, 4).

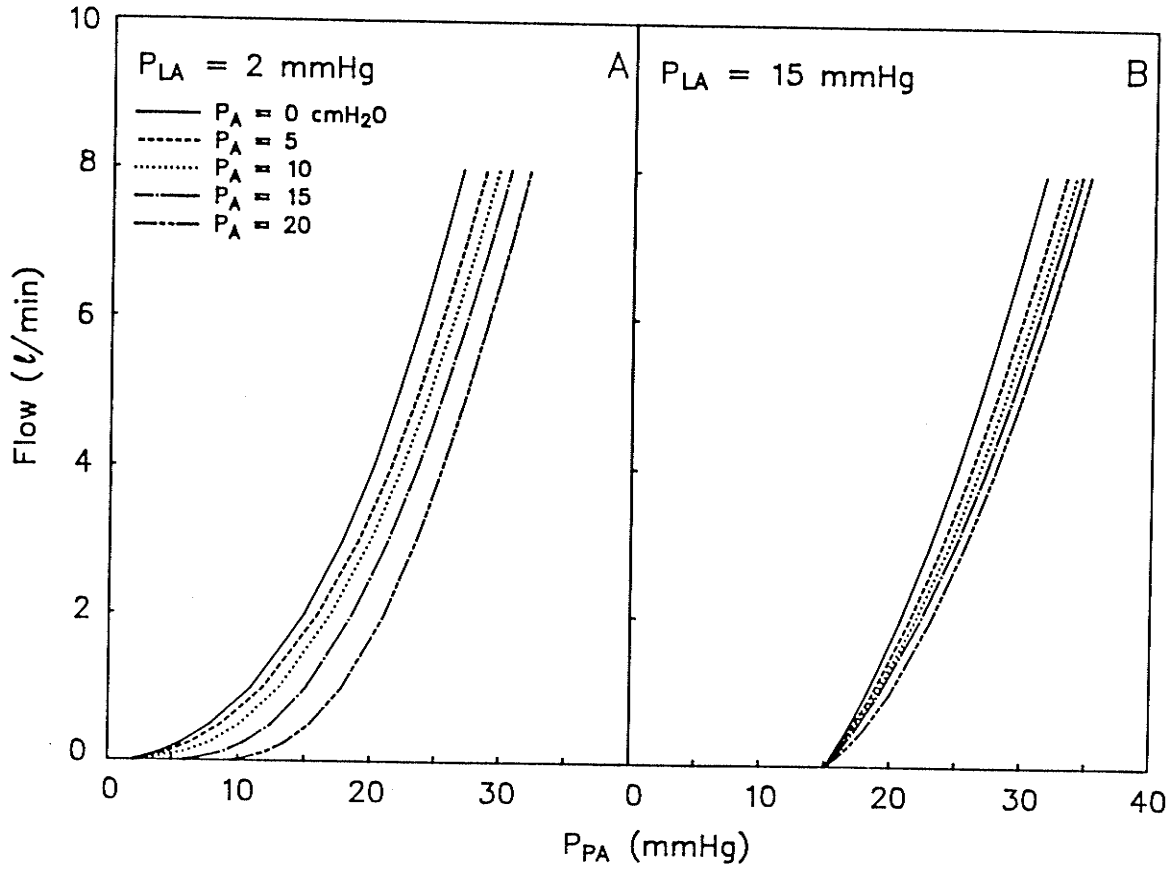

FIGURE 7. *P-F* relations generated with the multibranched model at various alveolar pressures (P_A) for both low (Panel A) and high (Panel B) P_{LA}.

Model predictions for P_z do not totally agree with observations made by Graham et al. (14) in isolated canine left lower lobes. In their study, raising P_A from 5 to 15 cmH_2O did not affect P_z (which was about 10 cmH_2O referenced to the bottom of the lobe). It is possible in our model to account for a fixed P_z that is higher than P_{LA} and that is independent of P_A (over the range $0 \leq P_A \leq P_z$) by introducing vascular tone. When vascular tone exceeds P_A it acts as the effective outflow pressure or P_z. However, in order to obtain a P_z that is lower than P_A it is necessary to introduce to the model additional channels that bypass the alveoli and thus allow P_{PA} to drop to levels below P_A. The time that was allowed, in the study of Graham et al. (14), for P_{PA} to stabilize (about 5 min) suggests that these vessels must have a very high resistance and therefore do not play a significant role in determining *P-F* relations under steady-state flow conditions.

As mentioned in "METHODS", R_{cmin} was selected arbitrarily to account for 20% of total resistance at reference conditions ($R_{T0,35}$). Because V_L (and hence P_A) affects alveolar and extra-alveolar vessels differently (i.e. raising P_A increases R of alveolar vessels and decreases R of extra-alveolar vessels) one anticipates the fractional contribution of R_{cmin} to $R_{T0,35}$ to affect the general behavior of the *P-F* relations while raising P_A. We have, therefore, compared *P-F* relations obtained when R_{cmin} is 5 and 50% of $R_{T0,35}$ with those shown in Figures 7A and

7B (obtained when R_{cmin} is 20% of $R_{T0,35}$). As expected P_z did not differ in any of these curves. The extent of right shift obtained with increasing P_A was roughly 20% less when R_{cmin} was 5% of $R_{T0,35}$ and 30% more when R_{cmin} was 50% of $R_{T0,35}$ compared to the shifts obtained in Figures 7A and 7B (figures not shown).

2. Response of the multibranched model in pathologic states

Vascular obstruction. With vascular obstruction $R_{0,35}$ of the occluded vessels becomes infinite and independent of P_{TM} while the behavior of the remaining vessels is kept "normal". Since each branch in the model represents several parallel channels, occlusion of some of the channels would remove some of the conductances, thus reducing the conductance of the branch by the same proportion (i.e. occluded vessels divided by total vessels) at all transmural pressures. Given the mathematical form used to compute R of each branch in the model (equations 13 and 14, CHAPTER 5), vascular occlusion can be simulated by simply increasing the value of $R_{0,35}$. To simulate occlusion of all vessels encompassed by one branch, $R_{0,35}$ for that branch is inputted as an infinitely high number (10^6 was used in the simulation). To simulate occlusion of half of the vessels in a branch $R_{0,35}$ for the branch is doubled, and so on.

Figure 8 shows *P-F* relations at P_A of 5 cmH_2O and P_{LA} of 5 mmHg when all vessels are intact (solid line), and when multiple occlusions (dashed line) caused obstruction of all vessels represented by R_{2a} (i.e. $R_{2a0,35} = 10^6$) as well as most vessels represented by R_{3c} and R_{4h} ($R_{3c0,35}$ increased 15 times and $R_{4h0,35}$ 20 times their normal values, respectively). This selection was arbitrary. However, the results were qualitatively similar when other combinations were utilized. The *P-F* relationship with vascular occlusion continues to show the same general characteristics as in the absence of occlusion; the slope of the relation progressively increases as *F* increases finally reaching a near linear segment and constant slope. The slope of the *P-F* curve at any *F* is, however, lower than in the absence of occlusion. There is, accordingly, no tendency for the two lines to become parallel; the lines continue to diverge as *F* increases (*cf* increased tone). Significantly, P_{op}, determined by extrapolation of the linear segment (*dots*), in the presence of occlusion is shifted to the right, a finding that may be erroneously attributed to a co-existent increase in P_{crit} (e.g. 6, 7, 13, 21, 27).

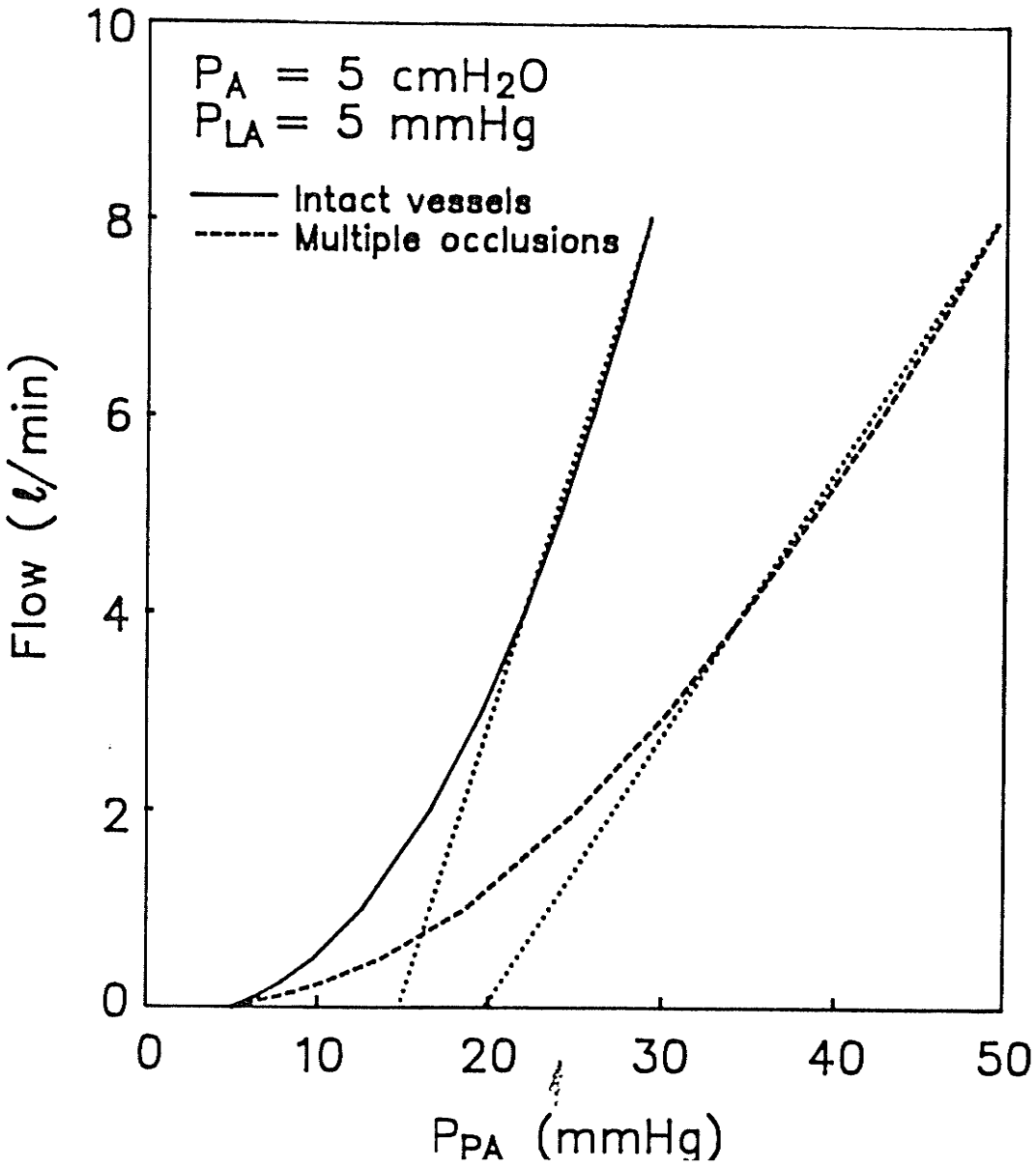

FIGURE 8. *P-F* relations with all vessels intact (*solid line*) and with multiple occlusions (*dashed line*) causing obstruction of all vessels represented by R_{2a} as well as most vessels represented by R_{3c} and R_{4h} (Figure 1). Dotted lines show the effect of extrapolating the nearly linear segments to zero flow.

Increased vascular tone. As in the case of the single vessel, vascular tone was modeled as a radial force opposing P_V, thereby reducing effective P_{TM}. Vessel area at a given effective P_{TM} (and hence $R_{0,35}$) are unaltered. Figure 9 shows *P-F* relations generated without added tone (*solid lines*) and with 3 levels of added tone, equivalent to 5, 10, and 15 mmHg, respectively. Left and right panels depict the responses at low (2 mmHg) and high (20 mmHg) P_{LA}. In the top two panels (A and B), tone was applied uniformly to all extra-alveolar vessels. In the middle pair (C and D) tone was applied to all precapillary vessels and in the bottom two panels (E and F) tone was applied to the third arterial generation only (i.e. R_{3a} to R_{3d}, Figure 1). In all cases H_t was 14 cm, P_A was zero, and pressures were referenced to LA.

As might be expected, when P_{LA} is low (*left*) addition of tone causes a right-ward shift in the minimum pressure required to initiate flow (i.e. P_z). The shift in P_z in panel E is less than in panels A and C since gravity forces the opening of the lowest constricted vessel (R_{3d}) at a lower P_{PA}. In all cases, however, the lines diverge from the no-tone line until a critical horizontal displacement has been reached. Above this level the *P-F* lines are shifted in a parallel fashion to the no-tone line, and to each other. The *F* at which the parallel shift begins is generally in the normal *F* range (2 to 4 *l*/min). Also as might be expected, the shift in the *P-F* relationship is greater at higher

tone levels. However, for a given P_T the shift is less at higher P_{LA}. The magnitude of shift also decreases as a function of the proportion of the vascular segment subjected to the applied tone.

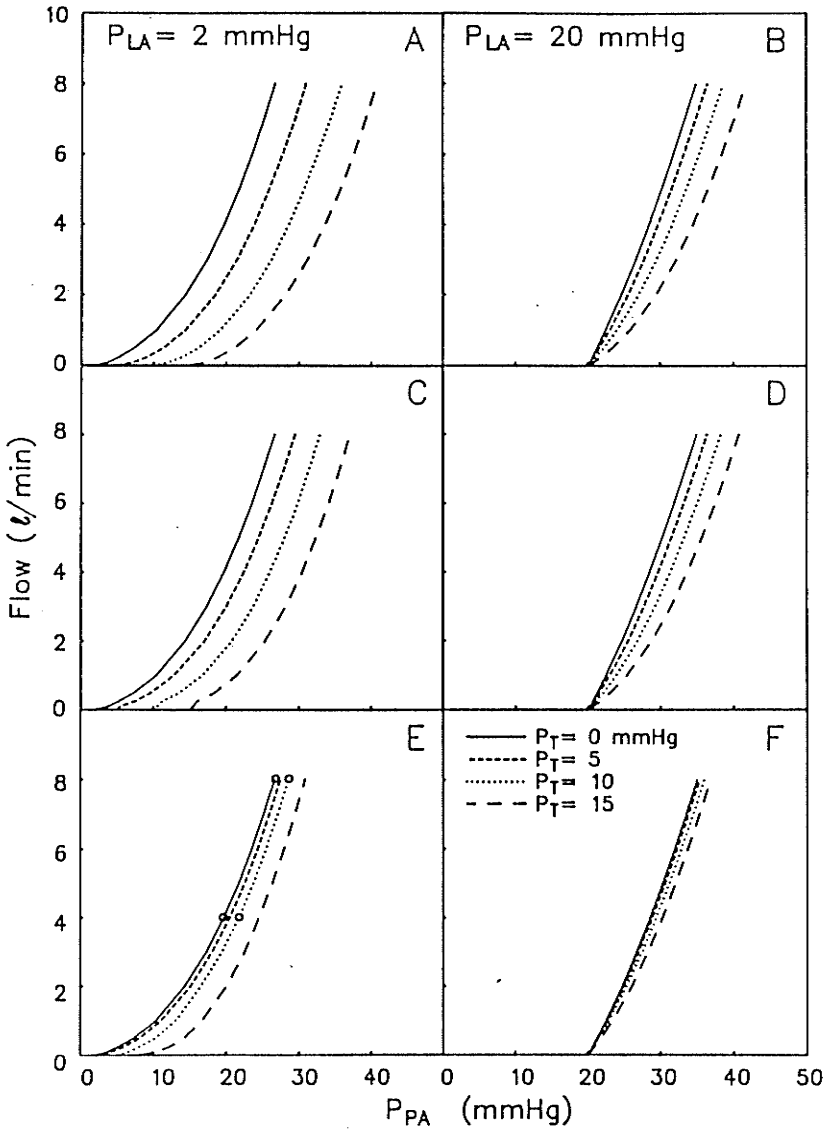

FIGURE 9. *P-F* relations without added tone (*solid lines*) and with 3 levels of added tone (5, 10, and 15 mmHg). Left and right panels show the response at low (2 mmHg) and high (20 mmHg) P_{LA}, respectively. Panels A and B, represent the condition when tone was applied uniformly to all extra-alveolar vessels; panels C and D represent the condition when tone was applied to all precapillary vessels; and panels E and F represent the condition when tone was applied to the third arterial generation only.

SEE FIGURE NEXT PAGE

FIGURE 10. Actual pressures (in mmHg), resistances (in mmHg/*l*/min) and flow (*l*/min) at different points in the model. Pressures are written at bifurcations; Resistances are written in series with the branches; Flow rates are the boxed-in values at the capillary level. Left panels were obtained at a flow of 4 *l*/min and right panels were obtained at a flow of 8 *l*/min. Panels A and B were obtained without tone. Panels C and D were obtained with a tone of 10 mmHg added to all vessels in the third arterial generation. Panels E and F were obtained with a tone of 10 mmHg was added to the second to last venous generation (R_2'). P_A equals zero, H_t equals 14 cm, and P_{LA} is 2 mmHg for all panels. All pressures are referenced to LA. Not all pressure values are shown. Missing values can be calculated from data provided. P is flow weighted mean of all pressures at the respective level. R is resistance calculated from the difference in P along the generation and total flow.

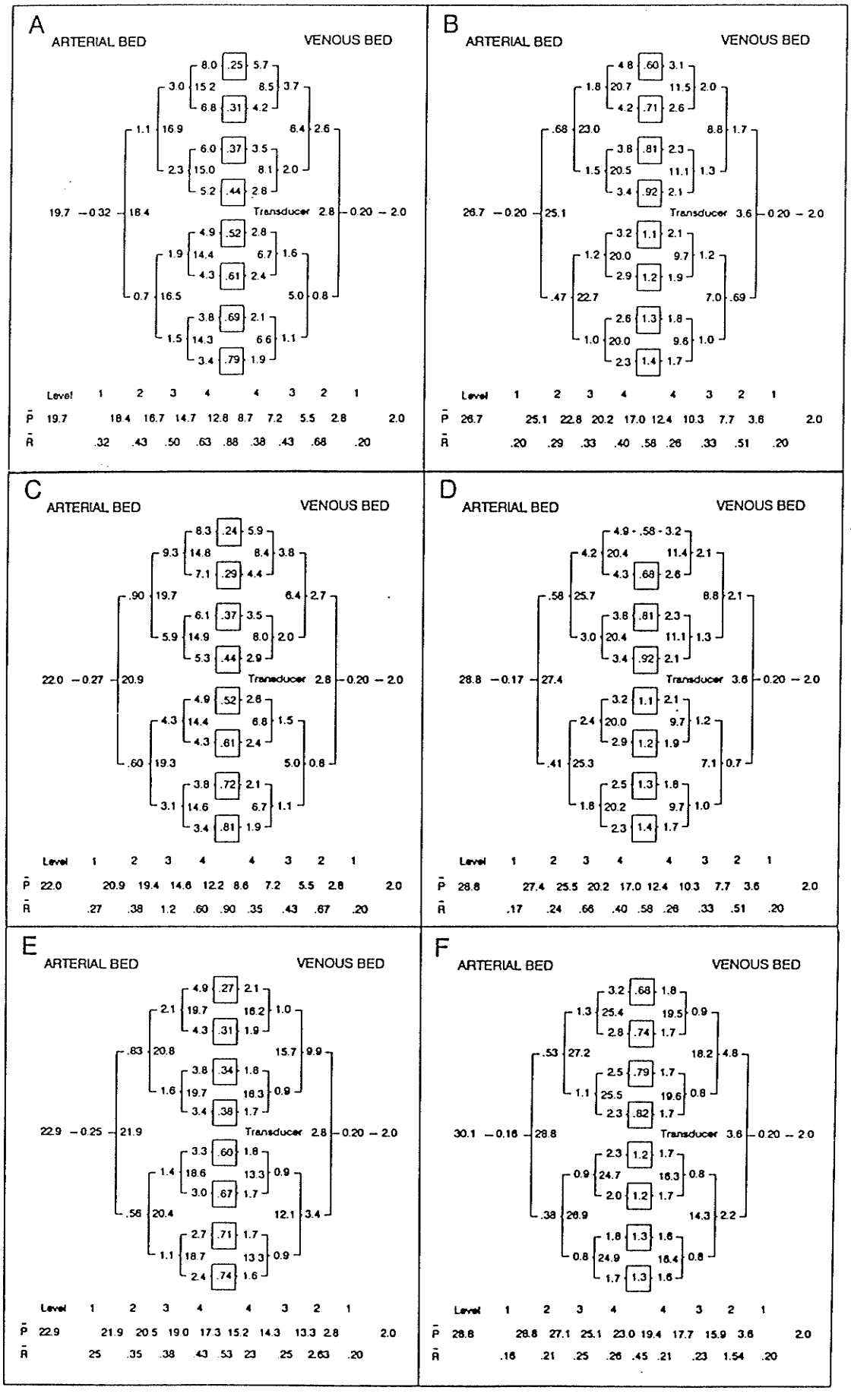
A
ARTERIAL BED
VENOUS BED
8.0 .25 5.7
3.0 15.2 8.5 3.7
6.8 .31 4.2
1.1 16.9 6.4 2.6
6.0 .37 3.5
2.3 15.0 8.1 2.0
5.2 .44 2.8
19.7 −0.32 18.4 Transducer 2.8 0.20 − 2.0
4.9 .52 2.8
1.9 14.4 6.7 1.6
4.3 .61 2.4
0.7 16.5 5.0 0.8
3.8 .69 2.1
1.5 14.3 6.6 1.1
3.4 .79 1.9
Level 1 2 3 4 4 3 2 1
P̄ 19.7 18.4 16.7 14.7 12.8 8.7 7.2 5.5 2.8 2.0
R̄ .32 .43 .50 .63 .88 .38 .43 .68 .20
B
ARTERIAL BED
VENOUS BED
4.8 .60 3.1
1.8 20.7 11.5 2.0
4.2 .71 2.6
.68 23.0 8.8 1.7
3.8 .81 2.3
1.5 20.5 11.1 1.3
3.4 .92 2.1
26.7 −0.20 25.1 Transducer 3.6 0.20 − 2.0
3.2 1.1 2.1
1.2 20.0 9.7 1.2
2.9 1.2 1.9
.47 22.7 7.0 .69
2.6 1.3 1.8
1.0 20.0 9.6 1.0
2.3 1.4 1.7
Level 1 2 3 4 4 3 2 1
P̄ 26.7 25.1 22.8 20.2 17.0 12.4 10.3 7.7 3.6 2.0
R̄ .20 .29 .33 .40 .58 .26 .33 .51 .20
C
ARTERIAL BED
VENOUS BED
8.3 .24 5.9
9.3 14.8 8.4 3.8
7.1 .29 4.4
.90 19.7 6.4 2.7
6.1 .37 3.5
5.9 14.9 8.0 2.0
5.3 .44 2.9
22.0 −0.27 20.9 Transducer 2.8 0.20 − 2.0
4.9 .52 2.8
4.3 14.4 6.8 1.5
4.3 .61 2.4
.60 19.3 5.0 0.8
3.8 .72 2.1
3.1 14.6 6.7 1.1
3.4 .81 1.9
Level 1 2 3 4 4 3 2 1
P̄ 22.0 20.9 19.4 14.6 12.2 8.6 7.2 5.5 2.8 2.0
R̄ .27 .38 1.2 .60 .90 .35 .43 .67 .20
D
ARTERIAL BED
VENOUS BED
4.9 .58 3.2
4.2 20.4 11.4 2.1
4.3 .68 2.6
.58 25.7 8.8 2.1
3.8 .81 2.3
3.0 20.4 11.1 1.3
3.4 .92 2.1
28.8 −0.17 27.4 Transducer 3.6 0.20 − 2.0
3.2 1.1 2.1
2.4 20.0 9.7 1.2
2.9 1.2 1.9
.41 25.3 7.1 0.7
2.5 1.3 1.8
1.8 20.2 9.7 1.0
2.3 1.4 1.7
Level 1 2 3 4 4 3 2 1
P̄ 28.8 27.4 25.5 20.2 17.0 12.4 10.3 7.7 3.6 2.0
R̄ .17 .24 .66 .40 .58 .26 .33 .51 .20
E
ARTERIAL BED
VENOUS BED
4.9 .27 2.1
2.1 19.7 16.2 1.0
4.3 .31 1.9
.83 20.8 15.7 9.9
3.8 .34 1.8
1.6 19.7 16.3 0.9
3.4 .38 1.7
22.9 −0.25 21.9 Transducer 2.8 0.20 − 2.0
3.3 .60 1.8
1.4 18.6 13.3 0.9
3.0 .67 1.7
.56 20.4 12.1 3.4
2.7 .71 1.7
1.1 18.7 13.3 0.9
2.4 .74 1.6
Level 1 2 3 4 4 3 2 1
P̄ 22.9 21.9 20.5 19.0 17.3 15.2 14.3 13.3 2.8 2.0
R̄ .25 .35 .38 .43 .53 .23 .25 2.63 .20
F
ARTERIAL BED
VENOUS BED
3.2 .68 1.8
1.3 25.4 19.5 0.9
2.8 .74 1.7
.53 27.2 18.2 4.8
2.5 .79 1.7
1.1 25.5 19.6 0.8
2.3 .82 1.7
30.1 −0.16 28.8 Transducer 3.6 0.20 − 2.0
2.3 1.2 1.7
0.9 24.7 16.3 0.8
2.0 1.2 1.7
.38 26.9 14.3 2.2
1.8 1.3 1.6
0.8 24.9 16.4 0.8
1.7 1.3 1.6
Level 1 2 3 4 4 3 2 1
P̄ 28.8 28.8 27.1 25.1 23.0 19.4 17.7 15.9 3.6 2.0
R̄ .16 .21 .25 .26 .45 .21 .23 1.54 .20

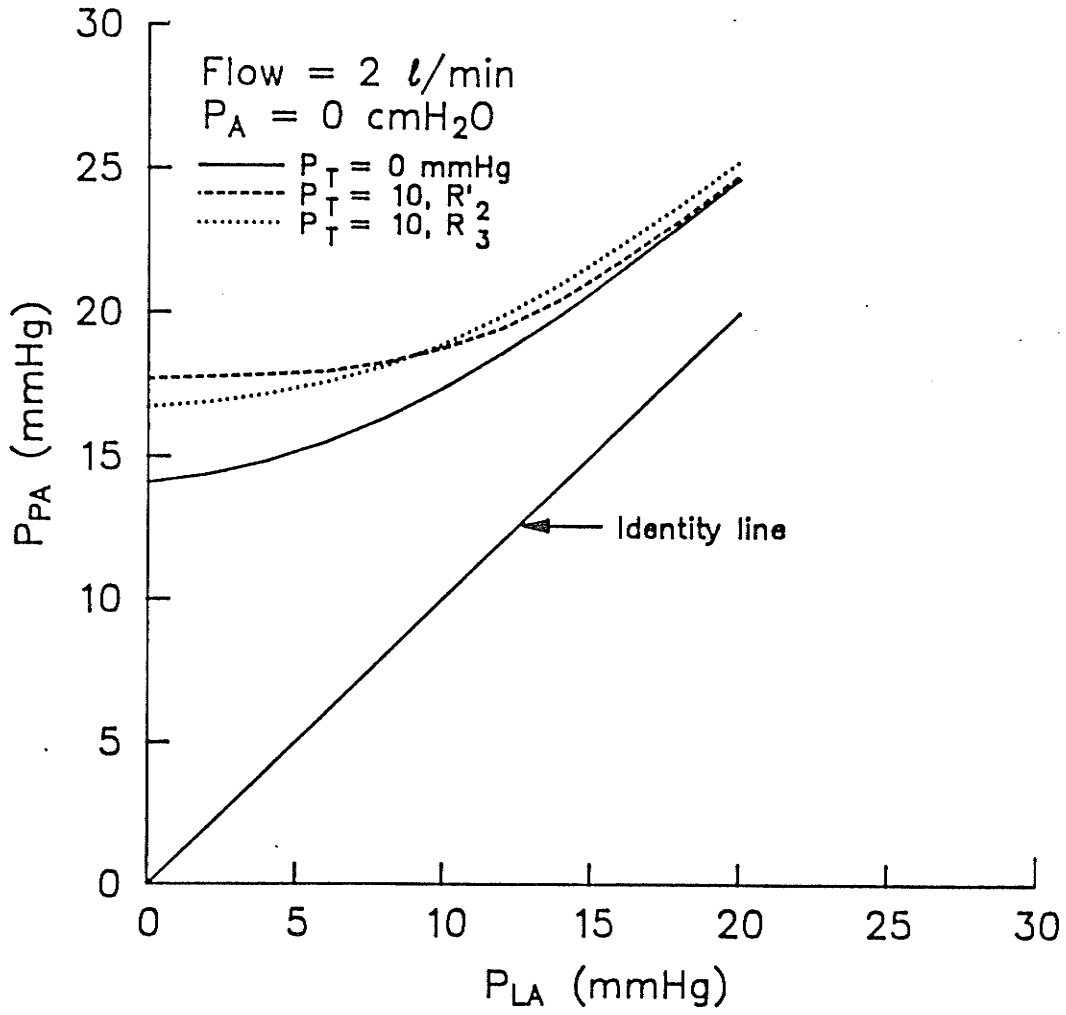

FIGURE 11. P_{LA}-P_{PA} relations without tone (*solid line*), with tone equivalent to 10 mmHg applied at the third arterial generation (*dotted line*) and at the second to last venous generation (*dashed line*).

A parallel shift in the *P-F* relationship could result from an increase in P_{crit} at some level along the vascular bed, or it may be fortuitous (see below). If the effect of tone is via the former mechanism (i.e. increased P_{crit}) then one might expect that adding tone would cause a parallel shift only when the level of added tone is such that the most downstream end of the constricted segment becomes, effectively, the site of critical closure (i.e. effective $P_{TM} < 0$). Adding tone above this level should cause a further parallel shift of the same magnitude as the extra added tone. Our results refute this explanation. It is evident that adding tone causes a roughly parallel shift even when P_{LA}, and hence transmural pressures throughout the circulation are in excess of the added tone (Figure 9, panels B, D, and F). Under these conditions a critical closure site cannot be postulated. In addition, if the parallel shift obtained with an added tone of 5 mmHg at low P_{LA} is secondary to P_T acting as P_{crit} at some segment, then subsequent increases in tone should cause a parallel shift equivalent to the extra-added tone. This was not the case (compare Figures 9A, B, and C). We conclude, therefore, that the parallel shift beyond a certain *F* is an incidental, and rather routine, response to an increase in tone resulting from complex effects of *F* on the resistance of, and pressure gradient along, the constricted and non-constricted segments, given the mechanical properties of pulmonary vessels. A good case in point is the response to added tone at one

generation only leaving other generations unaffected (as in Figure 9E). Thus, Figure 10 provides intravascular pressures and resistances at various points in the tree. Panels A and B pertain to the simulation with no added tone at flow rates of 4 and 8 *l*/min, respectively (left pair of circles in Figure 9E). Panels C and D show results obtained when a tone of 10 mmHg is added at the third arterial generation while all other variables are left unchanged (right pair of circles in Figure 9E). All pressures were referenced to LA. Note that:

1) Even though the *P-F* relationship without tone is linear in this *F* range (i.e. 4 to 8 *l*/min, solid line, Figure 9E) there is no waterfall at any level at either flow rate; P_{out} for all vessels is above P_{crit} (Figure 10, panels A and B)[1].

2) A vertical *F* gradient (note boxed numbers at capillary level), resulting from a vertical gradient in resistances, is evident. The latter is due to the effect of gravity or P_G (-7 to +7 cmH_2O from top to bottom to be added to displayed pressures).

3) Addition of tone equivalent to 10 mmHg to all branches of R_3 generation caused unequal increases in R at the different levels (compare Figures 10A with 10C and 10B with 10D). For example, R_{3a}, at 4.0 *l*/min, increased by 6.3 units whereas R_{3d} increased only by 1.6 units. This is because vessels at different levels are operating at different regions of their P_{TM} vs. R relationship (Figures 2A and 2B, CHAPTER 5) on account of gravity. Notwithstanding the different effects on R, the

vertical distribution of *F* was little affected (compare boxed values in Figure 10, panels A and C, or B and D). As a result, pressures downstream from the affected segment were almost unchanged.

4) When a tone of 10 mmHg was added to R_3 at 4.0 *l*/min, ΔP along the relevant branches increased, on average, by only 2.8 mmHg (compare ΔP along R_3 at bottom of panel C vs. ΔP along R_3 at bottom of panel A). P_{PA} increased less (i.e. 22.0-19.7 = 2.3 mmHg) on account of some decrease in R of the two upstream generations. At the higher *F* (Figure 10, panels B and D) the same added tone resulted in a smaller increase in R_3, again because the vessels are operating on a flatter region of their P_{TM} vs. R relationship (on account of greater P_V). The smaller increase in R_3 and greater *F* cancel each other out, resulting in a similar increase in ΔP across R_3 at both flow rates. Hence, the parallel shift. In neither case was there a waterfall at the site of constricted vessels. Thus, at R_{3a}, at 4.0 *l*/min (Figure 9, panel C), downstream pressure was 10.4 mmHg (14.8 mmHg referenced to LA as shown in figure less 4.4 mmHg for gravity) whereas P_{crit} was 10 mmHg. At lower branches and higher *F* downstream pressure exceeds P_{crit} by even greater amounts.

We wanted to see if the same magnitude of tone, applied at more distant sites (where the vessels are operating on a steeper part of their P_{TM} vs. R relationship) produces different results. Figures 10E and 10F show the effect of adding a tone of 10 mmHg

at the second to last venous generation (R_2', Figure 1) at 4.0 and 8.0 *l*/min, respectively. Under these conditions a waterfall exists since downstream pressures were only 2.8 and 3.6 mmHg at 4 and 8 *l*/min, respectively, while P_{crit} was 10 mmHg. ΔP along this generation increased much more than when the same amount of tone was applied upstream. For example, average ΔP across R_2' at 4.0 *l*/min increased from 2.7 (without tone, Figure 10A) to 10.5 mmHg (with tone, Figure 10E), a 7.8 mmHg increase as opposed to 2.8 mmHg (see above). Nonetheless, P_{PA} increased by only 3.2 mmHg, not much different from when tone was applied upstream. When tone is applied downstream it causes a greater rise in pressure immediately upstream to the constricted segment. However, a greater segment of the circulation lies upstream, and hence subject to distention. More of the increased pressure is thus lost on account of upstream distention eventually causing P_{PA} to rise to about the same amount. Applying tone distally also causes a parallel shift; P_{PA} increased 3.2 and 3.4 mmHg at 4.0 and 8.0 *l*/min, respectively (Figure 10A vs. Figure 10E and Figure 10B vs. Figure 10F). Similar results were obtained when tone was applied at other levels. It follows that similar qualitative responses (i.e. parallel shift) and nearly identical quantitative responses are obtained regardless of where the tone is applied and whether or not a waterfall results.

The effect of increasing P_{LA} on P_{PA} when tone (10 mmHg) was applied upstream (R_3 generation, no waterfall) or downstream (R_2' generation, waterfall present) is shown in Figure 11. The two curves are compared with the relationship obtained before adding tone. With venous constriction (dashed line) there is a segment where the slope is true zero (P_{LA} 0 to 6 mmHg). However, over the same P_{LA} range, the slope without the waterfall is not sufficiently different from zero to be detectable experimentally.

The data presented in Figures 9 to 11 indicate that the *P-F* and P_{LA}-P_{PA} relations have no discriminating ability in identifying the presence or absence of a waterfall. In addition, the slope of the P_{LA}-P_{PA} relation is of no use in determining the proportion of the lung in zone 2 perfusion. A parallel shift in the *P-F* relationship will always occur whenever vessels are subjected, uniformly (in the vertical sense) to a collapsing force. Furthermore, the magnitude of the parallel shift is not uniquely related to the magnitude of the collapsing force. The longitudinal extent of applied force (i.e. how many generations are affected) and P_{LA} both affect the extent of this shift (Figure 9). It is evident that these conclusions apply equally to the effect of increasing P_A, which operates in the same fashion as vasomotor tone except at the alveolar level.

When vascular tone is applied unequally to parallel channels, the results (figures not shown) are intermediate between those of mechanical obstruction (e.g. Figure 8) and those

of uniformly applied tone (Figure 9). For example, if a P_T of 30 mmHg is applied to one branch only, the *P-F* relation diverges from the *base line* relation until pressure upstream to the constricted segment exceeds P_{crit} for the vessel. Thereafter, the *P-F* relation becomes parallel to *base line*.

3. Relation to previous models

Models of the pulmonary circulation have been previously reported by various investigators. Permutt et al. (23) used a mechanical model consisting of Starling resistors arranged in parallel, one above the other, to account for *P-F* relationships of the pulmonary circulation. The lung was divided into two zones, one in which $P_{LA} \leq P_A$ and the other in which $P_{LA} > P_A$ [corresponding to zones 2 and 3, as defined by West et al. (30), respectively]. Total flow in each zone was obtained by integrating segmental (in the vertical sense) flow over a specified lung height for that zone, and total pulmonary blood flow was derived by combining flows from both zones. McDonald and Butler (20) used a similar model, except that their model consisted of four similar collapsible tubes connected in parallel and supported at different heights, in a box, to represent capillaries at different heights in an air-filled lung. Although both models could portray some characteristics of the *P-F* relationships seen in isolated lungs, both lacked extra-alveolar vessels and their contribution to the total *P-F* relationship. In

addition, both models were constructed from collapsible yet non-distensible tubing. In a later study, West et al. (31), using a computer model, were also able to simulate non-linearities in the *P-F* relationship. Their model consisted of 50 interconnected vessels each having its own R and its own P_{crit} before which *F* could not occur. Following that point, a region with a linear *P-F* relationship (i.e. fixed R) was assumed. Resistances and critical pressures of each element were randomly chosen. While the model helped explain non-linearities in the *P-F* relationship, again the model did not include extra-alveolar vessels.

To accommodate for extra-alveolar vessels, Dawson et al. (5) divided each parallel unit into three potential Starling resistors connected in series (an arterial segment that is connected to an alveolar segment which is in turn connected to a venous segment). P_x for the alveolar segment was assumed equal to P_A, whereas P_x for the arterial and venous segments were assumed equal to the sum of smooth muscle tone and counter radial traction forces produced by lung inflation. Although an improvement over prior models this latter model was still constructed from extra-alveolar vessels that were collapsible but not distensible. In addition, P_x values for the arterial and venous segments were arbitrarily chosen and were not based on experimental data.

Recently, Zhuang et al. (32) have presented a more complete model of the pulmonary circulation for steady-state flow conditions. Their model was based on direct measurements of anatomical and elasticity data obtained in isolated cat lungs. Although a detailed explanation of their model is beyond the scope of this paper, in brief, it consisted of a single sheet-flow model (10, 11) connected in series to an arterial and venous branching systems. The sheet-flow theory of Fung and Sobin (10, 11) was used to calculate pulmonary capillary *P-F* relationships at the alveolar level and an analogous "fifth-power law" was used for the arterial and venous branching systems. Model predictions in their study were compared to previously reported data. Krishnan et al. (15), in a more recent study, also compared the results of the model of Zhuang et al. (32) to a series of steady-state results obtained in isolated cat lungs. Our model differs from that of Zhuang et al. (32) in several respects:

First, the number of branching orders in the Zhuang model (11-17 orders) is considerably higher than the number of orders in our present model (4 orders). Although this negates the main advantage of the Zhuang model, namely the use of actual anatomical data (length, diameter, etc.), it permitted us to simulate parallel non-homogeneities, which would be unmanageable otherwise. We believe that the number of branching orders in the present model represents a good balance between the desire to

keep the model as simple as possible, while having the possibility to change individual resistances independently. Second, distensibility of the vascular bed in relation to P_{TM} (i.e pressure-diameter relations) in the Zhuang model was assumed constant. The relations reported for dogs are quite different. As shown in Figures 1A and 1B (CHAPTER 5, reproduced from Figures 7A and 7B, *ref.* 28, respectively), for arteries, area and not diameter is linearly related to pressure while for veins linearity is maintained over a very small range of P_{TM} (0 to 8 cmH_2O). Third, P_x in the Zhuang model was assumed constant and equal to either P_A or P_{p1} [depending on vessel size in the study of Zhuang et al. (32), and on the branching order in that of Krishnan et al. (15)]. P_x, however, as shown in Figures 1A and 1B (reproduced from Figures 11A and 11B, *ref.* 28, respectively) is highly dependent on the state of lung inflation and the magnitude of P_v (see also 16, 17). Fourth, in order to accommodate for increased vessel length with lung inflation, an increase in the number of branching orders is necessary in the Zhuang model (32). In the present model, however, changes in vessel length secondary to changes in lung volume are incorporated into the model. Fifth, vascular tone and gravity effects included in the present model, were not included in the Zhuang model.

E. FOOTNOTES

Footnote 1. Vascular pressures shown in Figure 10 are referenced to LA. To obtain actual P_V at any level, the effect of gravity (P_G) should be added to the indicated values. For this simulation P_G is -7 cmH_2O (≈5 mmHg) at the highest level and +7 cmH_2O at the lowest. Because P_A in this simulation is zero, and P_X is also zero (Figure 1, CHAPTER 5) and since no tone was added in panels A and B, $P_{crit} = P_X$ is equal zero for all branches.

F. GLOSSARY

α: compliance of the capillary sheet, in $\mu m/cmH_2O$.

μ: viscosity of blood.

0,35: when applied as subscript to a statement refers to the value of the statement at reference conditions of $P_{TP} = 0$ and $P_{pas} = 35$ cmH_2O.

A: vessel cross-sectional area (lumen).

A_i: cross-sectional area of segment i.

A_{max}: highest lumen cross-sectional area reported by Smith and Mitzner (28) [i.e. at P_{pas} of 30 cmH_2O].

A_o: lumen area at optimal muscle length (l_o).

C_L: a constant describing the fractional lung volume change per unit pressure change.

F: flow.

F_{crit}: critical flow at which the cross-sectional area of the most upstream segment of a vessel is the same with and without added tone.

F_{max}: maximal flow, as allowed by the wave-speed limitation theory, in a given segment and for a given P_v.

F_T: total flow.

H: capillary sheet thickness.

H_{art}: thickness at the arterial end of a capillary sheet.

H_{max}: maximum sheet thickness.

H_o: capillary sheet thickness when intravascular pressure (P_v) equals alveolar pressure (P_A).

H_t: lung height.

H_{ven}: thickness at the venous end of a capillary sheet.

l: vessel length

LA: left atrium.

l_{max}: vessel length at maximal (P_{TP} = 30 cmH_2O) lung volume.

l_o: optimal muscle length, length at which muscle produces maximal tension.

P-F: pressure-flow.

PA: pulmonary artery.

P_{art}: intravascular pressure at the arterial end of a capillary sheet.

P_{crit}: critical opening pressure, the minimal pressure required to open an individual vessel.

P_G: pressure produced by gravitational forces.

P_{in}: inflow pressure.

P_{LA}: left atrial pressure.

P_{max}: pressure at which a capillary sheet reaches its maximum thickness (H_{max}) and becomes non-distensible.

P_{min}: minimal P_{Tot} below which vessel compliance becomes zero or negative with treatments 1 and 2 of P_T (Figure 5).

P_o: pressure produced by active tension when smooth muscle layer is at l_o.

P_{op}: opening pressure, obtained from the extrapolated pressure intercept of the linear segment of a *P-F* relationship.

P_{out}: outflow pressure.

P_{PA}: pulmonary arterial pressure.

P_{pas}: passive pressure (i.e. in the absence of vasomotor tone).

P_{pl}: pleural pressure.

P_T: pressure due to vasomotor tone.

P_{TM}: transmural pressure.

P_{Tot}: total pressure, the sum of P_T and P_{pas}.

P_{TP}: transpulmonary pressure.

P_V: intravascular pressure.

P_{ven}: intravascular pressure a the venous end of a capillary sheet.

P_x: perivascular pressure.

P_z: the pressure at which flow commences in a vessel.

r: radius.

R: resistance. When followed by a "'" pertains to venous resistance and when combined with a numerical followed by a lower case letter refer to Figure 1, part II of this communication for exact location of the vessel in the multibranched model.

R_{ar}: resistance of an arterial extraalveolar pulmonary vessel.

R_{c1}: first (of two) subdivision of a capillary sheet resistance (see text for further explanation).

R_{c2}: second (of two) subdivision of a capillary sheet resistance (see text for further explanation).

R_c: capillary sheet resistance.

R_{cmin}: minimal capillary sheet resistance.

R_{DS}: downstream resistance.

R_i: resistance of segment i.

r_l: lumen radius.

r_m: radius of smooth muscle layer.

$R_{n(i)}$: vessel ranking relative to a reference point used to calculate gravitational pressure (P_G).

r_o: lumen radius when smooth muscle layer is at l_o.

R_T: total resistance.

R_V: vascular resistance.

R_{ve}: resistance of a venous extraalveolar pulmonary vessel.

T: tension.

T_{max}: maximal active tension obtained at l_o.

V_L: lung volume.

V_{Lmax}: maximal (i.e. at P_{TP} = 30 cmH_2O) lung volume.

V_M: minimal (i.e. at P_{TP} = 0) lung volume as a fraction of V_{Lmax}.

WS: wave-speed.

Z: the change in P_{PA} (ΔP_{PA}) as a fraction of a step change in P_{LA} (ΔP_{LA}); $\Delta P_{PA}/\Delta P_{LA}$ in the multibranched model and $\Delta P_{in}/\Delta P_{out}$ in the single vessel model.

G. REFERENCES

1. Banister, J., and R.N. Torrance. The effects of the tracheal pressure upon flow: pressure relations in the vascular bed of isolated lungs. *Quart. J. Exptl. Physiol.* 45:352-367, 1960.

2. Barer, G.R., and E. Nüsser. Pulmonary blood flow in the cat. The effect of positive pressure respiration. *J. Physiol.* 138:103-118, 1957.

4. Carlill, S.D., H.N. Duke, and M. Jones. Some observations on pulmonary hemodynamics in the cat. *J. Physiol.* 136:112-121, 1957.

5. Dawson, C.A., R.L. Jones, and L.H. Hamilton. A pulmonary circulation model based on forward and retrograde perfusion of isolated lungs. *J. Appl. Physiol.* 35(1):113-110, 1973.

6. Ducas, J., D. Duval, H. Dasilva, P. Boiteau, and R.M. Prewitt. Treatment of canine pulmonary hypertension: effects of norepinephrine and isoproterenol on pulmonary vascular pressure-flow characteristics. *Circulation* 75(1):235-242, 1987.

7. Ducas, J., L. Girling, U. Schick, and R.M. Prewitt. Pulmonary vascular effects of hydralazine in a canine preparation of pulmonary thromboembolism. *Circulation* 73:1050-1057, 1986.

8. Edwards, W.S. The effects of lung inflation and epinephrine on pulmonary vascular resistance. *Am. J. Physiol.* 167:756-762, 1951.

9. Fishman, A.P. Pulmonary Circulation. In: *Handbook of Physiology - The Respiratory System*, edited by A.P. Fishman and A.B. Fisher. Circulation and Nonrespiratory Functions. Bethesda, MD; Am. Physiol. Soc.; 1985, Sect. 3., vol. I, chapt. 3, p. 93-166.

10. Fung, Y.C., and S.S. Sobin. Elasticity of the pulmonary alveolar sheet. *Circ. Res.* 30:451-469, 1972.

11. Fung, Y.C., and S.S. Sobin. Pulmonary alveolar blood flow. *Circ. Res.* 30:470-490, 1972.

12. Glazier, J.B., Hughes, J.M.B., Maloney, J.E., and West, J.B. Vertical gradient of alveolar size in lungs of dogs frozen intact. *J. Appl. Physiol.* 23:694-705, 1967.

13. Graham, R., C. Skoog, W. Macedo, J. Carter, L. Oppenheimer, J. Robson, and H.S. Goldberg. Dopamine, dobutamine, and phentolamine effects on pulmonary vascular mechanics. *J. Appl. Physiol.* 54:1277-1283, 1983.

14. Graham, R., C. Skoog, L. Oppenheimer, J. Rabson, and H.S. Goldberg. Critical closure in the canine pulmonary vasculature. *Circ. Res.* 50(4):566-572, 1982.

15. Krishnan, A., J.H. Linehan, D.A. Rickaby, and C.A. Dawson. Cat lung hemodynamics: comparison of experimental results and model predictions. *J. Appl. Physiol.* 61(6):2023-2034, 1986.

16. Lai-Fook, S.J. A continuum mechanics analysis of pulmonary vascular interdependence in isolated dog lobes. *J. Appl. Physiol.* 46(3):419-429, 1979.

17. Lai-Fook, S.J., and R.E. Hyatt. Effect of parenchyma and length changes on vessel pressure-diameter behavior in pig lungs. *J. Appl. Physiol.* 47(4):666-669, 1979.

18. Lopez-Muniz, R., N.L. Stephens, B. Bromberger-Barnea, S. Permutt, and R.L. Riley. Critical closure of pulmonary vessels analyzed in terms of Starling resistor model. *J. Appl. Physiol.* 24(5):625-635, 1968.

19. Maloney, J.E., S.A. Rooholamini, and L. Wexler. Pressure-diameter relations of small blood vessels in isolated dog lung. *Microvasc. Res.* 2:1-12, 1970.

20. McDonald, I.G., and J. Butler. Distribution of vascular resistance in the isolated perfused dog lung. *J. Appl. Physiol.* 23(4):463-474, 1967.

21. Mink, S.N., H.S. Unruh, and L. Oppenheimer. Vascular and interstitial mechanics in canine pulmonary emphysema. *J. Appl. Physiol.* 59:1704-1715, 1985.

22. Mitzner, W., and I. Huang. Interpretation of pressure-flow curves in the pulmonary vascular bed. In: *The Pulmonary Circulation in Health and Disease*. Edited by J.A. Will, C.A. Dawson, E. Kenneth Weir, and C.K. Buckner. Academic Press, Inc. 1987. P. 215-230.

23. Permutt, S., B. Bromberger-Barnea, and H.N. Bane. Alveolar pressure, pulmonary venous pressure, and the vascular waterfall. *Med. Thorac.* 19:239-260, 1962.

24. Permutt, S., P. Caldini, A. Maseri, W.H. Palmer, T. Sasamori, and K. Zierler. Recruitment versus distensibility in the pulmonary vascular bed. In: *The Pulmonary Circulation and Interstitial Space*, edited by A.P. Fishman, Chicago, IL:Hecht, 1969, p. 375-390.

25. Permutt, S., and R.L. Riley. Hemodynamics of collapsible vessels with tone: the vascular waterfall. *J. Appl. Physiol.* 18:924-932, 1963.

26. Roos, A., L.J. Thomas, Jr., E.L. Nagel, and D.C. Prommas. Pulmonary vascular resistance as determined by lung inflation and vascular pressures. *J. Appl. Physiol.* 16(1):77-84, 1961.

27. Shoukas, A.A., M.J. Brunner, A.E. Frankle, A.S. Greene, and C.H. Kallman. Carotid sinus baroreceptor reflex control and the role of autoregulation in the systemic and pulmonary arterial pressure-flow relationship of the dog. *Circ. Res.* 54:674-682, 1984.

28. Smith, J.C., and W. Mitzner. Analysis of pulmonary vascular interdependence in excised dog lobes. *J. Appl. Physiol.* 48(3):450-467, 1980.

29. West, J.B., and C.T. Dollery. Distribution of blood flow and the pressure-flow relations of the whole lung. *J. Appl. Physiol.* 20:175-183, 1965.

30. West, J.B., C.T. Dollery, and A. Naimark. Distribution of blood flow in isolated lung relation to vascular and alveolar pressure. *J. Appl. Physiol.* 19:713-724, 1964.

31. West, J.B., A.M. Schneider, and M.M. Mitchell. Recruitment in networks of pulmonary capillaries. *J. Appl. Physiol.* 39(6):976-984, 1975.

32. Zhuang, F.Y., Y.C. Fung, and R.T. Yen. Analysis of blood flow in cat's lung with detailed anatomical and elasticity data. *J. Appl. Physiol.* 55(4):1341-1348, 1983.